EPRI | ELECTRIC POWER RESEARCH INSTITUTE

Spent Fuel Transportation Applications—Assessment of Cladding Performance

A Synthesis Report

WARNING:
Please read the Export Control Agreement on the back cover.

Spent Fuel Transportation Applications—Assessment of Cladding Performance

A Synthesis Report

1015048

Final Report, December 2007

EPRI Project Manager
A. Machiels

ELECTRIC POWER RESEARCH INSTITUTE
3420 Hillview Avenue, Palo Alto, California 94304-1338 • PO Box 10412, Palo Alto, California 94303-0813 • USA
800.313.3774 • 650.855.2121 • askepri@epri.com • www.epri.com

DISCLAIMER OF WARRANTIES AND LIMITATION OF LIABILITIES

ORGANIZATION(S) THAT PREPARED THIS DOCUMENT

Anatech Corp.

NOTE

For further information about EPRI, call the EPRI Customer Assistance Center at 800.313.3774 or e-mail askepri@epri.com.

CITATIONS

This report was prepared by

ANATECH Corp.
5435 Oberlin Drive
San Diego, California 92121

Principal Investigator
J. Rashid

This report describes research sponsored by the Electric Power Research Institute (EPRI).

The report is a corporate document that should be cited in the literature in the following manner:

Spent Fuel Transportation Applications—Assessment of Cladding Performance: A Synthesis Report. EPRI, Palo Alto, CA: 2007. 1015048.

REPORT SUMMARY

This report summarizes the results of EPRI's multi-year research effort to assess cladding performance under normal and hypothetical accident conditions of spent nuclear fuel transportation.

Background

The structural performance of high-burnup spent fuel cladding during dry storage and transportation has been the subject of research and evaluation at EPRI for several years. The major issues addressed in this research program have included the following:

- Characterization and development of predictive models for damage mechanisms perceived to be potentially active during dry storage
- Modeling and analysis of deformation processes during long-term dry storage
- Development of cladding failure models and failure criteria, considering cladding material and physical conditions during dry storage and transportation
- Failure analysis, considering end-of-dry-storage conditions, of spent fuel systems subjected to normal and accident conditions of transport, prescribed in Part 71 of Title 10 of the Code of Federal Regulations (10 CFR 71)

While issues related to dry storage have largely been resolved, transportation issues have not, at least for spent fuel with discharge burnups greater than 45 GWd/MTU. A research program was launched in late 2002 following two NRC-industry meetings held on September 6, 2002 and October 23, 2002. The aim of the research program was to assess the performance of high-burnup spent fuel cladding under normal and accident conditions of transportation, as prescribed by 10 CFR 71, considering the physical characteristics and mechanical properties of cladding at the end of dry storage. Since its inception in the fall of 2002, the research program has resulted in the publication of eight EPRI reports.

Objectives

To present a synthesis of the information contained in eight previously published EPRI reports, which collectively form a part of a technical basis intended to facilitate resolution of regulatory issues associated with the transportation of spent nuclear fuel characterized by discharge burnups greater than 45 GWd/MTU.

Approach

The research team reviewed the large body of modeling and analysis work carried out during the past several years and then organized it into three technical areas. The first technical area examines dry storage effects on cladding geometry (due to creep) and hydride morphology in the cladding alloy (due to hydride re-orientation). The second technical area deals with the

development of failure models and failure criteria for application to transportation accident analysis. The third technical area applies the above-described developments to the evaluation of fuel rod failures in transportation casks subjected to loading conditions specified in 10 CFR 71.

Results

The results of the analytical studies conducted during the past several years indicate that damage to high-burnup spent fuel under prescribed regulatory conditions of dry storage and transportation will not impair its operational management. Dry storage effects on cladding physical and material conditions, including creep-related deformations, have the potential to impact fuel rod performance during transportation. Specifically, cladding resistance to failure under the dynamic loading of transportation accidents depends on fuel-cladding gap size and radial hydride formation, both of which could—to a limited extent—evolve during long-term dry storage. The results of the hypothetical accident analysis indicate that cladding failure would be bi-modal—taking the form of 1) a state of failure initiation at the cladding inside diameter (ID) remaining as part-wall damage, with less than a 2% probability of occurrence and 2) a through-wall failure with a probability of 1E-5. The response analysis under normal conditions of transport shows a large margin against fuel rod failures. The grids and guide tubes, which form the structural elements of the fuel assembly, are predicted to remain structurally competent. As a result, the geometric form of the spent fuel assemblies will not be substantially altered.

EPRI Perspective

Failure to resolve, in a timely manner, regulatory issues associated with interim dry storage and transportation of high-burnup spent fuel would result in severe economic penalties and in operational limitations to nuclear plant operators. The Nuclear Regulatory Commission (NRC) Spent Fuel Storage and Transportation (SFST) Division issued Revision 3 of Interim Staff Guidance 11, *Cladding Considerations for Transportation and Storage of Spent Nuclear Fuel*, in November 2003. Revision 3 contains generic acceptance criteria for the dry storage of spent fuel, but does not specify any such criteria for the transportation of high-burnup (>45 GWd/MTU) spent fuel. Proposed approaches for resolving technical issues associated with fuel assembly integrity under hypothetical transportation accident conditions have been discussed with SFST. The results are documented in eight EPRI reports: 1009694, June 2004; 1009693, December 2004; 1009929, June 2005; 1011816, September 2005; 1011817, December 2005; 1013447, October 2006; 1013448, December 2006, and 1015049 (June 2007). This report provides a synthesis of the work reported in these eight reports. For completeness, past work related to the dry storage phase in the life cycle of managing spent fuel is summarized, given that transportation may occur after an extended period of dry storage. Two additional reports assessing criticality risks during transportation of spent fuel (1013449, December 2006) and addressing effects of fuel relocation on nuclear reactivity (1015050, June 2007) provide further information intended to generically resolve the high-burnup spent fuel transportation issue.

Keywords

Spent Fuel
High Burnup
Transportation
Spent Fuel Cladding
Dry Storage
Failure Analysis

ABSTRACT

This report summarizes the results of a multi-year research effort to assess cladding performance under normal and hypothetical accident conditions of spent nuclear fuel transportation. To inform resolution of the issues involved, the following developments were undertaken:

1. Evaluation of Fracture Toughness Data for Zirconium Alloys and Application to Spent Fuel Cladding in Dry Storage.
2. Development of Creep Modeling and Analysis Methodology for Spent Fuel in Dry Storage.
3. Modeling of Hydride Precipitation and Re-orientation in Spent Fuel Cladding during Dry Storage.
4. Development of Metal/Hydride Mixture Model for Characterizing the Constitutive Behavior of Zircaloy Cladding with Mixed Hydride Structure.
5. Derivation of Failure Criteria for Zircaloy Cladding Using a Damage-Based Metal/Hydride Mixture Model.
6. Development of a Methodology for the Evaluation of Fuel Rod Failures under Accident Conditions.
7. Computation of Global Forces Acting on Spent Fuel Rods and Deformation Patterns Resulting from Transportation Accidents.
8. Modeling of Spent Fuel Rod Transverse Tearing and Rod Breakage Resulting from Transportation Accidents.
9. Probabilistic Modeling of Spent Fuel Rod Longitudinal Tearing Resulting from Transportation Accidents.
10. Modeling of Spent Fuel under Normal Conditions of Transport.

Items 1 and 2 in the above list were developed to evaluate the potential for cladding failure under the in-situ conditions of dry storage, such as creep rupture, failure due to a pre-existing crack becoming critical under the decaying temperature, or the slow extension of pre-existing cracks under the stress corrosion cracking (SCC) and the delayed hydride cracking (DHC) mechanisms. The results show that the spent fuel rod's internal chemical environment and its thermal and mechanical histories are not sufficient to promote the SCC and the DHC mechanisms in dry storage. Creep, however, has two opposing effects: The first is the beneficial effect of reducing internal gas pressure, which reduces the hoop stress, consequently dampening the evolution of radial hydrides. The second effect is the increase in the fuel-cladding gap, which negatively impacts the cladding resistance to failure under the dynamic loading of drop accidents. Item 3 modeled the evolution of the hydride structure in dry storage, and using the hydride structure predicted by the model, a damage-based metal/hydride mixture model (Items 4 and 5) was

developed to predict the evolution of cladding failure and failure-mode configurations during drop accidents. Integrating these models into a detailed finite-element-based analysis simulation of the hypothetical transportation accident (Items 6, 7 and 8), cladding failure frequency and failure-modes patterns were calculated. The results were then incorporated into a probabilistic analysis methodology employing Monte Carlo simulations (Item 9) to calculate failure probabilities. The same methodology was applied to normal conditions of transport using the 0.3-m drop as a surrogate event for normal conditions of transportation. The results of the hypothetical accident analysis indicate that cladding failure is bi-modal: a state of failure initiation at the cladding ID remaining as part-wall damage, with less than a 2% probability of occurrence; and a through-wall failure with a probability of 1E-5. The response analysis under normal conditions of transport (Item 10) shows large margin against fuel rod failures. The grids and guide tubes, which form the structural elements of the fuel assembly, are predicted to remain structurally competent, which maintains the assemblies in a non-reconfigured state.

CONTENTS

LIST OF FIGURES

LIST OF TABLES

1
INTRODUCTION

The structural performance of high-burnup spent fuel cladding during dry storage and transportation has been the subject of research and evaluation at EPRI for several years. The major issues addressed in this research program have included:

- Characterization and development of predictive models for damage mechanisms perceived to be potentially active during dry storage,
- Modeling and analysis of deformation processes during long-term dry storage,
- Development of cladding failure models and failure criteria considering cladding material and physical conditions during dry storage and transportation, and
- Failure analysis, considering end-of-dry-storage conditions, of spent fuel systems subjected to normal and hypothetical accident conditions of transport prescribed in Part 71 of Title 10 of the Code of Federal Regulations, (10 CFR 71) [1].

A first phase of this research program dealt with storage issues and produced the three reports listed below, which were submitted for review to NRC's Spent Fuel Project Office (SFPO)[1]:

- 1001207, December 2000: "Creep as the Limiting Mechanism for Spent Fuel Dry Storage" [2].
- 1001281, January 2001: "Fracture Toughness Data for Zirconium Alloys – Application to Spent Fuel Cladding in Dry Storage" [3].
- 1003135, November 20001: "Creep Modeling and Analysis Methodology for Spent Fuel in Dry Storage" [4].

These documents led to extensive interactions with the SFPO in the form of presentations at NRC-Industry meetings and responses to Requests for Additional Information (RAIs) and clarifications. The scope of the NRC-Industry interactions is documented in the compendium EPRI Report 1009276 "Dry Storage of High-Burnup Spent Fuel – Responses to Nuclear Regulatory Commission Request for Additional Information and Clarification" [5], dated November 2003. These interactions contributed to the elimination of cladding creep as the limiting damage mechanism for dry storage of spent fuel, as was reflected in the second and third revisions of Interim Staff Guidance 11 [6, 7].

[1] Presently denominated Spent Fuel Storage and Transportation (SFST)

While issues related to dry storage have largely been resolved, transportation issues have not, at least for spent fuel with discharge burnup greater than 45 GWd/MTU. To that end, a second phase of the EPRI research program was launched in late 2002 following two NRC-Industry meetings held on September 6 and October 23, 2002. The objective of this second phase is the evaluation of the performance of high-burnup spent fuel cladding under accident and normal conditions of transportation, as prescribed by 10 CFR 71, considering the physical characteristics and mechanical properties of the cladding at the end of dry storage. The following documents were completed during the second phase of the program, and collectively provide a generic assessment of the structural performance of high-burnup spent fuel rod cladding during transportation.

- 1009694, June 2004: "Development of a Metal/Hydride Mixture Model for Zircaloy Cladding with Mixed Hydride Structure" [8].
- 1009693, December 2004: "Failure Criteria for Zircaloy Cladding Using a Damage-based Metal/Hydride Mixture Model" [9].
- 1009929, June 2005: "Spent Fuel Transportation Applications: Fuel Rod Failure Evaluation under Simulated Cask Side Drop Conditions" [10].
- 1011816, September 2005: "Application of Critical Strain Energy Density to Predicting High-Burnup Fuel Rod Failure, *Response to Comments from the Nuclear Regulatory Commission Staff*" [11].
- 1011817, December 2005: "Spent Fuel Transportation Applications: Global Forces Acting on Spent Fuel Rods and Deformation Patterns Resulting from Transportation Accidents" [12].
- 1013447, October 2006: Report 1009694, June 2004: "Spent-Fuel Transportation Applications: Modeling of Spent-Fuel Rod Transverse Tearing and Rod Breakage Resulting from Transportation Accidents" [13].
- 1013448, December 2006: "Spent Fuel Transportation Applications: Longitudinal Tearing Resulting from Transportation Accidents – A Probabilistic Treatment" [14].
- 1015049, June 2007: "Spent-Fuel Transportation Applications – Normal Conditions of Transport" [15].

The first four reports in the above list deal with mechanistic modeling of the evolution of damage in cladding with mixed hydride structure and the development of failure criteria as function of radial and circumferential hydride concentrations. Utilizing the developed failure criteria, the last four reports describe the results of failure analyses under the dynamic loading of cask drop events prescribed by 10 CFR 71 for normal and hypothetical-accident conditions of transport. These eight documents [8] to [15] collectively provide the background for constructing a defense-in-depth argument for the safe transportation of high-burnup spent fuel during its eventual journey from at-reactor independent spent fuel storage installations to a permanent repository, a centralized interim storage facility, or both.

Background

The first attempt to quantify spent fuel failure statistics under hypothetical transportation and handling accidents was carried out in the DOE-sponsored study by Sandia National Laboratories, "*A Method for Determining the Spent Fuel Contribution to Transport Cask Containment Requirements*", SAND90-2406, November 1992 [16]. The largest failure probabilities calculated in that study ranged from 5E-5 (rod breakage) to 2E-4 (pinhole rupture) for the regulatory-prescribed hypothetical transportation accidents. The cladding properties and technical bases for the failure evaluation conducted in the five-year Sandia study reflected the effects of burnup levels below 35 GWd/MTU. By the end of the 20th century, however, the basis for the SAND90-2406 evaluation became questionable as the burnup of fuel assemblies being discharged at the time was closer to 45 GWd/MTU and projected to be routinely over that level within a few years. Although dry storage issues had not yet fully emerged at the time of the Sandia study, storage-related degradation mechanisms, such as secondary stress corrosion cracking, delayed hydride cracking and creep rupture were briefly discussed in SAND90-2406. Also, briefly described were the effects of hydride re-orientation on cladding ductility (Marshal and Louthan [17] and Einziger and Kohli [18]), but the lack of sufficient data for formulating any failure models or failure criteria made those discussions somewhat premature. It should be noted in retrospect, however, that the lack of such information did not invalidate the failure prediction of SAND90-2406 because those failure predictions were based on bounding estimates of inner surface cracks assumed to have been present in the cladding as the result of the in-reactor pellet cladding interaction (PCI) damage mechanism. Because of their bounding nature, such pre-existing flaws would have qualified as surrogate representation of the above-cited damage mechanisms.

The earliest postulate for potential cladding failure during dry storage was put forward in an NRC licensing review of the CASTOR V/21 dry storage cask, USNRC 1985 [19]. The reviewers based their assessment for maintaining cladding integrity on a model derived from work by Raj and Ashby, 1975 [20] on creep-induced failure in metals by creep-cavity growth and grain-boundary sliding. The mechanism is known as "diffusion controlled cavity growth" (DCCG). Although NUREG-1536 [21] had endorsed the use of the DCCG model for setting maximum temperature limits for spent fuel dry storage, the NRC subsequently dismissed the model as being "overly restrictive", Draft ISG-11, 1999 [22], and relied upon the CSFM methodology, Gilbert et al., 2000 [23], in setting preliminary acceptance criteria. The latter established the 1% creep strain limit, for the dry storage of high-burnup spent fuel (> 45 GWD/MTU assembly average), ISG-11 Rev.1, 2000.

The major element introduced in Revision 1 of ISG-11 was setting the maximum temperature based on a creep strain limit of 1% as a means to preclude cladding perforation during dry storage. At the time, creep-related issues were the focus of EPRI's development effort for cladding behavior in dry storage. Two reports were completed: 1001207 (*"Creep as the Limiting Mechanism for Spent Fuel Dry Storage"*) and 1001281 (*"Fracture Toughness Data for Zirconium Alloys"*), and submitted to NRC in late 2000/early 2001. The first of these two reports contained detailed discussion of the then-postulated damage mechanisms, which included delayed hydride cracking (DHC), stress corrosion cracking (SCC) and creep rupture (CR). The main thesis of 1001207 is that creep, as the only deformation regime for the cladding under dry storage conditions, is the governing mechanism, and that SCC and DHC are non-operative mechanisms for spent fuel in dry storage. The latter was illustrated through a fracture mechanics based analysis using the information contained in 1001281. The above-described results were

discussed in a meeting between NRC and NEI/EPRI on April 18, 2001. A third report, 1003135 (*"Creep Modeling and Analysis Methodology for Spent Fuel in Dry Storage"*), which contained a large number of case analyses to illustrate the self-limiting nature of cladding creep under dry storage conditions, was submitted to NRC in October 2001. The submittal was followed by a series of meetings that took place in the period from March to July, 2002. Not long after that, Revision 2 of ISG-11 was issued at the end of July 2002; Rev. 2 set the maximum temperature limit at 400°C and established restrictions on thermal cycling during vacuum drying. The change came as a result of increased understanding of the creep phenomenon as it relates to spent fuel dry storage, both through joint USNRC- and EPRI-sponsored experimental research, Einziger et al. [24], EPRI-sponsored analytical research, as well as experimental/analytical work by Goll et al. [25], Limon et al. [26], Bouffioux et al. [27], and others. The technical evidence represented in this body of work provided support for the following statement in ISG-11, Rev.2: *"the staff had reasonable assurance that creep under normal conditions of storage will not cause gross degradation of the cladding and that the geometric configuration of the spent fuel will be preserved provided that the peak cladding temperature not exceed 400°C"*.

Finally, the last revision of ISG-11 (Rev. 3) published in November 2003, clarified some of the terms of Rev. 2, but left unresolved the transportation of high-burnup spent fuel; the central issue being the then-unknown effect of radial hydrides on fuel reconfiguration during transportation accidents. This issue became the focus of the EPRI program starting in late 2002 following two NRC-Industry meetings in September and October 2002.

Report Contents

The large body of modeling and analysis work carried out during the past several years is organized into three technical areas. The first technical area examines cladding performance during dry storage considering a number of potential failure mechanisms (Section 2). The second technical area deals with the development of failure models and failure criteria for application to transportation accidents analysis (Section 3). The third technical area applies the above-described developments to the evaluation of fuel rod failures in transportation casks subjected to hypothetical accident (Section 4) and normal loading conditions (Section 5). Conclusions are presented in Section 6.

2
DRY STORAGE APPLICATIONS

Beginning-of-Storage Initial Conditions

The physical and material conditions of spent fuel rods at the beginning of dry storage constitute the initial conditions for the analytical evaluation of potential threats to cladding integrity during dry storage, and subsequently, transportation when such initial conditions will have been modified by years or decades of storage. These initial conditions include: rod internal pressure, cladding oxide thickness and hydrogen content, cladding hydride structure, and initial flaws in the cladding, which may have been caused by pellet-cladding interaction (PCI) during reactor operation.

Rod Internal Pressure

Rod internal pressure data at the start of dry storage, compiled from various sources, are shown in Figure 2-1. Although the data are not extensive, they are, nevertheless, considered representative.

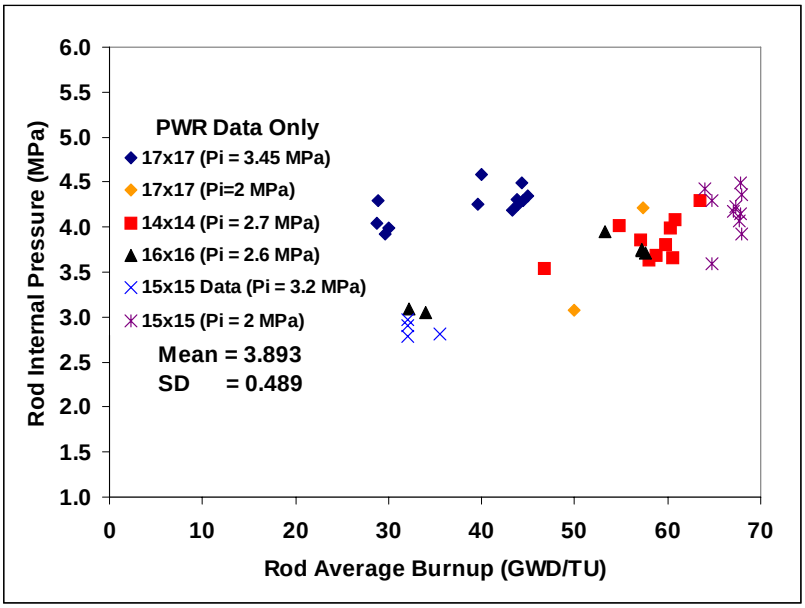

Figure 2-1
End-of-Life (EOL) PWR Rod Internal Pressure at 25°C

For standard PWR rods, the end-of-life (EOL) internal pressure data shown in Figure 2-1 at 25ºC have a mean of 3.89 MPa and a standard deviation of 0.49 MPa. Higher EOL pressures, by a factor of 2, can be found in fuel rods containing boron-coated pellets (BCP). Rod internal pressure is the primary source of loading for the damage mechanisms that may be operative during dry storage.

Oxide Thickness and Hydrogen Content

Cladding hydrogen content and effective wall thickness are correlated to the cladding outer-surface zirconium oxide. The maximum outer-surface oxide layer thickness data, as a function of fuel rod average burnup, are shown in Figure 2-2 for UO_2 fuel rods with low-tin Zircaloy-4 cladding material irradiated to burnup levels greater than 60 GWd/MTU. Figure 2-2 contains more than 4,400 measurements from commercial fuel rods irradiated in reactors worldwide [14].

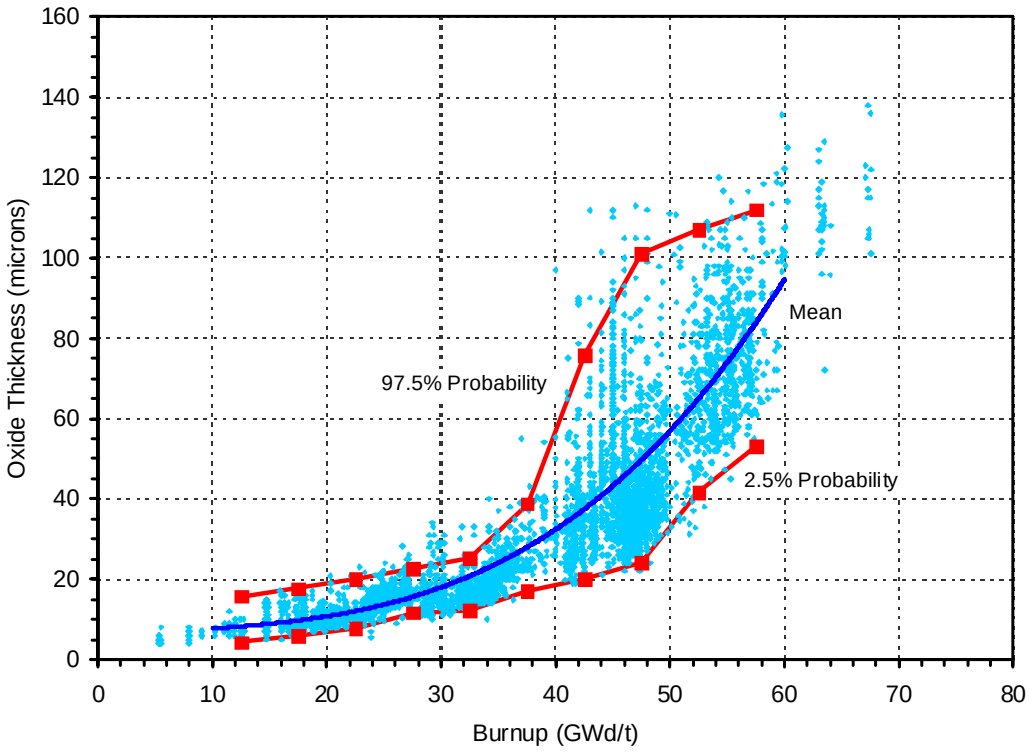

Figure 2-2
Cladding Outer Surface Oxide Layer Thickness versus Rod Average Burnup

Using the information in Figure 2-2, the maximum wall thickness average (MWTA) hydrogen content is calculated using a hydrogen evolution model, which uses as input: the oxide layer thickness, the hydrogen pick-up fraction, the cladding wall thickness and the Pilling-Bedworth ratio. The results are shown in Figure 2-3 where the maximum wall-average hydrogen content in low-Sn Zircaloy-4 cladding is plotted as a function of burnup. Also shown for comparison are measurements from irradiated commercial PWR fuel rods [14]. For discharge burnup in the range of 60-65 GWd/MTU, the average hydrogen concentration is 600 ppm and the maximum oxide thickness is 100 μm, which corresponds to a metal loss of 70 μm (assuming 100% theoretical density for zirconium oxide, which is conservative).

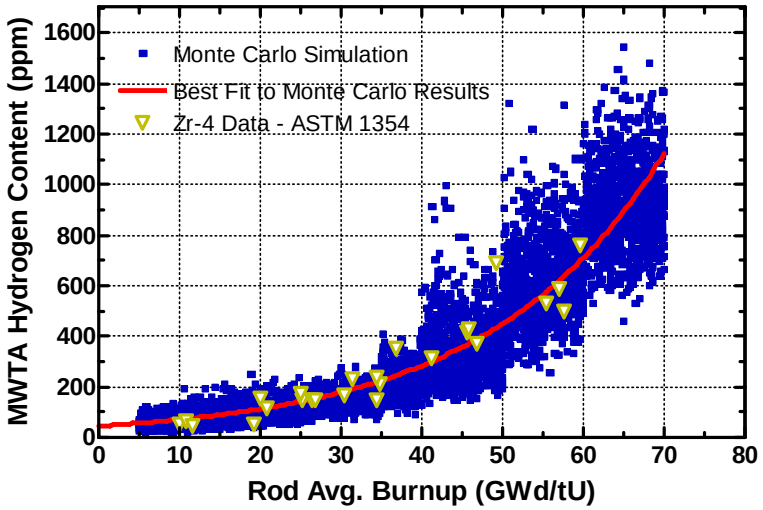

Figure 2-3
Maximum Wall Thickness Average (MWTA) Hydrogen Content in Low-tin Zircaloy-4 Cladding

Cladding Hydride Structure

The cladding hydrogen content described above exists mostly in the form of circumferential hydrides distributed in the wall in the manner shown in Figure 2-4. Although the mathematical idealization depicted in this figure show near zero hydrogen concentration at the ID, the actual hydride concentration there is of the order of 50-100 ppm. As will be shown later in this paper, the average hydrogen concentration is the quantity of interest that enters cladding integrity modeling and analysis.

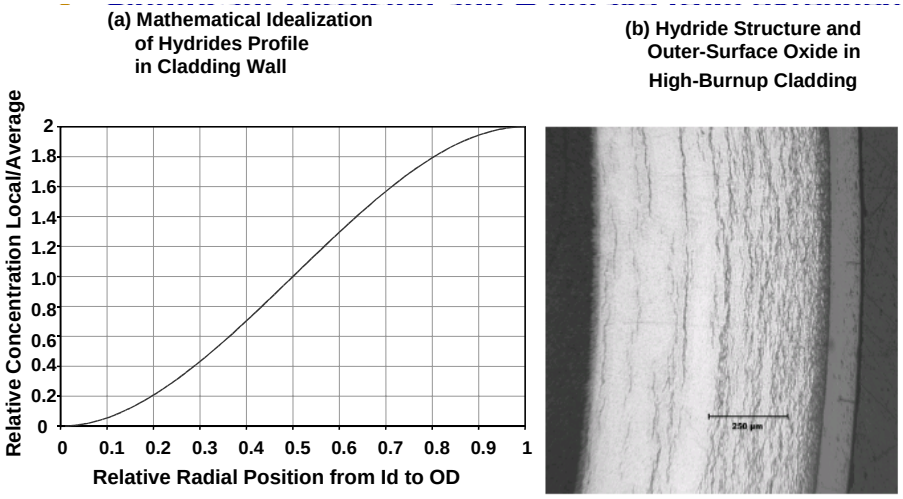

Figure 2-4
Hydrides Distribution (b) and Mathematical Idealization (a) in High-Burnup Cladding With an Average Hydrogen Concentration of ~600 ppm

Pre-Existing Part-Wall Cracks

In this work, spent fuel placed in dry storage casks is considered not to contain failed, i.e., leaky, rods. However, part-wall cracks in intact rods may exist, as they can be caused by pellet-cladding interaction (PCI) during power ramps. The importance of such cracks lies in the fact that they can be precursors for three other damage mechanisms, namely, creep rupture, intergranular stress corrosion cracking (IGSCC), and delayed hydride cracking (DHC). These mechanisms have been invoked as potentially damaging for spent fuel in dry storage on the basis that long-term exposure to the thermal and fission-product environment, to which cladding is exposed, produces ideal conditions for such damage mechanisms to be operable. A bounding value for the in-reactor depth of PCI cracks can be estimated using fracture mechanics, as described in detail in EPRI-1001207 [2]. A summary is presented below.

PCI cracks are initiated by stress corrosion cracking (SCC) in a two-stage process: (1) a pellet-cladding mechanical interaction (PCMI) stress above a threshold value activates a crack nucleation stage during which a crack tip is formed, and (2) a crack-extension stage when the crack-tip stress intensity reaches the stress corrosion cracking fracture toughness K_{ISCC}. For irradiated Zircaloy, data surveyed in EPRI-1001207 [2] shows 200 MPa and 4.7 MPa$\sqrt{m}$ for Stage-I SCC threshold stress and K_{ISCC}, respectively. After the SCC crack has extended to a given length, the fracture process is completed by mechanical fracture, which is governed by the K_{IC} property. A compilation of fracture toughness values can be found in EPRI-TR-1001281, 2001 [3], which gives a fracture toughness K_{IC} of 20 MPa$\sqrt{m}$ for T>280°C, 500<H≤750 ppm, which are typical in-reactor conditions at high burnup. This K_{IC} value is valid for mechanical fracture in reactor, un-assisted by SCC. The stress intensity factor is calculated from $K_I = 1.12\sigma(\pi a)^{1/2}$, where σ is the stress (200 MPa threshold) and a is the crack size. Equating the stress intensity factor to the fracture toughness, the maximum crack size that remains sub-critical during reactor operation can thus be calculated. For failure by SCC, using K_{ISCC} of 4.7 MPa$\sqrt{m}$, the maximum sub-critical crack size is calculated to be 140 µm. Repeating the calculations for failure by

mechanical rupture, conservatively assuming a stress value equal to high fluence cladding yield strength of 700 MPa at 300°C, and using a K_{IC} value of 20 MPa√m, the maximum sub-critical crack length is 200 μm. However, by the above calculations, such a crack size could not exist under SCC conditions, which means that the maximum initial flaw would not exceed 140 μm, or 28% of the remaining cladding thickness in a 17x17 fuel configuration with an estimated 100-μm oxide thickness. The initial crack size calculated above is used to evaluate the potential for crack extension during dry storage, under creep or by SCC and DHC mechanisms, as is discussed below.

Threats to Cladding Integrity During Dry Storage

Several mechanisms were postulated for spent fuel in dry storage, which are passive damage-producing processes that may not be subject to operational control. These are: (1) creep, potentially leading to creep rupture; (2) crack extension of pre-existing cracks by mechanical fracture under the internal gas pressure; (3) stress corrosion cracking (SCC); (4) delayed hydride cracking (DHC); and (5) hydride re-orientation. This latter mechanism has greater relevance to spent fuel transportation, as will be discussed in a later section. The conditions that govern these damage mechanisms are strongly dependent on the initial thermo-mechanical and physical states of the cladding when first placed in dry storage. These include temperature; stress; hydrogen concentration, and hydride morphology. Each of these conditions plays a role, to varying degrees, in determining the deformation rate and ultimately cladding failure potential. The benign effects of these damage mechanisms for spent fuel in dry storage are discussed in greater detail in EPRI reports: 1001207, *"Creep as the Limiting Mechanism for Spent Fuel Dry Storage"*, 2000 [2], and 1003135, 2001, *"Creep Modeling and Analysis Methodology for Spent Fuel in Dry Storage"* [4]. A summary of the results is presented herein, but first the cladding temperature history in dry storage is described, being the common activation function for the above-cited damage mechanisms.

Temperature History

The cladding temperature history at the hottest axial position of the fuel rod is shown in Figure 5-2 for a 40-year dry storage period. In the thermal calculations performed in 1003135 [4], the boundary and initial conditions were adjusted to match the initial peak cladding temperature of 400°C prescribed by ISG-11 Rev. 2. The equation in the figure is a mathematical fit of the calculated temperatures in Kelvin.

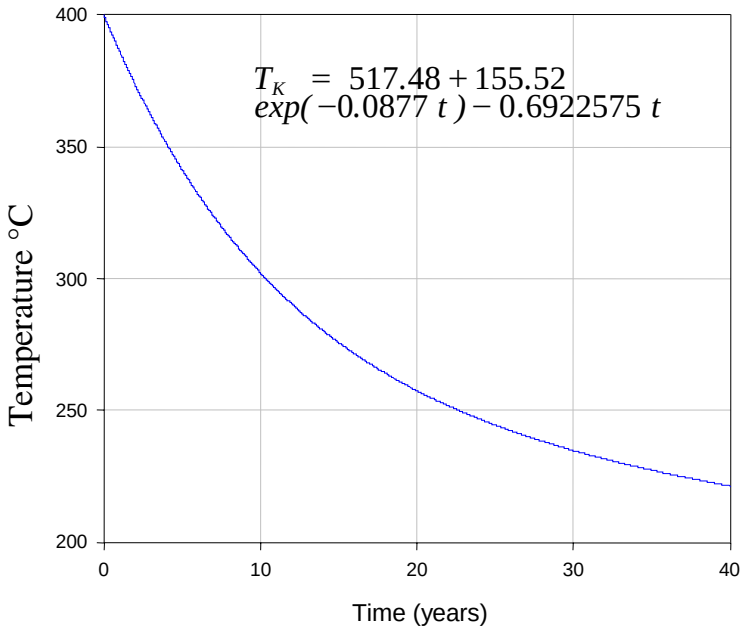

Figure 2-5
Cladding Temperature History for High-Burnup Spent Fuel in Dry Storage Casks

The temperature-time history shown above is such that it can subject the cask's contents to passive damage-producing processes that may not be subject to operational control. As seen in the figure, peak cladding temperature during dry storage can, in principle, remain higher than 300°C for a period as long as ten years. The effects of this temperature history on SCC, DHC, and creep are summarized below.

The SCC and DHC Mechanisms

The SCC and DHC are passive processes that require special environments to become operative. However, as described in 1001207, 2000 [2] and summarized below, the spent fuel environment in dry storage is not conducive to the initiation of either mechanism.

Let us consider, first, the chemical condition for SCC. The two chemical species that have been invoked for activating the SCC mechanism during reactor operation are iodine and cadmium-in-cesium. Fission product iodine in spent fuel rods is in the form of cesium iodide, and for iodine to be operative there must be a release of elemental iodine from cesium iodide by gamma or other forms of high-energy radiation (Cubiccioti and Davies [28]), a condition that is not duplicated in spent fuel storage. On the other hand, cadmium-bearing cesium is in a liquid state at room temperature and has a high boiling point of 671°C, which indicates that during in-reactor irradiation the majority of the cesium, being in gaseous state, would have been released to the plenum, where it would condense because of the lower temperature. The entire inventory will have condensed to a liquid form upon reactor shutdown and removal of the fuel to the spent fuel pool, and will remain in liquid form during dry storage, i.e., inert with respect to SCC activation.

With respect to stress, a survey of the SCC data shows that for relevant temperatures (above 300°C), the threshold stress for inducing failure by SCC in Zircaloy-2 is approximately 360 MPa and 180 MPa for unirradiated and irradiated materials, respectively, Roberts et al. [29]. Threshold values for stress-relieved Zircaloy-4 samples are 300 MPa and 200 MPa for unirradiated and irradiated materials, respectively, Brunisholz and Lemaignan [30]. These threshold stress values are above the pressure-induced hoop stress during dry storage, as can be verified by applying Figure 2-1 to the maximum dry storage temperature of 400°C. Based on the above, neither the chemistry nor the stress conditions of spent fuel rods are sufficient to support the SCC damage mechanism in dry storage.

The DHC process evolves in two stages: crack initiation governed by a K_{IH} value of 5.0-6.0 MPa$\sqrt{m}$, transitioning to stable crack growth at nearly constant velocity driven by stress intensity at a K_I value around 9.0-10.0 MPa$\sqrt{m}$. The time to failure is governed by the highly temperature dependent rate of hydrogen diffusion from the bulk of the material to the crack tip. An important condition that promotes the diffusion of hydrogen to, and the precipitation of hydrides in, the crack tip zone is the tri-axial tensile field surrounding the crack tip, a condition that exists in plane strain test specimens but would not be present, at least to the same degree, in the plane-stress geometry of the cladding. With the continuous hydrogen diffusion to the crack tip, the local hydrogen concentration rises until it exceeds the solubility limit locally and hydrides begin to precipitate ahead of the crack tip. When the hydride reaches a critical size, it fractures, allowing the crack to advance until it is arrested in the tougher Zircaloy material past the hydride, where a new highly stressed crack tip is formed. The process is repeated, and the crack continues to propagate in this manner until failure by plastic instability. Providing that stress conditions are satisfied, the temperature history in spent fuel would not preclude DHC; the slowly decreasing temperature with time during dry storage is almost the ideal recipe for maintaining crack growth in the manner described above. Therefore, the key to precluding failure by DHC is to prevent the initiation of Stage-I, which is primarily controlled by the stress intensity at a pre-existing crack tip. Using the maximum initial crack size of 28% of the cladding thickness determined earlier as a possible initial condition for spent fuel cladding, and using a conservative hoop stress value of 150 MPa, we calculate a stress intensity factor K_I of 3.5 MPa$\sqrt{m}$, which is below the K_{IH} value of 5.0-6.0 MPa$\sqrt{m}$ cited above for initiating DHC. These bounding calculations indicate that DHC would not be an operative mechanism for spent fuel in dry storage.

Creep Rupture

The creep rupture phenomenon as it relates to spent fuel in dry storage is examined in greater detail in 1003135, 2001 [4], and its derivative paper in the IAEA International Conference on Storage of Spent Fuel [31]. It is shown that creep-induced deformations under dry storage conditions are self-limiting, counter to the creep rupture process; the reason being that under conditions of dry storage the creep rate is continuously decreasing due to the decaying temperature and the relaxation of internal pressure due to the expanding void volume of the fuel rod. This, however, is counteracted by partial thermal recovery of irradiation damage [32], which enhances the creep rate and slows down the effect of temperature decay and volume expansion on the creep deformation, but would not be sufficient to reverse it. Many case studies can be found in 1003135, but the two cases shown here are selected to illustrate two important points: (a) creep rupture has been modeled and can be correctly predicted, and (b) creep

deformations under dry storage conditions are self limiting and cannot transition to the tertiary creep regime, which is the onset of creep rupture. Figure 2-6 depicts model prediction of creep-rupture tests conducted under stress and temperature combinations shown in the figures. The case with an initial stress of 386 MPa is a pressurized tube specimen; the other is a tube specimen loaded axially. As shown in the Figure, the highest data points are the final measurements just before failure, and were taken at an intact section away from the rupture opening, which would represent the global strain response, rather than the local strain at the failure location.

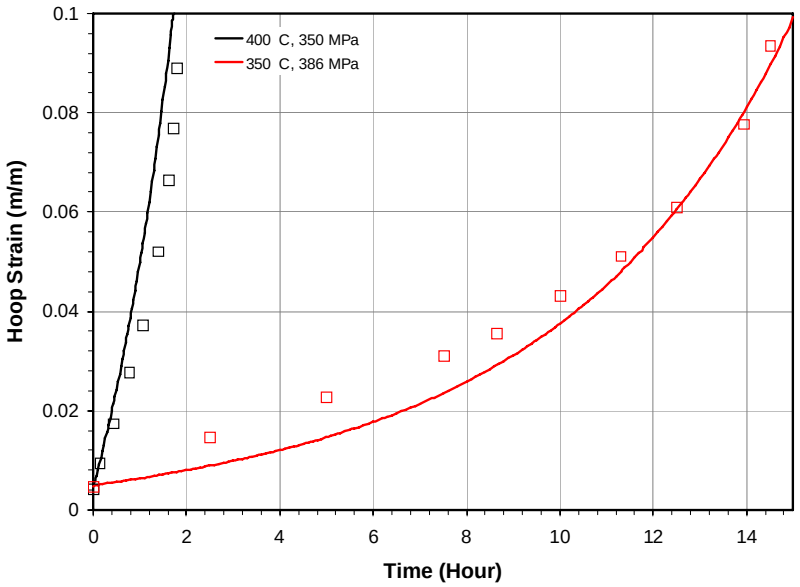

Figure 2-6
Analysis of Creep Rupture Tests of Un-irradiated Cladding

In contrast with the un-bounded phenomenon of creep rupture illustrated in the preceding example, the creep response of a spent fuel rod in dry storage is self-limiting. This is illustrated in an analysis of a high-burnup spent fuel rod considering a worst-case condition of the cladding, which is described as having an oxide thickness of 120 μm and a hydride lens of depth equal to 50% of the as-received thickness in a 17x17 assembly and extending 60 degrees circumferentially. To maximize the damage effects of the oxide and the hydride lens, they are treated as metal loss and the lens is assumed to extend several diameters axially, which is highly conservative, but it permits the creep analysis to be carried out in two-dimensions, i.e., r-θ representation of the cross section. The pressure is chosen to approximate maximum beginning-of-storage pressure, and a 40°C temperature rise is superimposed on the 400°C initial storage temperature to simulate a 24-hour drying cycle of 8-hour ramp up, 8-hour dwell time, and 8-hour ramp down. Figure 2-7 depicts the strain history of the cladding, which shows the asymptotic behavior of creep deformations.

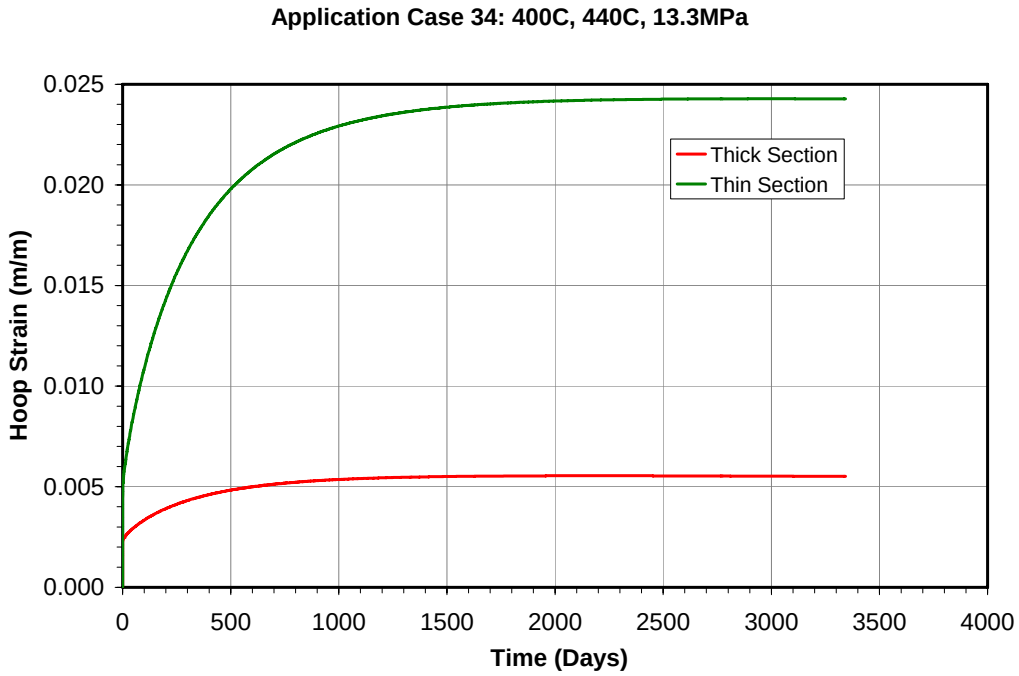

Figure 2-7
Creep Response of a Fuel Rod With Hydride Lens

From Storage to Transportation

The temperature history depicted in Figure 2-5 represents the most important parameter for evaluating spent fuel behavior during dry storage and post-storage transportation accidents. The beginning-of-storage conditions of spent fuel rods presented earlier, consisting of oxide thickness, hydrogen concentration and fission gas content, remain virtually unchanged during dry storage. However, the temperature and temperature-induced effects, such as the precipitation of radial hydrides, the fuel-cladding gap, and the gas pressure change slowly with time. These conditions are interdependent: the cladding hoop stress and decaying temperature set the conditions for the precipitation of radial hydrides, but at a reduced rate because of decreasing stress due to the effects of thermal creep on expanding fuel-cladding gap that increases the void volume and reduces the pressure. As will be discussed in the next chapter, the radial hydrides concentration and the change in the fuel-cladding gap constitute the most important effects of dry storage on transportation. Significant effort was dedicated in the EPRI research program to these parameters and related phenomena, as described in the following two reports and conference paper: "*Creep Modeling and Analysis Methodology for Spent Fuel in Dry Storage*", 1003135, November 20001 [4], "*Development of a Metal/Hydride Mixture Model for Zircaloy Cladding With Mixed Hydride Structure*", 1009694, June 2004 [7], and "*Hydride Precipitation in Spent Fuel Cladding During Storage*", ICEM05 Paper #1038, September 2005 [33]. The following is a synthesis summary of that material.

Fuel-Cladding Gap at the End of Dry Storage

The size of the fuel-cladding gap due to creep is computed after 40 years of dry storage using the methodology of 1003135 [4], the temperature history shown in Figure 2-5 and the EOL rod internal pressure data depicted in Figure 2-1. Table 2-1 lists gap size as function of beginning-of-storage (BOS) temperature and hoop stress. The creep calculations take into consideration the time variation of fuel rod temperature and pressure during dry storage. The boxed value in the table represents the gap width to be used in the accident analysis described in the next chapter.

Table 2-1
Gap Size (μm) as a Function of Initial Temperature and Hoop Stress

Hoop Stress (MPa)	BOS Temperature					
	320	340	360	380	400	410
0	0.00	0.00	0.00	0.00	0.00	0.0
50	1.87	2.02	3.44	3.44	6.45	9.7
100	3.87	4.44	10.3	10.3	22.3	34.1
150	6.08	7.50	23.3	23.3	51.5	75.4
200	8.59	11.9	46.5	46.5	94.7	129.9
250	11.9	19.4	80.0	80.0	145.8	190.2

Radial Hydride Concentration at the End of Dry Storage

The hydride precipitation model described in References [5] and [33] is used to calculate the increase in radial hydride concentration at the end of the 40-year dry storage. These calculations are illustrated in Figures 2-8 and 2-9, and Table 2-2. Figure 2-8 shows the dependence of the hoop stress on time, and Figure 2-9 shows the evolution of radial hydrides under the stress histories of Figure 2-8 and the temperature history of Figure 2-5. Table 2-2 lists the radial hydride concentrations for assumed beginning-of-storage stresses and temperatures.

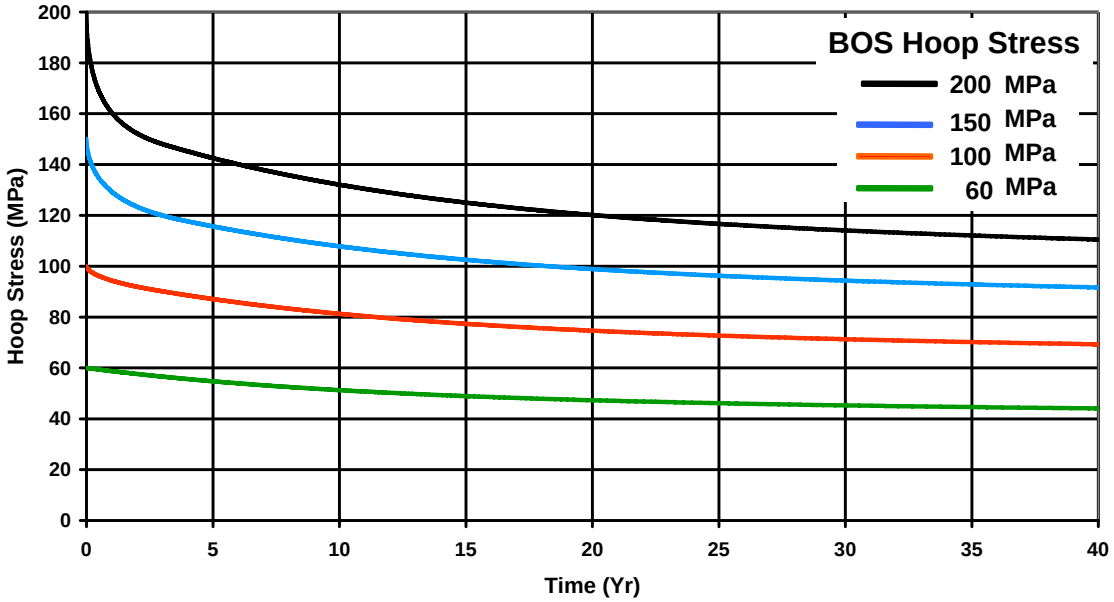

Figure 2-8
40-Year Cladding Hoop Stress Histories for an Initial (BOS) Temperature of 400°C

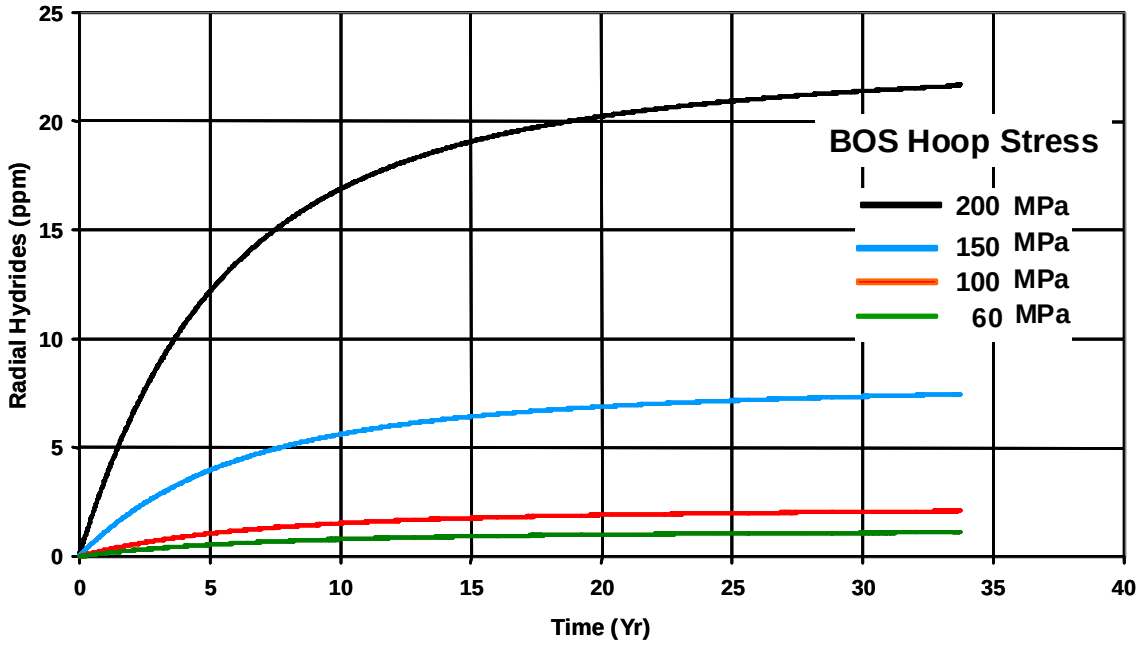

Figure 2-9
40-Year Radial Hydride Evolution for a BOS Temperature of 400°C at Various BOS Hoop Stresses

Table 2-2
Radial Hydride Concentration (ppm) as a Function of BOS Temperature and Hoop Stress

Hoop Stress (MPa)	Temperature (°C)									
	410	400	390	380	370	360	350	340	330	320
200	29.1	21.6	16.0	11.7	8.6	6.3	4.6	3.4	2.5	1.8
190	23.6	17.4	12.9	9.5	7.0	5.1	3.8	2.8	2.0	1.5
180	19.0	14.1	10.4	7.7	5.7	4.2	3.1	2.3	1.7	1.2
170	15.3	11.4	8.4	6.3	4.6	3.4	2.5	1.9	1.4	1.0
160	12.4	9.2	6.9	5.1	3.8	2.8	2.1	1.6	1.2	0.9
150	10.0	7.4	5.6	4.1	3.1	2.3	1.7	1.3	1.0	0.7
140	8.0	6.0	4.5	3.4	2.5	1.9	1.4	1.1	0.8	0.6
130	6.5	4.9	3.7	2.7	2.1	1.5	1.2	0.9	0.7	0.5
120	5.2	3.9	2.9	2.2	1.7	1.3	1.0	0.7	0.5	0.4
110	4.1	3.1	2.4	1.8	1.3	1.0	0.8	0.6	0.4	0.3
100	2.7	2.1	1.6	1.2	0.9	0.7	0.5	0.4	0.3	0.2
90	2.1	1.6	1.2	0.9	0.7	0.5	0.4	0.3	0.2	0.2
80	1.4	1.1	0.8	0.7	0.5	0.4	0.3	0.2	0.2	0.1
70	0.9	0.7	0.6	0.4	0.3	0.3	0.2	0.2	0.1	0.1
60	0.6	0.5	0.4	0.3	0.2	0.2	0.1	0.1	0.1	0.1

For conditions corresponding to a hoop stress of 150 MPa and a temperature of 400°C at beginning of storage, an increase in radial hydride concentration is calculated to be in the range of 7-8 ppm, as shown in the box in Table 2-2 and the 150-MPa curve in Figure 2-9, after 40 years of dry storage. For an initial hoop stress of 200 MPa and 400°C, the increase in radial hydride concentration is calculated to be ~22 ppm. These values are small fractions of the hydrogen in solution in the Zircaloy matrix at 400°C. Given appropriate experimental conditions, such as those achieved during laboratory testing where the cladding can be maintained under constant hoop stress during cooling to room temperature, re-precipitation of a large fraction of the dissolved hydrogen as radial hydride can be readily obtained. This is illustrated in Figure 2-10, which depicts the increase in radial hydride concentration under three different testing conditions as function of initially applied hoop stress at 400°C. The top curve in the figure is for constant hoop stress during cooling to room temperature; the middle curve is for the case where the stress decays with absolute temperature only; and the lower curve simulates a fuel rod in dry storage in which the stress is decaying in response to the decreasing rod internal pressure due to expanding void volume resulting from cladding creep. As can be seen in Figure 2-10, the hydride precipitation model correctly predicts the laboratory case, which shows that about 95% of the hydrogen in solid solution precipitates as radial hydrides for an initial hoop stress of 200 MPa. For reference, the hydrogen solubility limit in Zry-4 at 400°C is ~210 ppm.

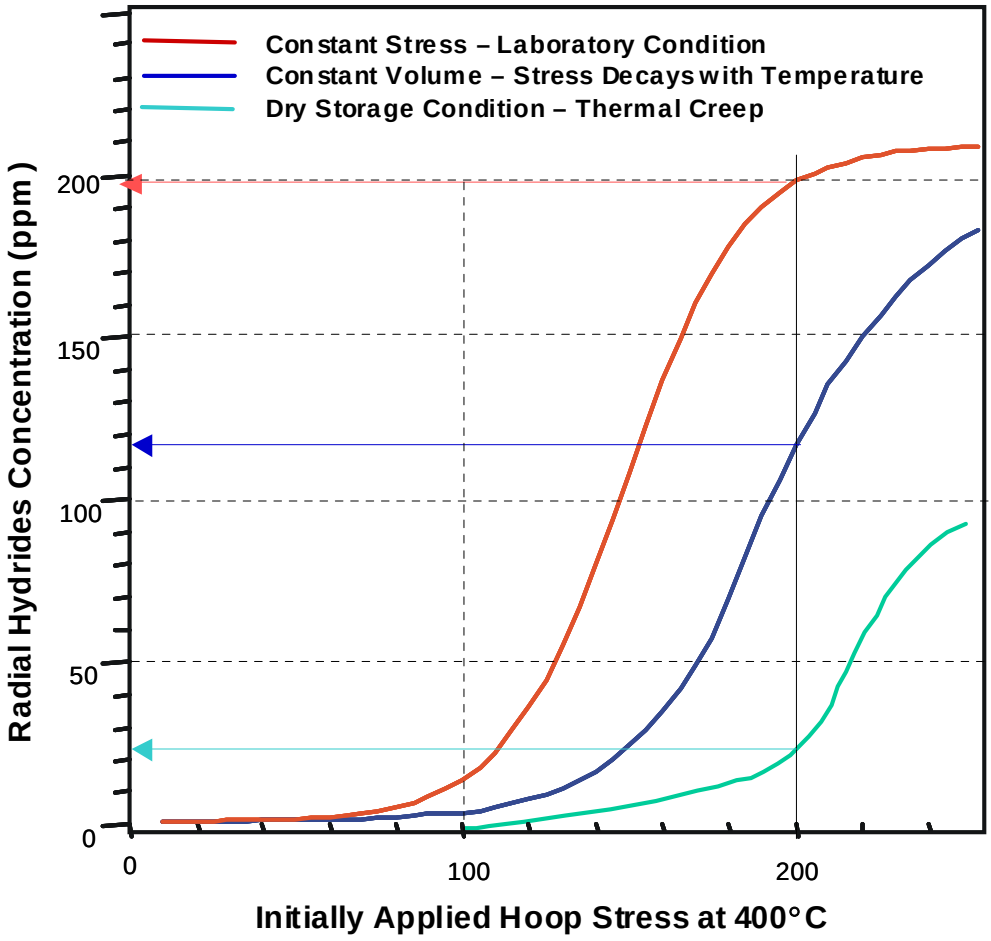

Figure 2-10
Radial Hydrides Concentrations for Three Stress Histories Under Cooling From 400°C

3
CLADDING FAILURE CRITERIA

As previously noted, the spent fuel conditions at the end of dry storage described in the preceding chapter define the cladding material conditions to be considered in the structural analysis of spent fuel under hypothetical accident and normal conditions of transport. This requires the availability of failure criteria applicable to the cladding mixed hydride structure that developed during dry storage. Reliable failure criteria that capture relevant mechanical behavior regimes of high-burnup cladding with both circumferential and radial hydrides are presently lacking, with limited near-term prospects for developing such criteria experimentally. Consequently, an alternative is to rely on the analytical development of the criteria described in 1009694, June 2004 [7] and 1009693, December 2004 [8], which is summarized below. The failure criteria development described in the above-cited reports is a two-step process: First, a failure model is developed which directly predicts cladding damage initiation and progression during the loading event; second, utilizing this model, a set of failure criteria are developed that can be applied in structural analysis in the traditional way. This made it possible, using the latter criteria, to calculate failure frequencies of spent fuel subjected to the hypothetical cask drop accident and normal conditions of transport, as will be described in following chapters.

Cladding Failure Model

Reports 1009694 [7] and 1009693 [8] describe the development of a material constitutive model for irradiated Zircaloy cladding containing circumferential and radial hydrides of general concentration and radial distribution. The cladding is modeled as a three-phase mixture composite consisting of a metal matrix in which circumferential and/or radial hydrides are embedded as lamellar structures. The hydride phases interact with the Zircaloy metal phase through rigorously enforced interface constraints that satisfy the necessary stress-equilibrium equations and strain-compatibility relations between the phases, consistently with the orientation of the hydrides platelets within each lamellar plane. This formulation renders the overall composite morphologically anisotropic, which is a departure from the simple classical mixture theory, and is specifically introduced to capture the direction-dependent effect of the hydrides on cladding integrity. This gives the model the necessary theoretical construct needed to enable the model to predict high burnup spent-fuel cladding behavior. An important feature of the model is a damage formulation that incorporates cladding failure as a constitutive property, which allows direct prediction of cladding failure as part of structural response analysis. The development of the model was accomplished in two stages as described below.

Two-Phase Mixture Model

The two-phase model considers a Zircaloy matrix in which either circumferential or radial hydride platelets are embedded, *but not both*, 1009694 [7]. The development of the two-phase model was highly significant in the sense that it established the validity of using the strain energy density (SED) as a basis for global failure criterion. This was done by first calibrating the model's internal parameters using the critical strain energy density (CSED) determined from test data; then using the calibrated model to predict the stress-strain curves measured in the tests. CSED data for eight well-characterized specimens from the NFIR program [34] were used to quantify a model parameter, called the hydride efficiency factor, as function of hydride concentration. The calibration calculations were performed iteratively until convergence on the best estimate value of the hydride efficiency factor among all specimens was achieved. Once calibrated, the model was applied to two axial tension tests, performed at room temperature (25°C), of irradiated guide tubes of about equal fast fluence levels in the range $7\text{-}8 \times 10^{25}$ n/m^2 (E>1 MeV). The first specimen contained 206 ppm of hydrogen in the form of uniformly distributed circumferential hydrides. The average hydrogen concentration in the second specimen was 411 ppm, also in the form of uniformly distributed circumferential hydrides. Figures 3-1 and 3-2 depict the measured true stress-strain curves compared to the model's simulation. The measured curves in the figures exhibit a turn down behavior in the true stress following a peak value, which is akin to engineering stress vs. engineering strain curves. This type of behavior, which is not compatible with the true-stress vs. true-strain behavior of a single-phase material, is attributed to the fracture of the hydrides. The Two-Phase Mixture Model simulates this behavior through a two-parameter damage formulation, where one parameter defines the strain at which a single hydride fractures and the other defines the strain range over which fracture is completed for all the hydrides in the plane normal to the stress, (see details in 1009694). The accuracy of the model predictions shown in Figures 3-1 and 3-2 validates the CSED concept as an appropriate global failure criterion to use for spent fuel cladding.

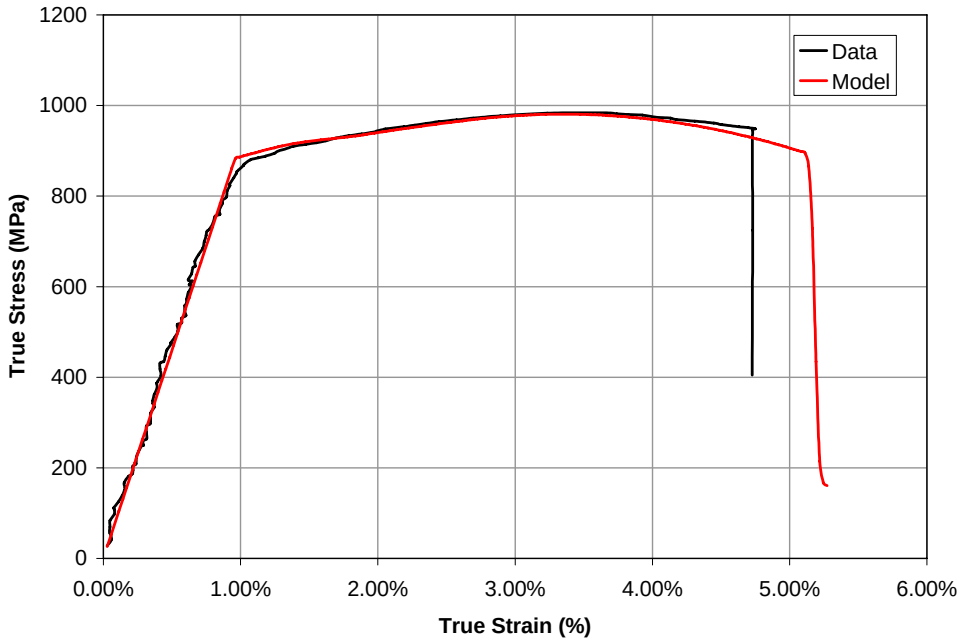

Figure 3-1
Stress-Strain Response of Irradiated Guide Tube Specimen, With 206 ppm Hydrogen, Tested at 25°C

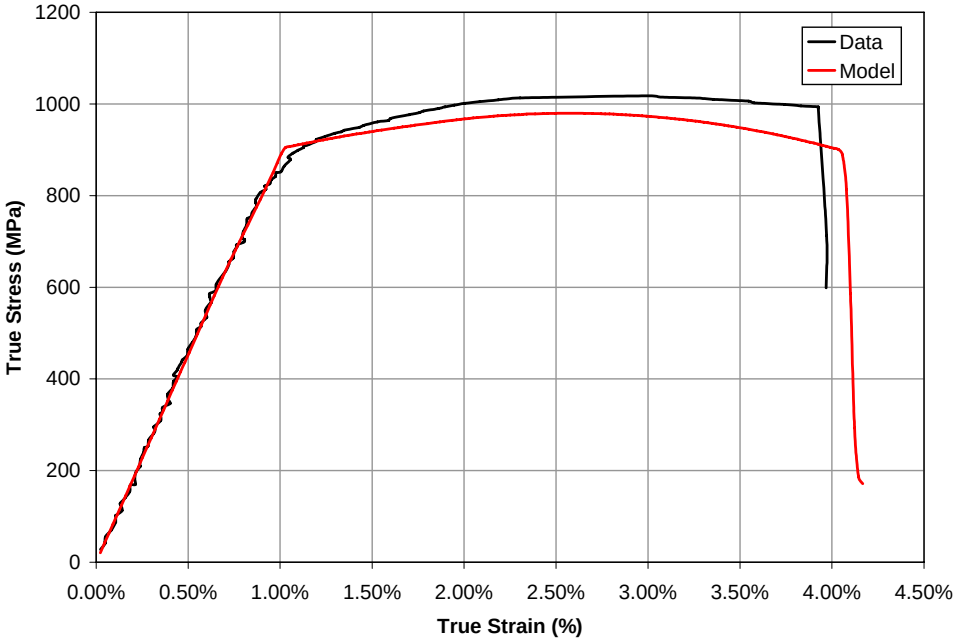

Figure 3-2
Stress-Strain Response of Irradiated Guide Tube Specimen, With 411 ppm Hydrogen, Tested at 25°C

Three-Phase Mixture Model

Based on the results of the two-phase model described above, the model formulation was extended to a three-phase composite, which enabled the treatment of the interaction between the radial and the circumferential hydrides, and provided a tool for the development of CSED as a failure criterion for high-burnup spent fuel rods subjected to dynamic loading after being exposed to the effects of decades of dry storage. The mathematical construct of the model is described in detail in 1009693 [8]; here we illustrate the prediction capabilities of the model. Three test specimens are selected from 1009693: two fuel-rod cladding (irradiated) specimens containing circumferential hydrides of about equivalent hydrogen concentrations tested at 25°C and 300°C, and one un-irradiated cladding specimen subjected to hydrogen charging followed by radial hydride treatment that produced a mixed hydride structure.

Figures 3-3 and 3-4 depict the results in terms of stress-strain curves computed at three radial positions in the cladding: outer surface, mid-wall, and inner surface. The measured stress-strain curves are shown in the figures. The analysis considers an idealized radial distribution of circumferential hydrides (see Figure 3-8 in a later discussion). As can be seen in the figures, the model predicts that cladding failure progresses from OD to ID, as would be expected, but the data are for the integral behavior of the specimen, and in most cases they lie closer to the ID curve. The figures are self-explanatory, showing reasonably good agreement.

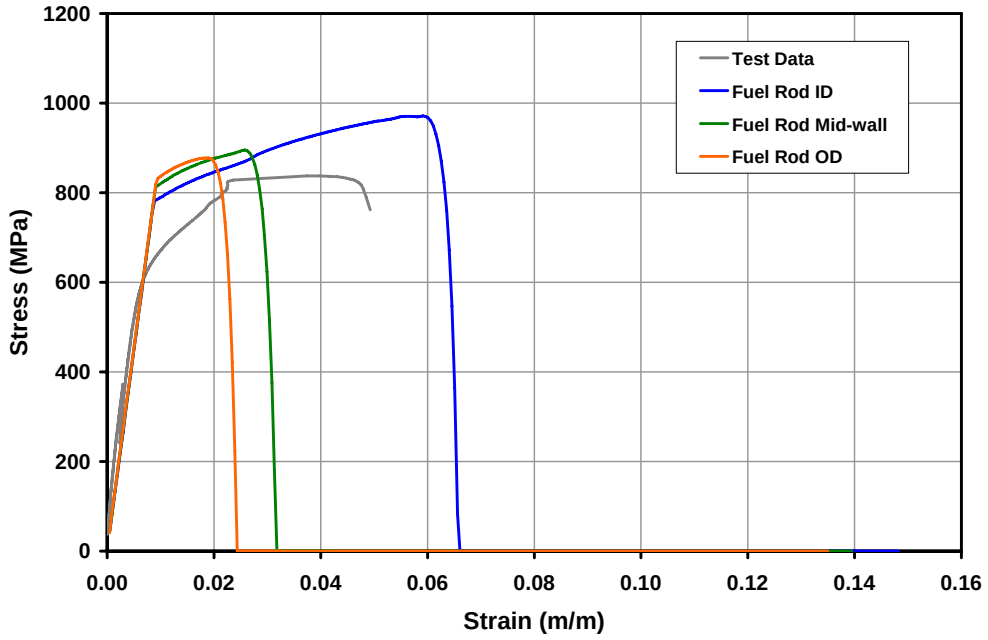

Figure 3-3
Stress-Strain Response of Irradiated Fuel Rod Cladding at 25°C – 356-ppm Average Hydrogen Concentration

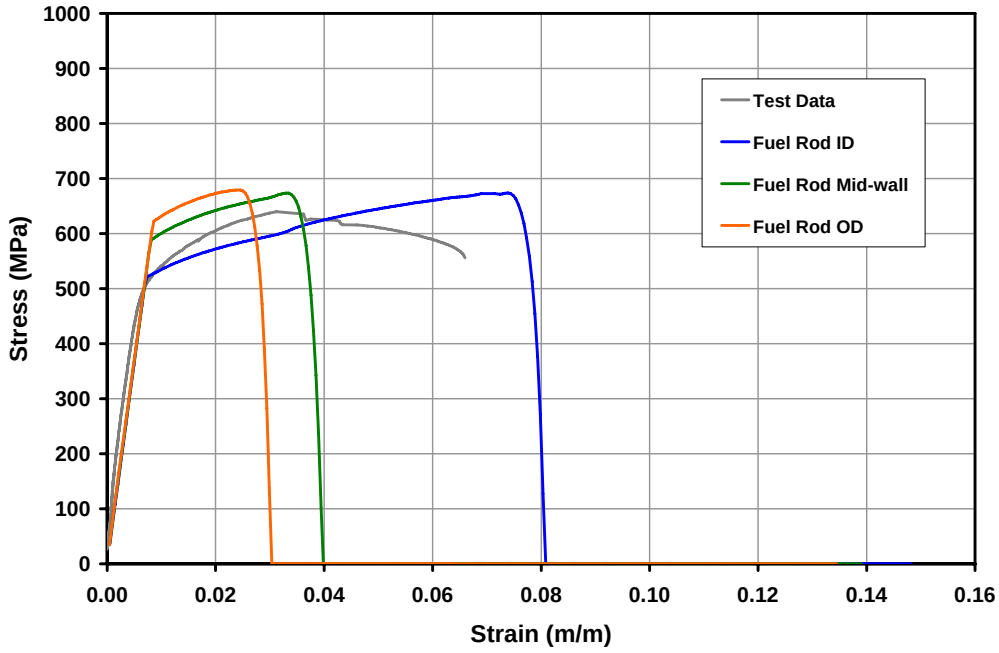

Figure 3-4
Stress-Strain Response of Irradiated Fuel Rod Cladding at 300°C – 400-ppm Average Hydrogen Concentration

The third example is for cladding with mixed hydride structure. Figure 3-5 shows a micrograph of as-hydrided specimen with ~220 ppm hydrogen (a), and after subjecting the specimen to radial hydrides (b), by cooling from 300°C under a hoop stress of 225 MPa. The laboratory testing was performed by INER, Kuo et al. [35], and the results were reported in Yagnik et al. [36]. By calculation, using the hydride precipitation model discussed in the preceding chapter, the radial hydride concentration is approximately 70 ppm. The stress-strain response is not available, but total elongation data for specimen (b) with mixed hydrides are ~17.5% in the axial direction and ~1.5% in the hoop direction, estimated, respectively, from Figures 8 and 9 of Ref. [36], the latter being the property most affected by radial hydrides.

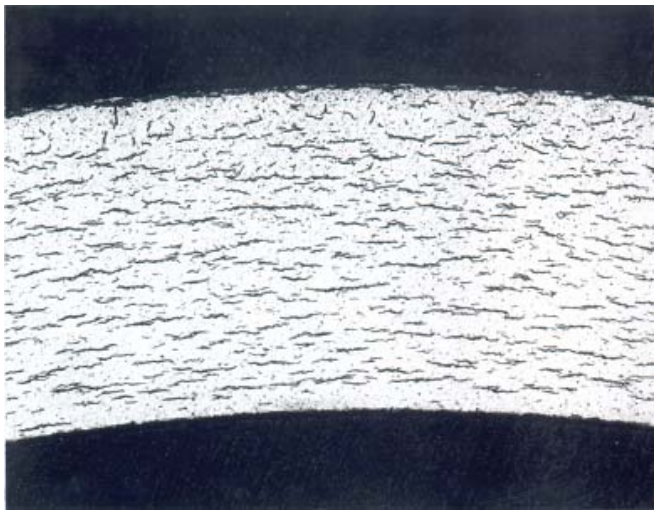

(a) As-Hydrided, ~200 ppm H

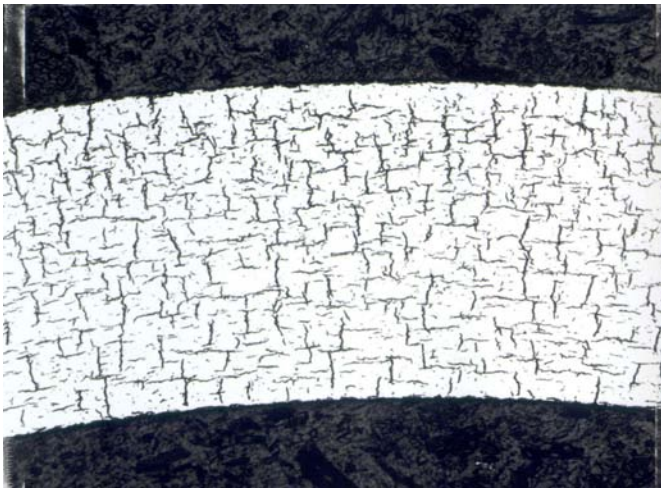

(b) 27% Radial Hydrides Counted at RT

Figure 3-5
Micrographs Showing Hydride Reorientation in Zry-4 Cladding Hydrided to ~220 ppm H
(a) As-Hydrided; (b) After Reorientation With a Hoop Stress of 225 MPa

Model predictions for this case are shown in Figures 3-6 and 3-7, depicting, respectively, the stress-strain curves for the specimen with circumferential hydrides, specimen Figure 3-5 (a), and its companion specimen with mixed radial and circumferential hydrides, Figure 3-5 (b). The figures also show the measured total elongation strain reported in Ref. [36]. As can be seen, the predicted failure strains are in reasonable agreement with the measured data.

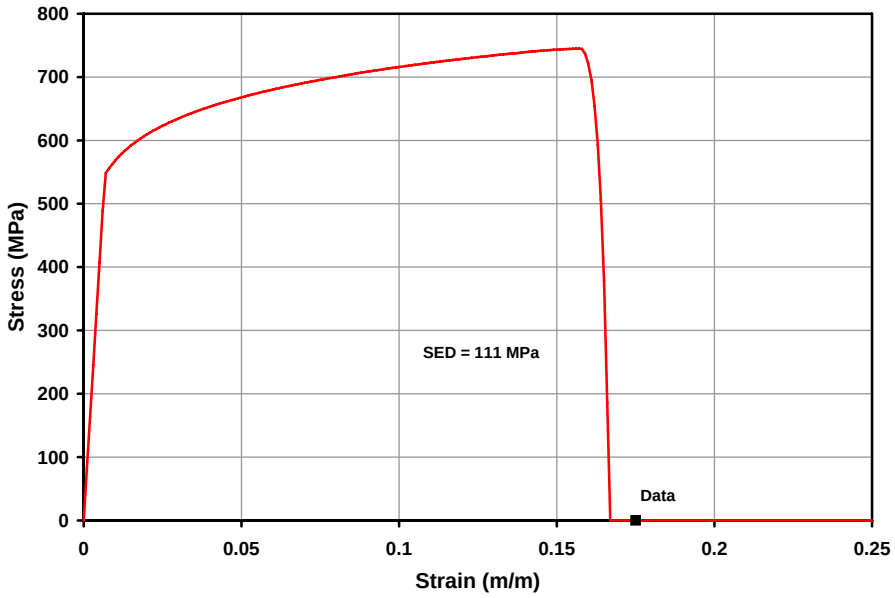

Figure 3-6
Axial Stress-strain Response, ~220-ppm Total and ~70-ppm Radial Hydrides, Tested at 25°C

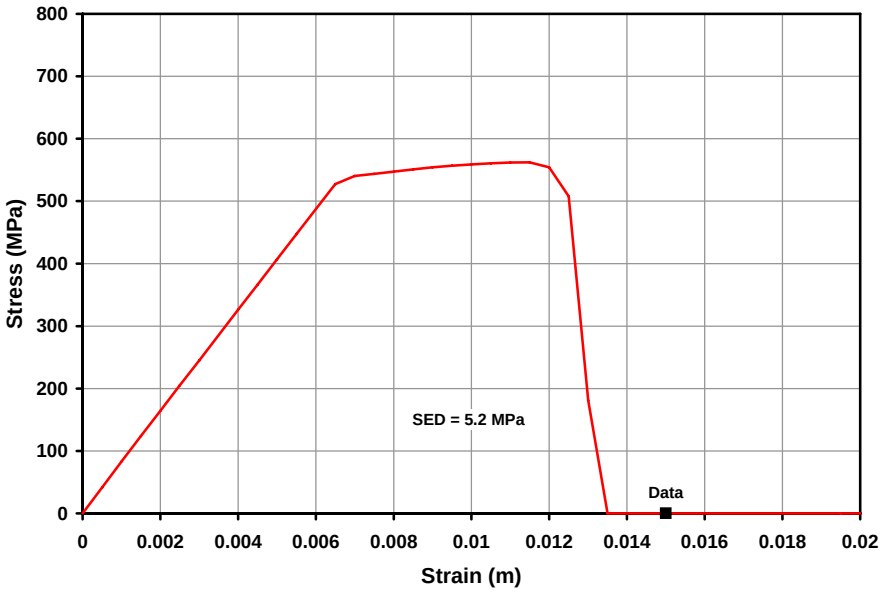

Figure 3-7
Azimuthal Stress-strain Response, ~220-ppm Total and ~70-ppm Radial Hydrides, Tested at 25°C

Development of Cladding Failure Criteria

The need for cladding failure criteria arises from the fact that the evaluation of fuel reconfiguration during cask drop events involves the failure analysis of all fuel rods in the cask, which makes it impossible to use the failure model as a constitutive property. Instead, the model is used to generate failure criteria of the type that can be applied in failure analysis following the accepted practice of comparing structural analysis results to the failure criteria. The metric used for judging cladding failure is the critical strain energy density (CSED), developed as function of circumferential and radial hydrides concentrations. Since the distribution of circumferential hydrides is strongly dependent on the radial position, unlike radial hydrides which tend to be uniformly distributed, the combined effect of radial and circumferential hydrides on CSED becomes position dependent. To help visualize the relative effect of both types of hydrides, an idealized description of the radial distribution of circumferential hydrides is presented in Figure 3-8. The integral under this curve times the average hydrogen concentration gives the total hydrogen content specified for the rod.

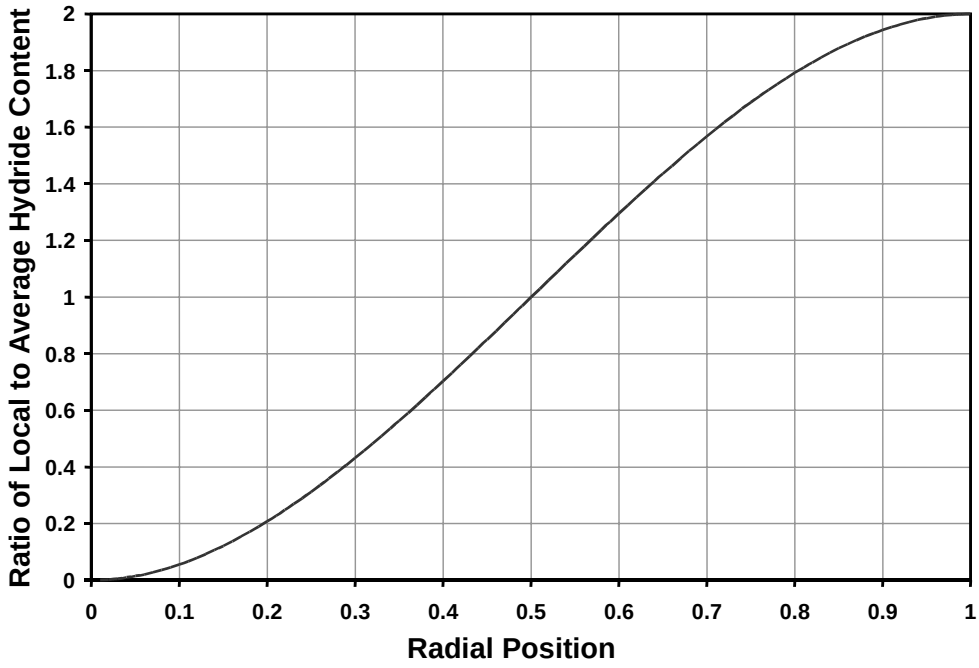

Figure 3-8
Idealization of Circumferential Hydride Distribution in Fuel Rod Cladding

The case of uniformly distributed hydrides is addressed first. The selected combinations of circumferential and radial hydrides cover the range of 0-1000 ppm for circumferential hydrides and 0-200 ppm for radial hydrides. Figure 3-9 shows the CSED as function of radial hydride concentration, with circumferential hydrides concentration as a parameter. It is observed that the model clearly identifies the coupling between the two orientations, with the effect of this coupling diminishing as the radial hydride concentration increases. For example, the dependence of CSED on circumferential hydride concentration continuously decreases with increasing radial hydrides until the CSED becomes independent of the circumferential hydride content at about 70 ppm hydrogen of radial hydrides. Table 3-1 is a numerical representation of Figure 3-9, which might be more convenient to use.

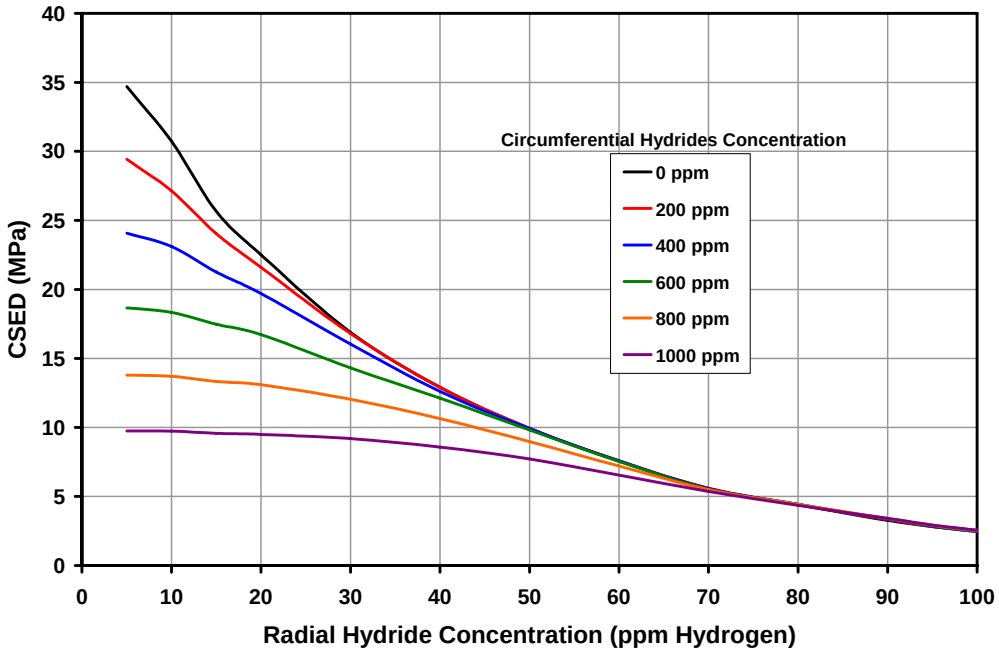

Figure 3-9
CSED vs. Radial Hydrides for Various Circumferential Hydride Concentrations at 25°C

Table 3-1
CSED (MPa) as a Function of Circumferential and Radial Hydride Concentration

Radial Hydrides (ppm)	Concentration of Circumferential Hydrides (ppm)										
	0	25	50	100	200	300	400	600	800	1000	2000
1	61.6	53.4	49.4	44.1	37.4	31.6	28.9	22.4	17.6	13.9	9.5
2	43.3	40.6	39.6	37.1	33.7	30.5	27.6	22.1	17.5	13.9	9.5
5	26.5	26.6	26.6	26.6	25.9	24.8	23.2	20.2	16.6	13.6	9.5
10	24.2	24.2	24.1	24.0	23.6	22.9	21.8	19.3	16.4	13.5	9.4
15	20.4	20.4	20.5	20.5	20.4	20.2	19.5	17.9	15.6	13.2	9.4
20	18.1	18.2	18.2	18.3	18.3	18.2	18.0	16.6	14.9	12.8	9.3
25	15.6	15.6	15.7	15.8	15.9	15.9	15.9	15.2	13.9	12.3	9.2
30	13.7	13.7	13.7	13.8	13.9	14.0	14.0	13.8	12.9	11.6	9.0
35	11.8	11.8	11.9	11.9	12.0	12.1	12.2	12.3	11.8	10.9	8.3
40	10.5	10.6	10.6	10.6	10.7	10.8	10.9	11.0	10.8	10.2	8.5
45	9.3	9.3	9.3	9.4	9.4	9.5	9.6	9.7	9.8	9.4	8.1
50	8.5	8.5	8.5	8.5	8.6	8.6	8.7	8.7	8.7	8.3	7.6
55	7.4	7.4	7.4	7.5	7.5	7.6	7.6	7.7	7.7	7.7	7.1
60	6.7	6.7	6.7	6.7	6.7	6.8	6.8	6.8	6.8	6.8	6.5
65	5.9	5.9	6.0	6.0	6.0	6.0	6.0	6.0	6.0	6.0	5.8
70	5.3	5.3	5.2	5.2	5.3	5.3	5.3	5.2	5.2	5.2	5.1
80	4.0	4.0	4.0	4.0	4.0	4.0	4.0	3.9	3.9	3.9	3.8
90	3.0	2.9	2.9	2.9	2.9	2.9	2.8	2.8	2.8	2.8	2.7
100	2.1	2.1	2.1	2.1	2.1	2.1	2.1	2.1	2.1	2.1	2.0
150	0.8	0.8	0.8	0.8	0.8	0.8	0.8	0.8	0.8	0.8	0.8

The CSED curves in Figure 3-9 were generated assuming both types of hydrides are uniformly distributed through the cladding thickness, which makes the criteria consistent with global failure analysis in which failure prediction implies through-wall failure. However, for evaluating partial through-wall failure, it is necessary to conduct local failure analysis, which requires developing CSED as function of local position in the cladding. Moreover, the CSED criteria in Figure 3-9 apply to loading regimes that lead to hoop stress as the dominant stress condition. Such a condition represents a failure mode that results in axial fracture under pinch type forces. For other failure modes, such as circumferential fracture under bending and/or axial forces, the dominant stress is axial, which does not engage radial hydrides. For such a failure regime, CSED is primarily a function of the circumferential hydride concentration, which varies as shown in Figure 3-8, and is highest at the cladding OD where the circumferential crack would initiate. Combining Figure 3-8 with uniformly distributed radial hydrides of various concentrations, CSED is obtained as function of radial hydrides for three positions in the cladding as shown in Figure 3-10. Similarly, Figures 3-11 through 3-13 depict the variation of CSED for circumferential fracture initiating at the cladding OD and extending through the wall to the ID.

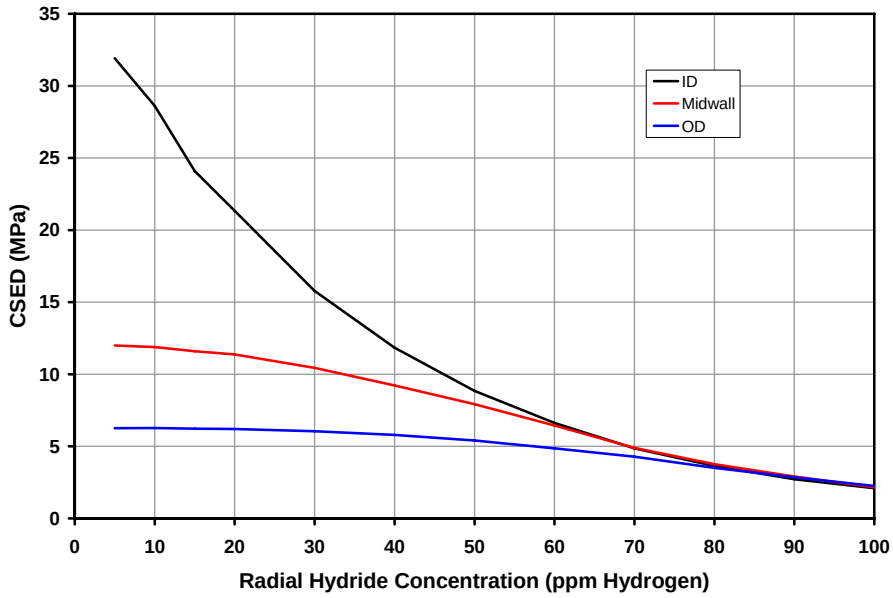

Figure 3-10
CSED vs. Radial Hydride Concentration at 25°C as Function of Radial Position for a Fuel Rod Cladding With 600-ppm Hydrogen Content, With Radially Varying Circumferential Hydrides as Depicted in Figure 3-8

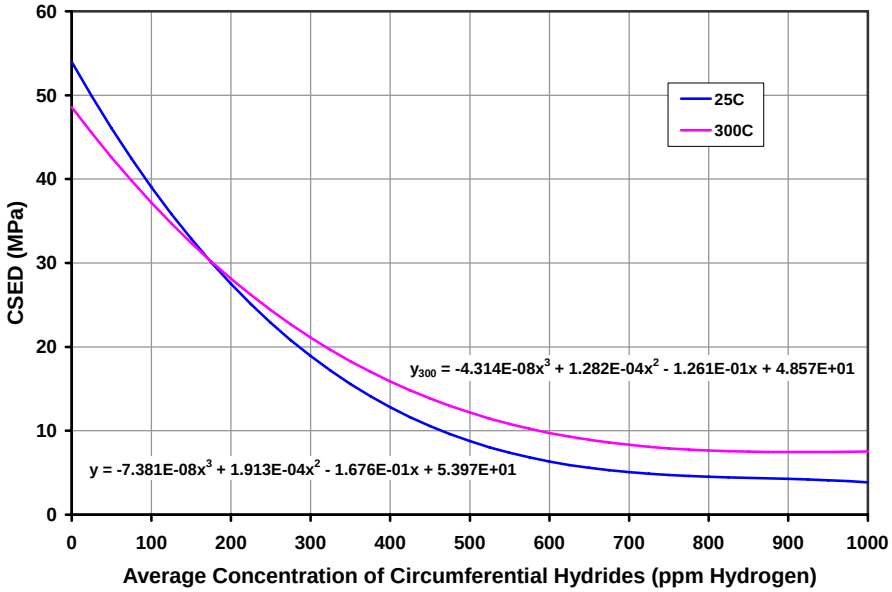

Figure 3-11
CSED vs. Average Hydrogen Concentration at Cladding OD for Fuel Rod Loaded Axially

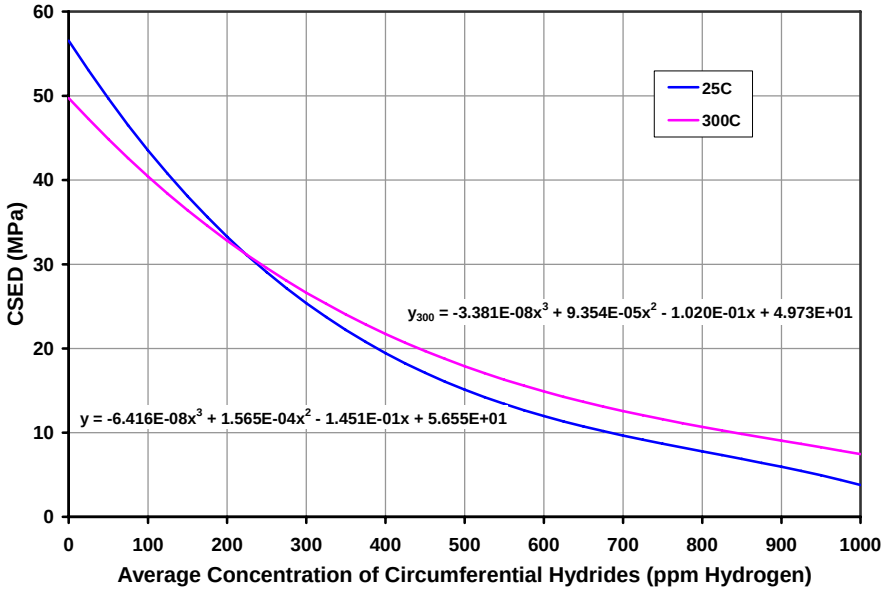

Figure 3-12
CSED vs. Average Hydrogen Concentration at Cladding Mid-wall for Fuel Rod Loaded Axially

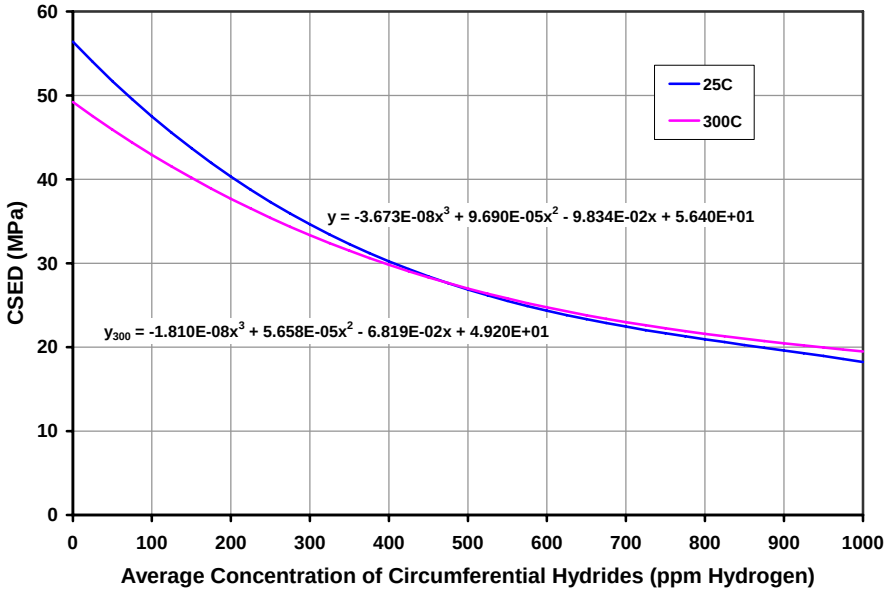

Figure 3-13
CSED vs. Average Hydrogen Concentration at the ID for Fuel Rod Loaded Axially

The five figures, Figure 3-9 through Figure 3-13, constitute a complete set of failure criteria for application in the failure evaluation of high-burnup spent fuel discussed in Chapters 4 and 5 for the hypothetical accident and the normal conditions of transport, respectively. The applicable domains for this failure analysis are: radial hydride concentration less than 22 ppm, circumferential hydride average concentration of 600 ppm +/- 50 ppm, and peak-to-average ratio of 2 for circumferential hydrides.

4
STRUCTURAL ANALYSIS AND FAILURE EVALUATION OF THE HYPOTHETICAL ACCIDENT

The first analytical effort for the failure evaluation of spent fuel under hypothetical accident conditions, as prescribed by10 CFR 71, was performed as part of a source term study by Sandia National Laboratory in Albuquerque, NM, in the late eighties/early nineties for low to intermediate burnup fuel (~35 GWd/MTU), SAND90-2406 [16]. The failure criteria adopted for determining failure frequency were based on cladding peak strain, in which the initiation of fracture implied total through-wall failure. Failure-mode-dependent failure probabilities were calculated for PWR fuel, for the three failure modes depicted in Figure 4-1, as follows: $2x10^{-4}$ for pinhole failure Mode-I, $5x10^{-5}$ for rod breakage Mode-II, and $2x10^{-5}$ for longitudinal slit Mode-III.

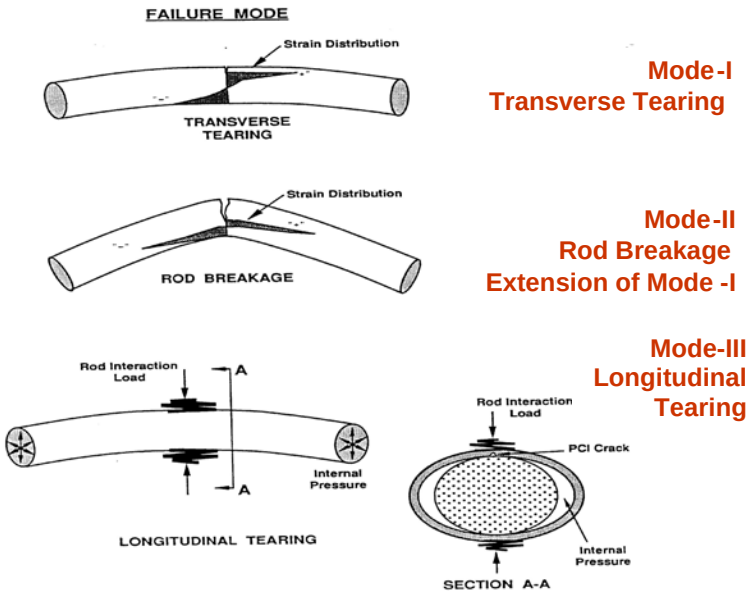

Figure 4-1
Possible Failure Modes Under Cask Drop in Horizontal Orientation, SAND90-2406 [16]

These failure probabilities are roughly within one order of magnitude, and failure in any of these three modes can be regarded as equally likely for intermediate-burnup fuel. However, this may not be the case for high-burnup spent fuel because of the role of radial hydrides, which uniquely affect Mode-III.

SAND90-2406 has charted the path for the structural modeling and failure analysis methodology developed in the present EPRI program, adapted to high-burnup spent fuel conditions and considering the effects of long-term dry storage. The detailed results are described in a series of reports, which are summarized in this chapter for the hypothetical accident and in the following chapter for the normal conditions of transport. To the former, the following EPRI reports are cited for further details:

1. 1009929, June 2005: "Spent Fuel Transportation Applications: Fuel Rod Failure Evaluation under Simulated Cask Side Drop Conditions" [10].
2. 1011816, September 2005: "Application of Critical Strain Energy Density to Predicting High-Burnup Fuel Rod Failure" – *Response to Comments from the Nuclear Regulatory Commission Staff*.[11]
3. 1011817, December 2005: "Spent Fuel Transportation Applications: Global Forces Acting on Spent Fuel Rods and Deformation Patterns Resulting from Transportation Accidents" [12].
4. 1013447, October 2006: "Spent-Fuel Transportation Applications: Modeling of Spent-Fuel Rod Transverse Tearing and Rod Breakage Resulting from Transportation Accidents" [13].
5. 1013448, December 2006: "Spent Fuel Transportation Applications: Longitudinal Tearing Resulting from Transportation Accidents – A Probabilistic Treatment" [14].

The regulatory definition of the hypothetical accident as a 9-meter drop of a transportation cask, which normally would be protected by impact limiters, onto an essentially unyielding surface is replaced in this analysis by a 9-meter drop of a bare cask onto a seismically designed concrete storage pad. This definition was shown in 1011817 to be conservatively equivalent to the regulatory definition. The analysis was carried out in three steps. In the first step, explicit-dynamics analyses are performed to calculate the global forces acting on the fuel rods. In the second step, the global forces are applied in local models of individual rods to calculate detailed cladding response. Finally, the local response is evaluated against the failure criteria. These results are summarized in this section, presenting the major findings with reference to the appropriate reports for further details.

Global Structural Analysis

Report 1011817, December 2005 [12] describes the modeling and analysis methodology for calculating global forces under the hypothetical accident conditions. Explicit-dynamics analyses were carried out employing detailed finite element models of the cask, the fuel assemblies, the fuel rods, and the cask's internal structures that hold the fuel assemblies in position. The finite element modeling of individual assemblies emphasized fuel rod responses at locations in the assembly where maximum forces would be expected, which include spacer grids at assembly mid-span and end-span positions, as shown in Figure 4-2.

With the view towards probabilistic evaluation of fuel rod failures, the structural model was constructed to capture the whole range of variation of dynamic forces in the cask, consisting of several detailed models of the assemblies positioned at various locations in the basket structure: at the bottom where the forces would be largest, at the top where the forces would be smallest and at the side position where intermediate level forces would be expected. The dynamic forces of significance to fuel rod failure evaluation consist of pinch forces caused by rod-to-rod impact, bending moments, and axial-extension and shear forces.

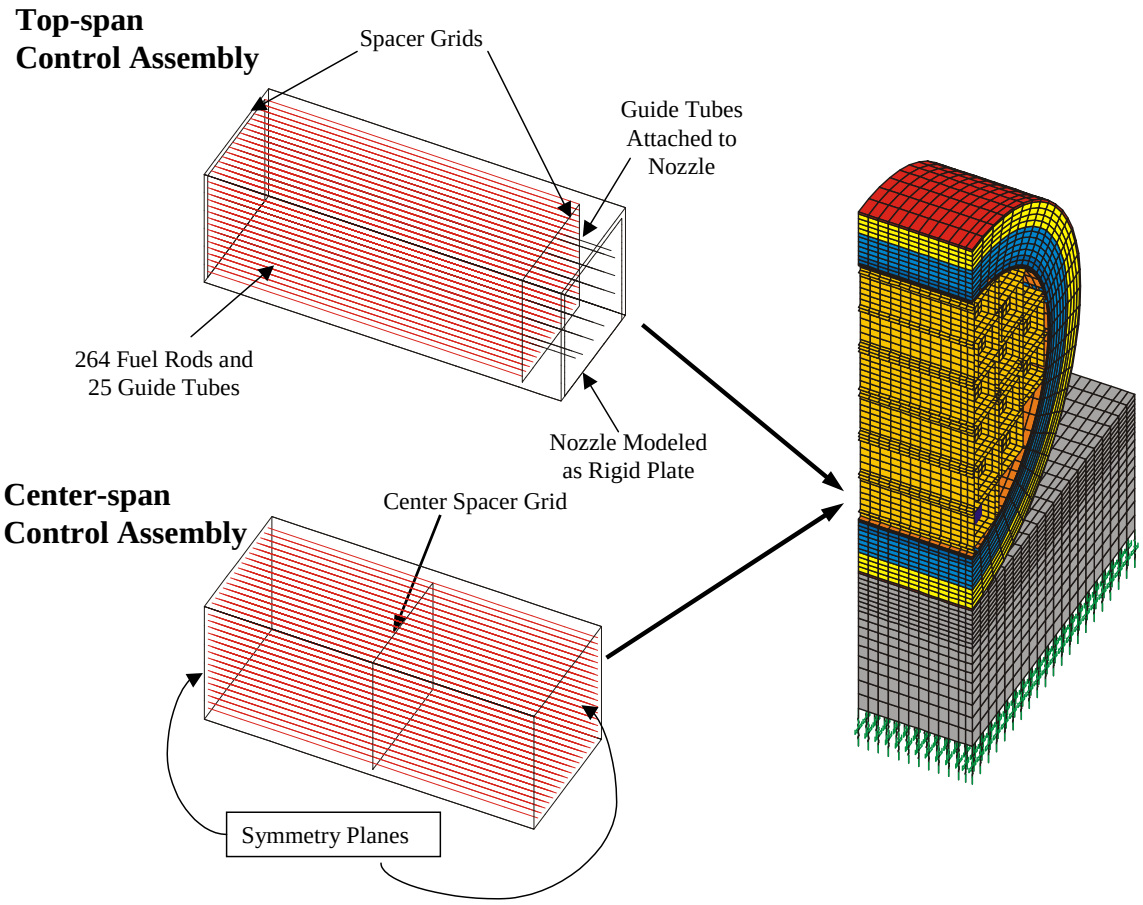

Figure 4-2
Control Assembly Models Within a Three-Dimensional Slice of the Global Structural Model

Assembly Deformations and Fuel Rods Force Response

Representative results are selected from 1011817 and presented in the following figures to illustrate global response of the assemblies and fuel rods to the dynamic loading. The spatial variation of fuel assembly dynamic response can be seen by comparing the deformation pattern of the least loaded top assembly, Figure 4-3, with that of the bottom-corner assembly, Figure 4-4. The time response of the maximum forces acting on fuel rods, which are the pinch forces (rod-to-rod contact forces), is illustrated in Figure 4-5.

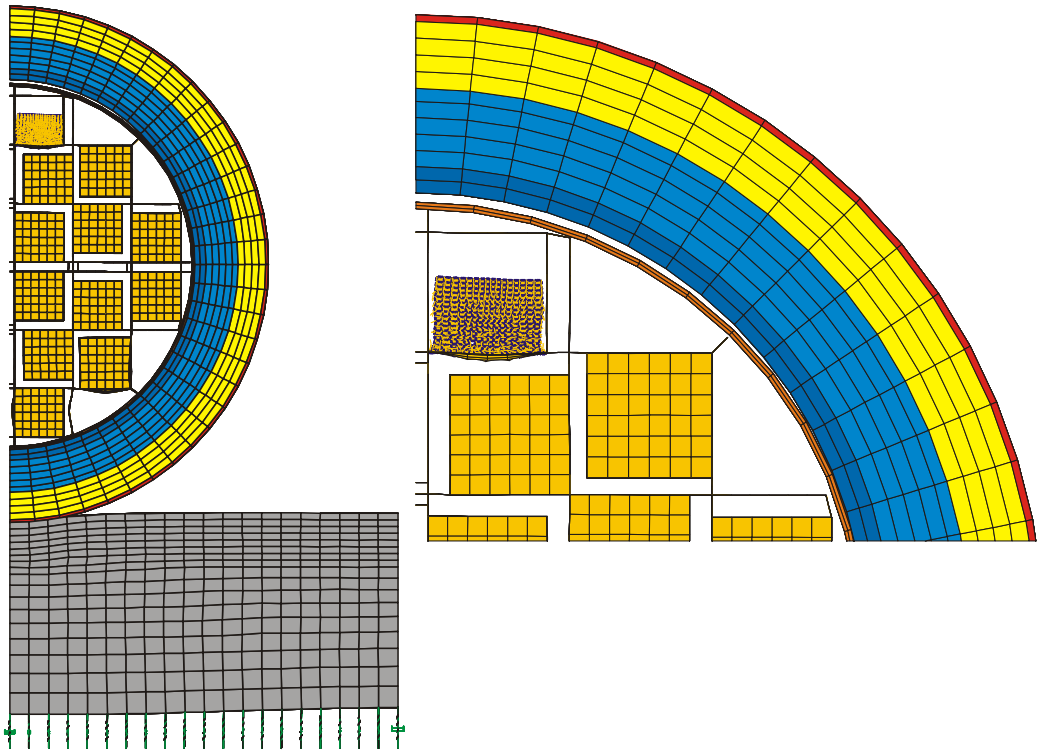

Figure 4-3
End Snapshot View at 20 ms of Cell 02 Assembly Deformations – No Displacement Magnification

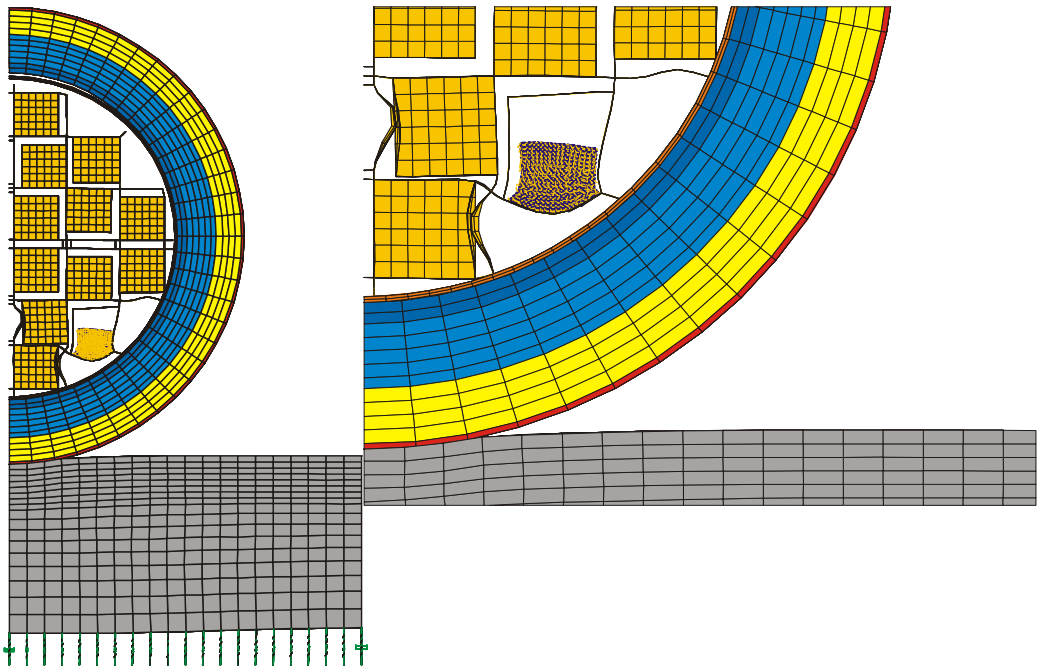

Figure 4-4
End Snapshot View at 20 ms of Cell 22 Assembly Deformations – No Displacement Magnification

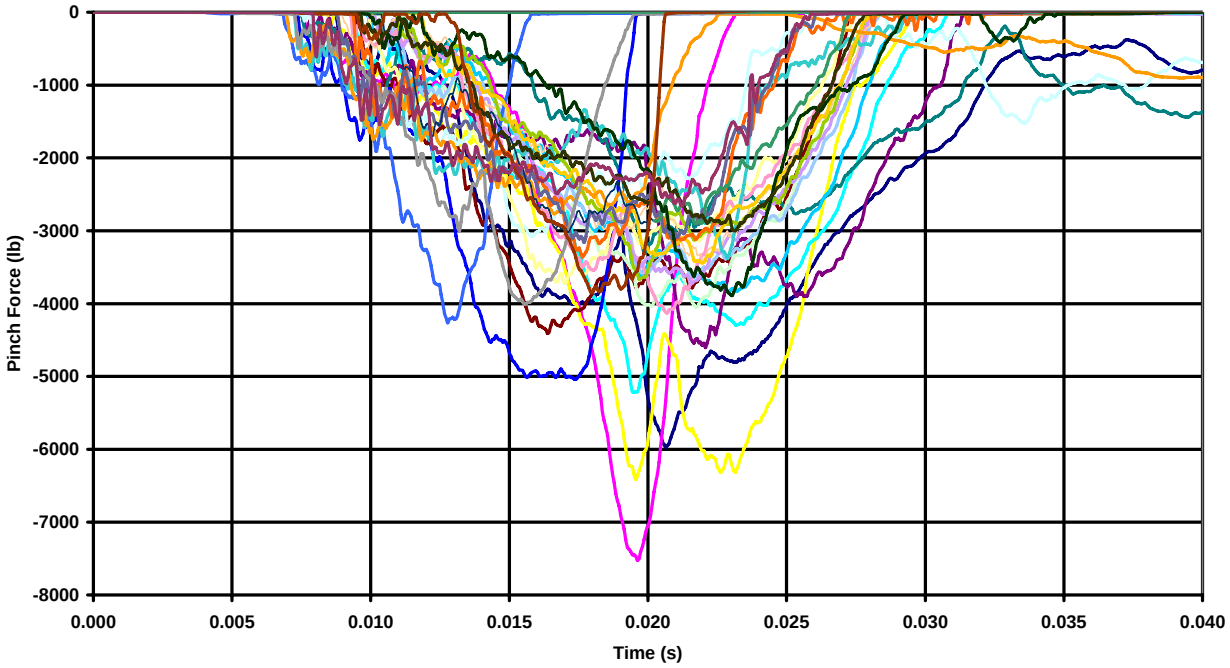

Figure 4-5
Bundle 22 Maximum Pinch Force Time Histories Center Model

Force Distributions

Frequency distributions of the forces and moments were obtained through the post-processing of the dynamic analysis results of the 867 rods, at the center spacer grid and the end-plate models, in the three assemblies that were modeled in detail. The distributions for the pinch force, the axial force and the bending moment are shown, respectively, in Figures 4-6, 4-7 and 4-8. Also shown on figures are the expected "Normal Distribution" probabilities. The pinch force frequency distribution and the frequency distribution of moments and axial forces are generally well approximated by the normal distribution. These distributions will be used in the probabilistic failure evaluation of the longitudinal tearing mode, which will be discussed in a later section.

The maximum pinch forces computed is 7.5 kips, but over 90% of the rods experience a pinch force less than half this maximum. The maximum axial force is 2.8 kips, and the largest bending moment is 300 in-lb. These forces will be used in the local modeling of individual fuel rods to evaluate failure initiation and potential propagation through the cladding wall. This is discussed next. It is important to point out that these forces were computed for the fuel rods modeled as beams; and as such they represent upper-bound values because, by beam theory, the fuel rods cross sections deform as non-compliant planes, which make the rods stiffer and attract higher forces. This beam-theory assumption will be absent in the local models failure analysis.

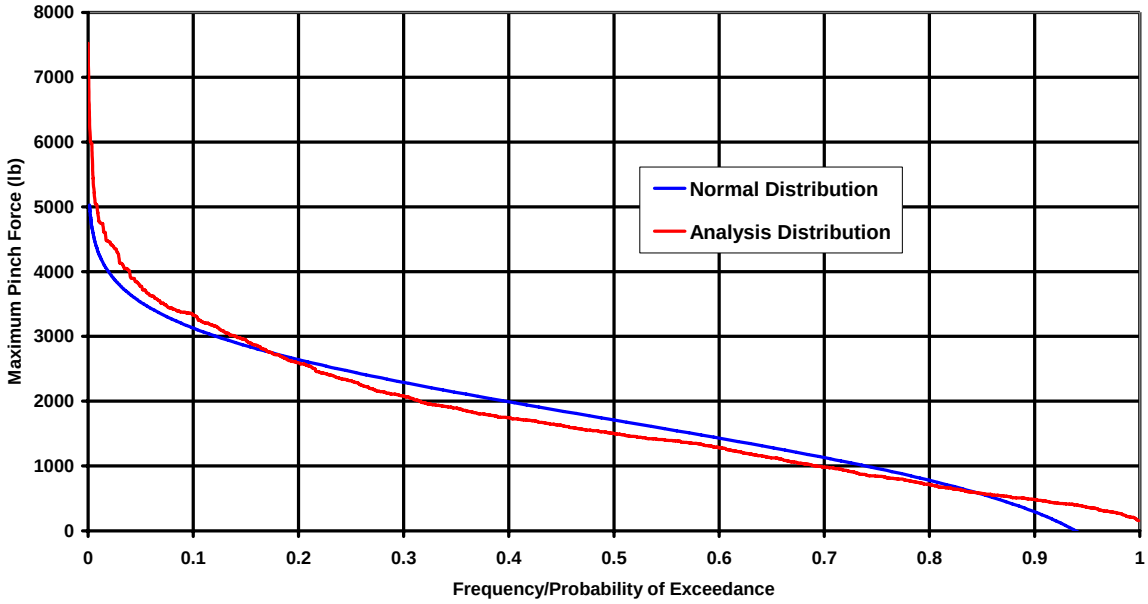

Figure 4-6
Maximum Pinch Force Frequency/Probability Distribution Center Model

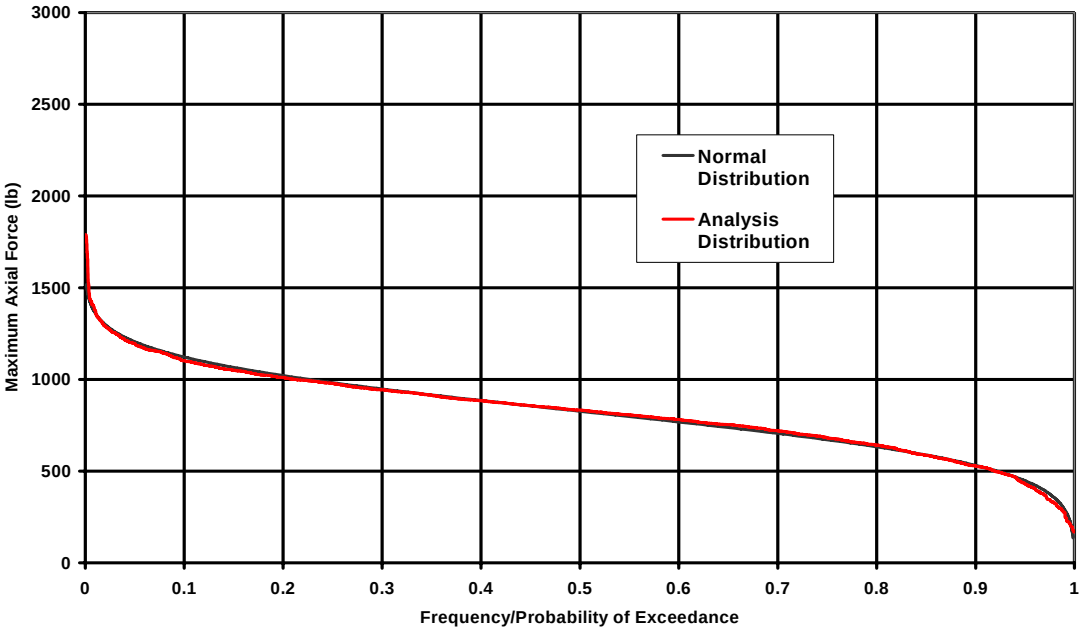

Figure 4-7
Maximum Axial Force Frequency/Probability Distribution Center Model

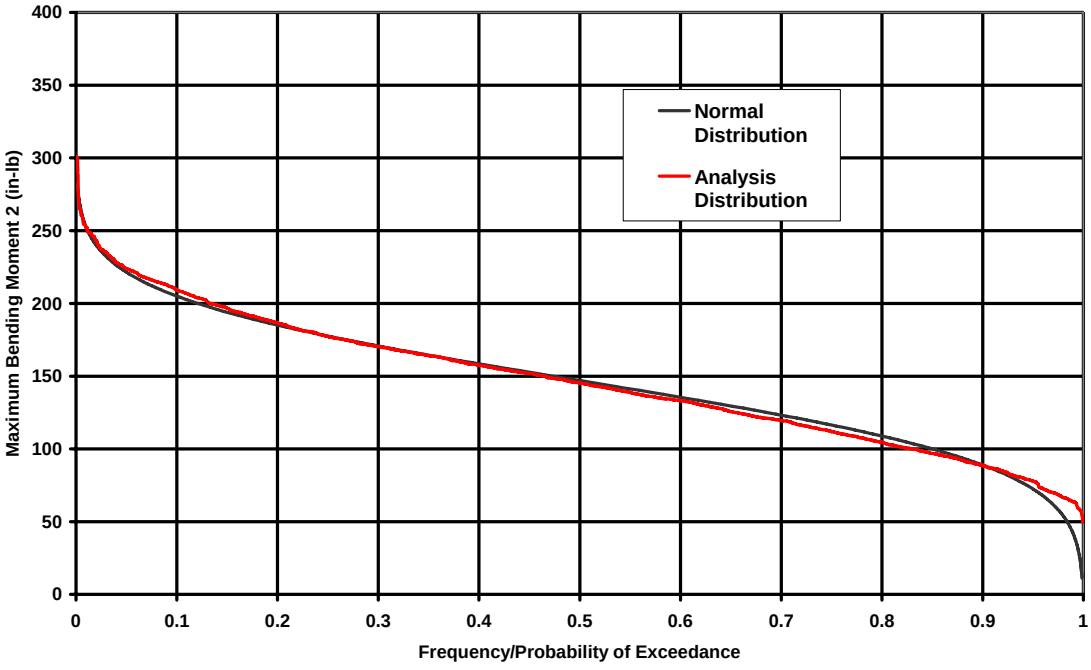

Figure 4-8
Maximum Bending Moment Frequency/Probability Distribution Center Model

Fuel Rods Local Model Representation for Failure Evaluation

The maximum forces and moments calculated in the global analysis are applied in detailed local models of individual fuel rods, such as the ones depicted in Figure 4-9. The use of either model is a matter of convenience and the choice of failure mode being evaluated.

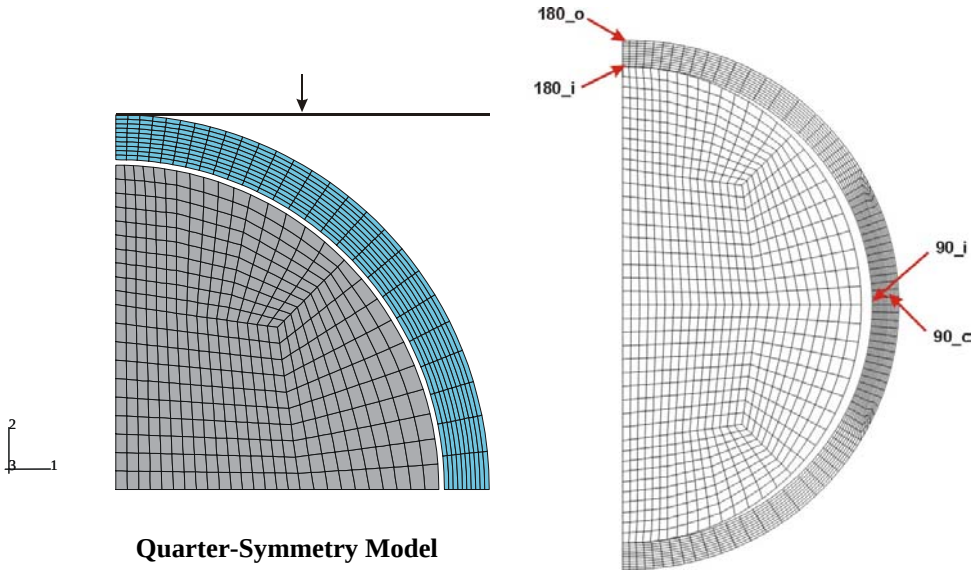

Figure 4-9
2D Finite Element Models for Local Failure Analysis

The fuel in Figure 4-9 is modeled with reduced stiffness to represent cracked pellets. A side study was conducted to calculate the cracked-pellet stiffness using the FALCON fuel behavior code [37] applied to a finite element r-θ model of a fuel rod cross section. The resulting force displacement response is depicted in Figure 4-10 for plane strain and plane stress cases. The curves show two-stage resistance to the pinch load, indicating the gradual engagement of the fuel pellet in resisting the load. The slope of the second stage of the curve describes the combined stiffness of the cladding and the cracked fuel pellet. The overall pinch-load stiffness of the fuel rod is calculated as the average of the slopes of the plane stress and plane strain curves. This stiffness was simulated in the local finite element model depicted in Figure 4-9 by reducing the fuel elastic modulus through repetitive calculations to find an effective fuel pellet modulus that matched the FALCON force-displacement curves. This resulted in reducing the fuel modulus to 20% of the un-cracked pellet modulus.

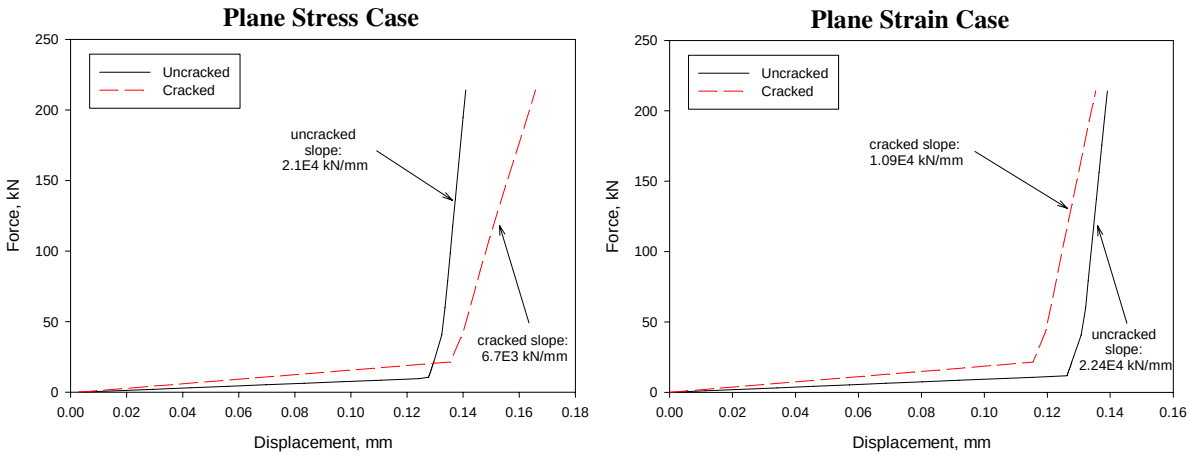

Figure 4-10
Stiffness of Fuel Rod Under Pinch Forces With the Effects of Fractured Fuel

The local response of the cladding is strongly dependent on the material and physical conditions that were determined to be present at the end of dry storage, as described in Chapter 2. These are discussed below.

Fuel Rods Conditions at the End of Dry Storage

The physical and material conditions of spent fuel rods at the end of dry storage constitute the initial conditions for the local failure evaluation under the hypothetical accident. Some of those initial conditions are the result of in-reactor service and remain virtually unchanged by dry storage; the others would have evolved during dry storage. The former include: irradiation hardening, OD corrosion layer thickness and cohesion, hydrogen concentration and initial hydride morphology, possible hydride lens at the OD, and incipient pellet-cladding interaction (PCI) cracks. Among the latter, the formation of radial hydrides and the increase in the fuel-cladding gap due to creep are the most important. Less important, but beneficial, effects such as the small amounts of annealing of irradiation hardening and radial homogenization of the hydrides are ignored for conservatism.

From an analytical perspective, the cladding initial conditions identified above are placed in three groups with respect to their effects on spent fuel failure evaluation:

(a) Burnup-dependent conditions, such as irradiation hardening and hydrogen content, are treated by modifying the cladding mechanical properties,

(b) Conditions, such as hydride morphology and radial hydrides concentration, are incorporated in the failure criteria discussed in the preceding chapter; and

(c) Geometric conditions, such as corrosion thickness, fuel-cladding gap, OD hydride lens, and incipient PCI cracks, are treated explicitly by constructing finite element models that include these geometric conditions.

It is relevant to mention that pre-existing PCI cracks were used as the initial damage conditions in the low-burnup analysis of SAND90-2406 [16]. For the high-burnup case, the formation of radial hydrides during dry storage would replace PCI as the stronger protagonist for failure analysis. However, the equivalence between PCI cracks and radial hydrides is not totally valid, because PCI cracks can exist only at the ID and become damaging only when they are located in close proximity to the impact points. This limited their contribution to failure, hence the small failure probability of 2E-5 calculated in SAND90-2406 for Mode-III. In the present case, the role of PCI cracks is relatively small compared to radial hydrides. For similar reasons, the same can be said about hydride lenses. The analytical study reported in 1009929, 2005 [10] shows that both conditions, namely, PCI crack and hydride lens, can be eliminated from further consideration. The study shows that under worst-case conditions, a factor >2 on a calculated pinch force of 6300 lbs is required to fail the cladding. This should be juxtaposed against the very small probability of having a PCI crack at the ID and a deep hydride lens at the OD in line with the maximum pinch force. A local effects analysis utilizing Figures 4-9 and 4-10 conducted in 1009929 shows a local crack-tip SED value rising to 70 MPa at a load factor 2.8, Figure 4-11. However, failure initiation would have occurred at a load factor >2, as determined from Figure 4-12 at an SED of 22 MPa, which is the CSED value estimated from Table 3-1, first row.

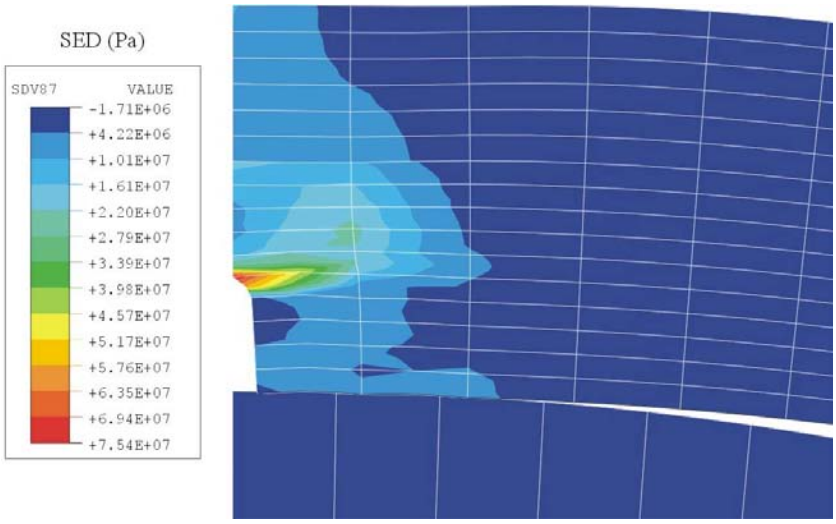

Figure 4-11
Strain Energy Density Distribution Under Pinch Load at Failure, Load Factor = 2.8

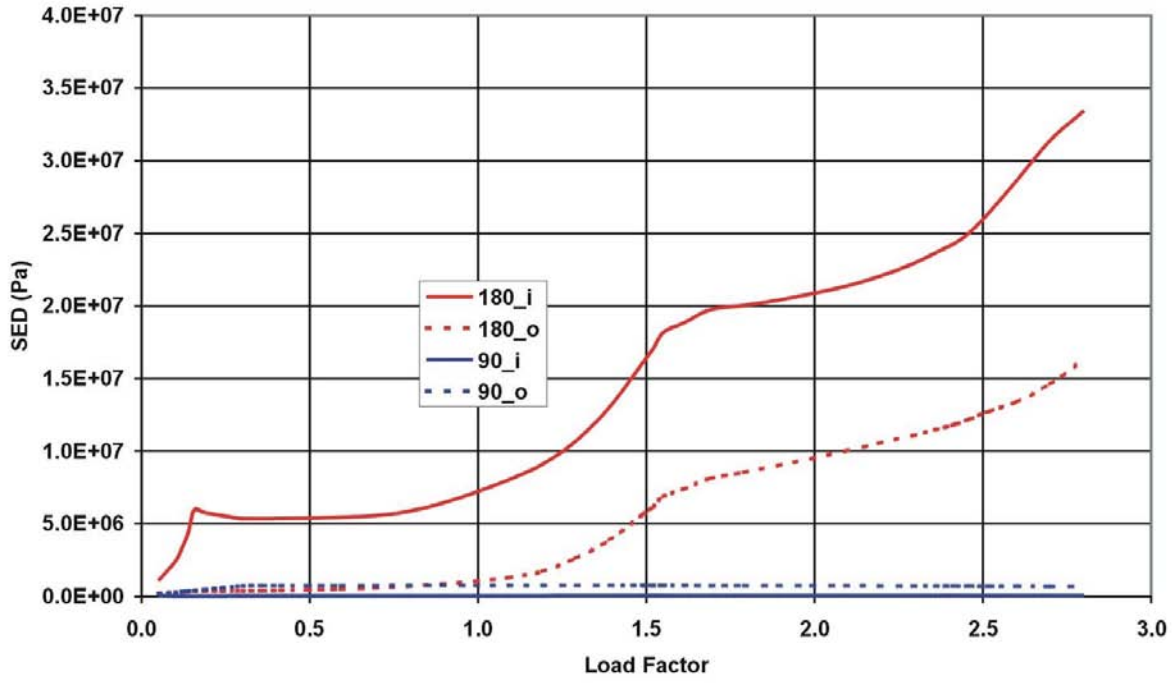

Figure 4-12
Strain Energy Density versus Pinch Force Load Factor

Based on the above results, PCI cracks and hydride lenses no longer need to be considered in the failure evaluation that follows. The remaining geometric initial conditions that need to be considered in the local finite element model are the corrosion layer thickness and the fuel-cladding gap. The former is conservatively treated as a cladding thickness reduction, and the latter is explicitly included in the finite element models shown in Figure 4-9. End of dry storage values for the gap thickness are listed in Table 3-1 in Chapter 3, which shows that ~52 μm represents the expected size of the gap, with an upper bound value of ~95 μm as a possible gap size under extreme conditions of cladding stress and temperature. An average value of 70 μm is considered a conservative upper limit of the gap size to be used in the local failure analysis. However, as will be shown, a gap-size distribution is used in the probabilistic failure analysis of the longitudinal tearing mode, which is the mode affected most by the gap size because of the effects of radial hydrides.

Failure Analysis of Fuel Rods in the Longitudinal Tearing Mode

The longitudinal tearing failure mode, Mode-III in Figure 4-1, is the mode that is affected by radial hydrides, and for this reason it was thought prudent to explore the effects of radial hydrides on cladding vulnerability as soon as a radial-hydride-dependent failure criterion was developed in the program. The results of that study were reported in 1009929, June 2005 [10]. Partial results are presented above in connection with the effects of PCI cracks at the ID in line with a hydride lens at the OD, which show that even for that combination of cladding damage sufficient margin against failure exists.

A subsequent more detailed analysis, reported in 1003448, 2006 [14], was performed to evaluate the failure probability for the longitudinal tearing mode. This required a precise definition for failure, which, in view of the bimodal response of the cladding due to fuel-cladding interaction, must distinguish between failure initiation that remains part-wall and complete through-wall failure. This is strongly dependent on the magnitude of cladding displacement before fuel-cladding contact begins to transfer the force to the pellets. If the fuel-cladding gap is sufficiently wide, such that cladding failure is initiated before fuel-cladding contact is established, the likelihood exists that crack extension through-wall would continue. On the other hand, if fuel-cladding contact occurs early in the loading history, then the driving force for crack extension would not be sufficient to overcome the pellet resistance. These two states of failure initiation are used as scenario for defining a "fail/no-fail boundary" where crack initiation prior to fuel-cladding contact is assumed to extend to complete through-wall failure regardless of what the analysis results indicate, and crack initiation post fuel-cladding contact is to be considered no-failure unless the analysis in fact shows damage progression to through-wall failure. These behavior states are illustrated by the analysis presented below.

Bi-Modal Response of Spent Fuel Rods – Fail/No-Fail Boundary

The bi-modal response regime is characterized by low-resistance deformation through open fuel-cladding gap followed by high resistance response under fuel-cladding interaction. A series of analyses were performed to quantify the fail/no-fail boundary of spent fuel rods subjected to pinch forces. The fail/no-fail boundary defines the demand/response relationship that distinguishes through-wall rupture from part-wall damage, as discussed above. This boundary is a strong function of the size of the fuel-cladding gap. The quarter-symmetry finite element model of a fuel rod cross section, shown in Figure 4-9, is analyzed under displacement-controlled conditions, considering several gap sizes ranging from zero to 200 μm. Again the cracked-pellet stiffness depicted in Figure 4-10 is used. Contour plot of the strain energy density (SED) is presented for illustration in Figure 4-13 for the 70-μm gap case. Figure 4-14 depicts the pinch force as function of displacement, which, in the quarter-symmetry model, is equal to the gap size. Very little force is required to close the gaps, as shown. This behavior is reversed for the SED, which is depicted in Figure 4-15, showing nearly unbounded behavior (solid-dashed red curve) prior to gap closure. It is interesting to note that it is possible to estimate from Figure 4-15 the maximum force that can be applied in a ring compression test; it is simply the asymptotic value of the dashed curve. Note that the SED showed no increase for any gap size beyond a pinch force of 4000 lb, which implies that increasing the severity effect of the accident beyond a certain level has little additional effect on cladding failure.

On closer examination of Figure 4-15, the information needed to define the fail/no-fail boundary is contained within the dotted circle. Figure 4-16, generated from that information, depicts SED (the demand) at the cladding ID as function of displacement (the response), computed at the instant of fuel-cladding contact (gap closure). SED values falling below the curve in Figure 4-16 is the response domain of an open gap, and failure initiation at the ID in that domain is assumed to extend to the OD. However, failure initiation in the SED-Displacement domain above the curve in Figure 4-16 would remain an ID part-wall failure. Thus, Figure 4-16, in combination with the failure criteria developed in Chapter 3, Figures 3-9, 3-10 and Table 3-1, fully characterize the fail/no-fail boundary, which is key input in the probabilistic failure evaluation.

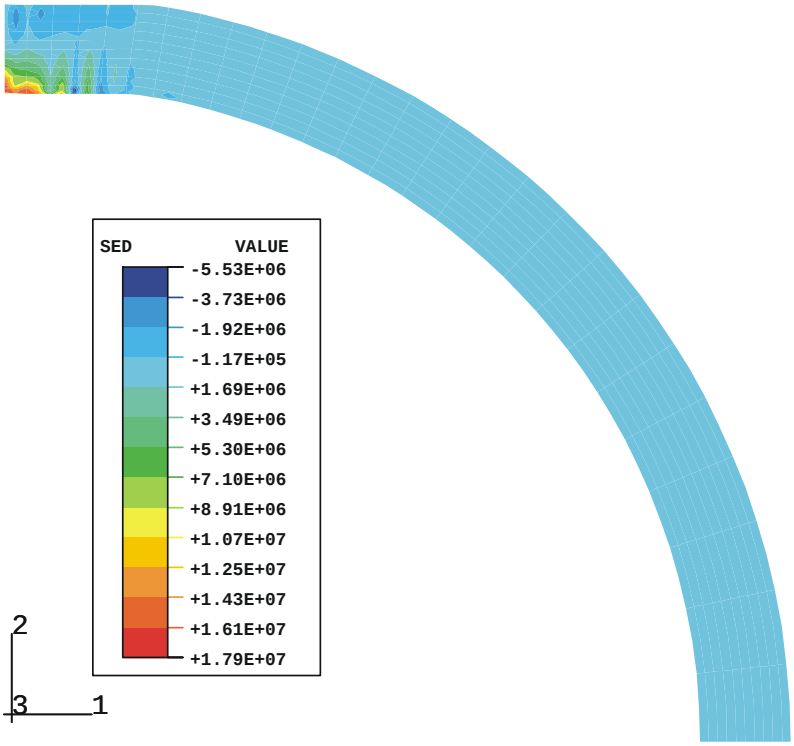

Figure 4-13
SED (Pa) at End of Loading for 70-µm Gap

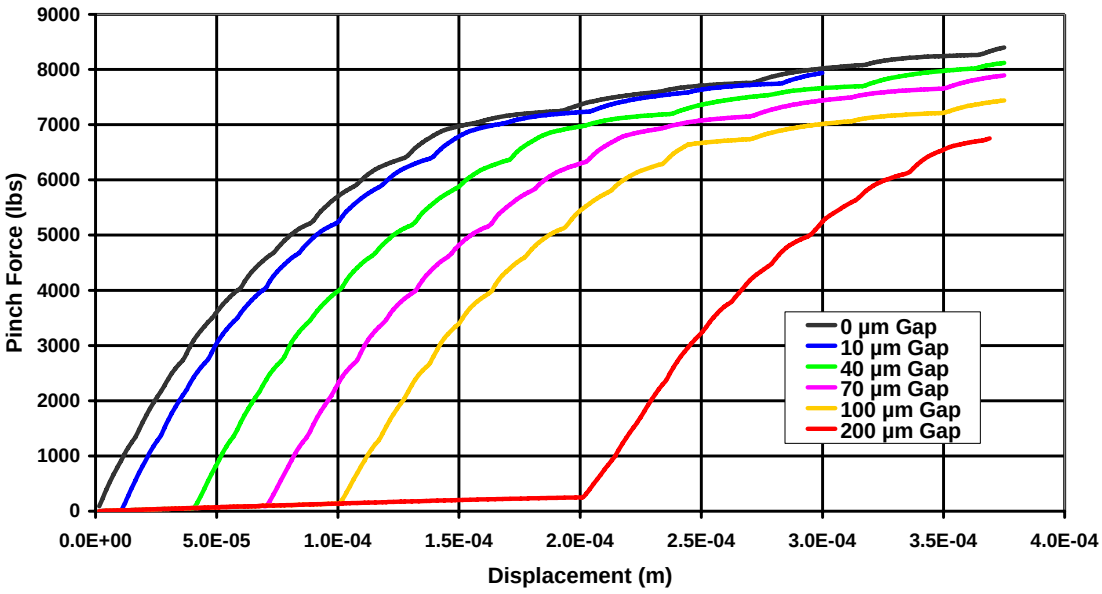

Figure 4-14
Pinch Force vs. Imposed Displacement

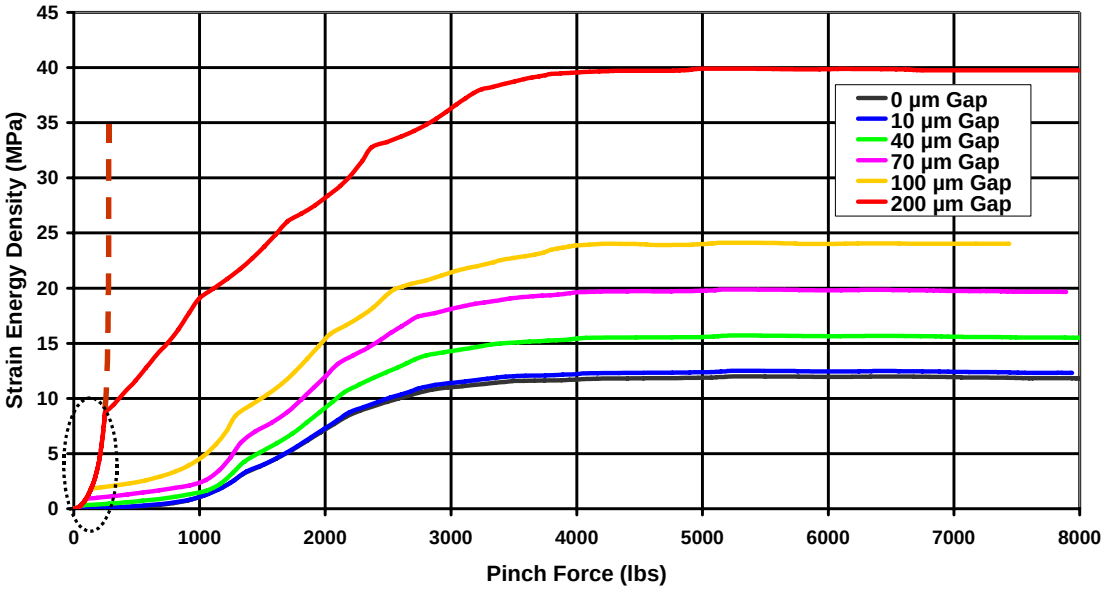

Figure 4-15
SED at Cladding ID as a Function of Pinch Force

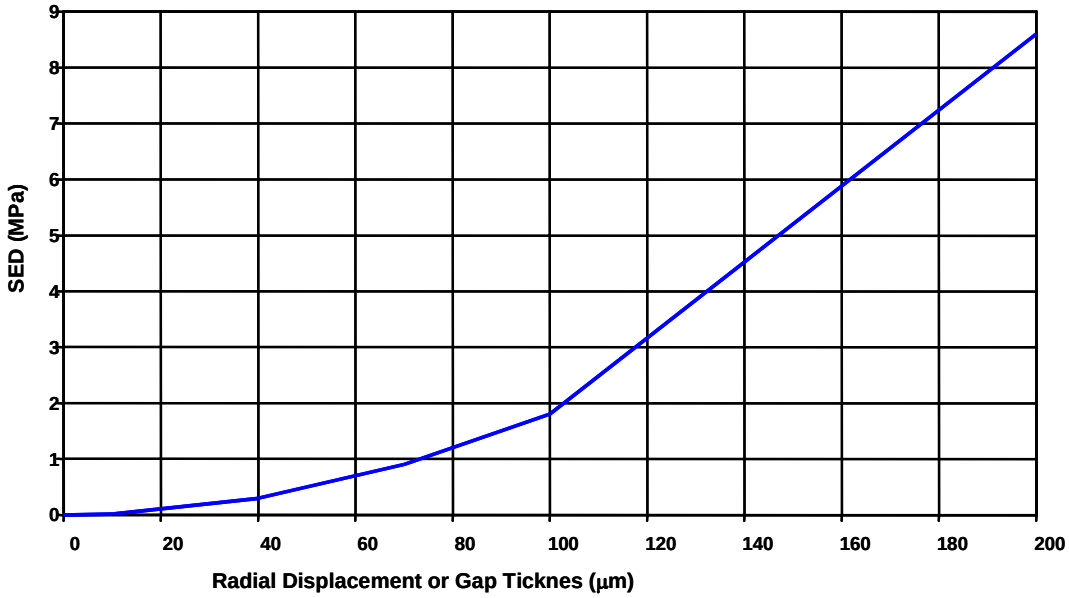

Figure 4-16
Strain Energy Density at the Instant of Gap Closure Defining the Fail/no-Fail Boundary

Longitudinal Tearing Failure Probability

It was shown in the preceding sub-section that cladding susceptibility to failure is strongly dependent on the onset of fuel-cladding contact, which is a direct function of the gap size. The definition of a "fail/no-fail boundary" makes it possible to distinguish between failure initiation that could progress to complete through-wall failure, (fail), and partial failure that remains as a local damage state (no-fail). According to this definition, a necessary and sufficient condition that a through-wall failure occurs is that failure be initiated prior to fuel-cladding contact. In the context of probabilistic evaluation, however, failure probability calculations will consider failure initiation only, but special calculations will be performed to quantify the probability of through-wall failure.

In the evaluation of these two failure states, Demand is defined as Strain Energy Density (SED); Capacity is defined as Critical Strain Energy Density (CSED); and failure is defined as Demand exceeding Capacity, i.e., $SED \geq CSED$. The probability of failure (P_F) is equal to the double integral of the joint probability density function (PDF) of SED and CSED over the failure domain defined by $SED \geq CSED$, as

$$P_F = \iint_{R \leq S} f_{R,S}(r,s)\, dr\, ds, \qquad \textbf{Eq. 4-1}$$

where *R* and *S* are CSED and SED, respectively; and $f_{R,S}(r,s)$ is their joint PDF. In the special case where *R* and *S* are statistically independent, i.e., $f_{R,S}(r,s) = f_R(r) \cdot f_S(s)$, the above double integral can be simplified into the following

$$P_F = \int_0^\infty F_R(s)\, f_S(s)\, ds = \int_0^\infty (1 - F_S(r))\, F_R(r)\, dr \qquad \textbf{Eq. 4-2}$$

In the above equation, F_X is the cumulative distribution function (CDF) of *X*, and f_X is the PDF of *X*. Note that PDF is the derivative of the CDF, as $f_X(x) = dF_x(x)/dx$.

Therefore, the key to determining the probability of failure is to establish the probability distributions of SED and CSED. Their probability distributions are, of course, functions of many basic random variables such as pinch force, circumferential and radial hydrides concentrations, gap size, cladding temperature, etc., which, in turn, have their own probability distributions. Knowing those distributions, the failure probability can be determined by solving Equation 4-1 or Equation 4-2. However, a closed-form solution is impossible, and the solution is obtained through Monte Carlo simulation. The overall procedure is outlined below:

1. Identify two sets of basic random variables, one set for CSED and another set for SED:

   Set-1 – CSED random variables: Circumferential Hydrides (Figures 2-3 and 2-4), Radial Hydrides (Table 2-2), Cladding Temperature (normal distribution over the range 350-410°C), Internal Rod Pressure (Figure 2-1, with a factor of 2 for Boron-coated Pellets (BCP)), and Material Failure Limits (Table 3-1 and Figures 3-9 and 3-10).

Set-2 – SED Random Variables: Pinch Force (Figure 4-6) and Fuel-Cladding Gap (Table 2-1).

2. Use Monte Carlo simulations to generate numerical PDFs for the random variables in Set-1, (Report 1013448 Figures 5-14, 5-15 and 5-16 for mixed (standard and BCP) fuel, and Figures 5-18, 5-19 and 5-20 for BCP fuel); then generate numerical PDFs for the CSED, (Report 1013448 Figures 5-17 and 5-20 for mixed and BCP fuel, respectively).
3. Use Monte Carlo simulations to generate numerical PDFs for the random variables in Set-2, (Report 1013448 Figures 5-29, 5-30 and 5-32), from which generate numerical PDFs (Report 1013448 Figures 5-31 and 5-33) for the SED for mixed and BCP fuel, respectively.
4. Obtain a numerical solution for Equation 4-1 by comparing the CSED and SED values from 2 and 3 above, as described below.

Calculation of the Probability of Failure Initiation

The double integral in Equation 5.1 can now be numerically calculated using Monte Carlo simulation to obtain the probability of failure as follows,

$$P_F = \iint_{R \le S} f_{R,S}(r,s)\, dr\, ds \approx \frac{n_f}{n_t}, \qquad \textbf{Eq. 4-3}$$

where n_f and n_t are the number of failures (i.e., cases where SED ≥ CSED) and the total number of simulations, respectively.

Based on 100,000 samplings, the probability of failure initiation at the cladding ID for a rod population consisting of 80% standard rods and 20% rods with boron-coated pellets is 1.61%. The probability of failure for a rod population consisting exclusively of rods with boron-coated pellets is 2.47%. As an illustration, Figure 4-17 shows the CDF of the SED and CDF of the CSED, respectively, for a mixed rod population. Figure 4-18 shows the same information for a rod population with boron-coated pellets exclusively. The horizontal separation between these curves illustrates why low failure probabilities are predicted.

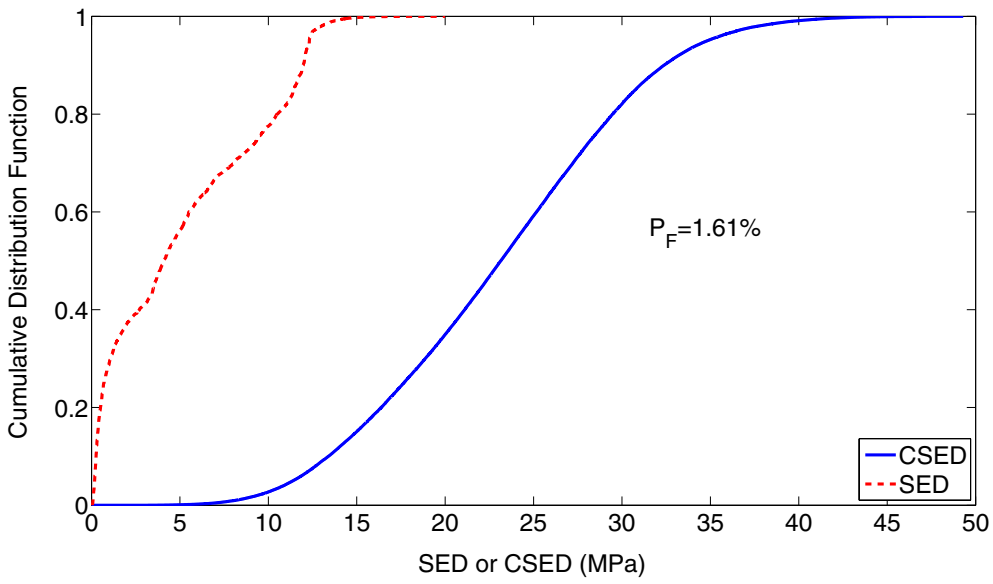

Figure 4-17
Monte Carlo Simulation CDF of SED and CSED for Standard-Design PWR Rods

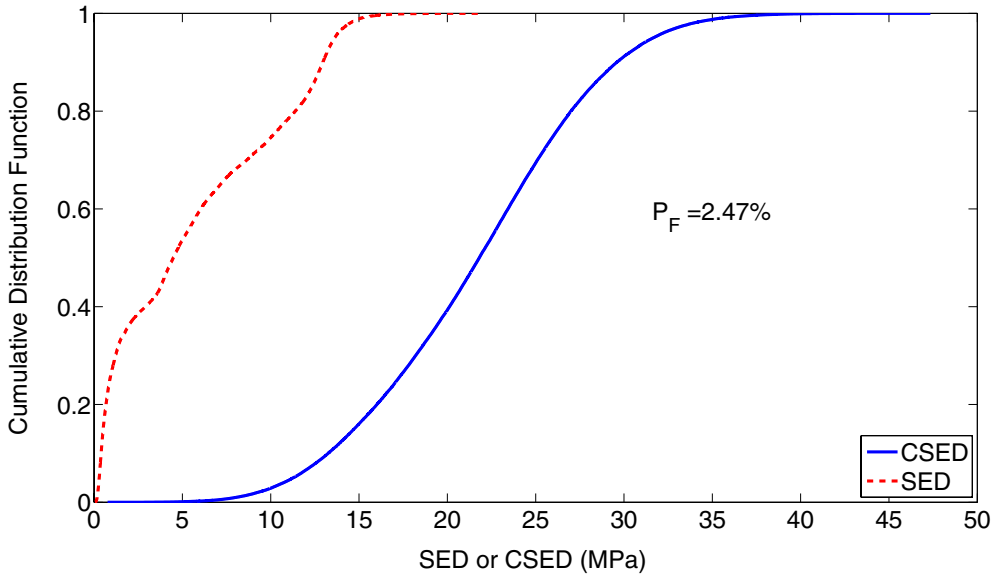

Figure 4-18
Monte Carlo Simulation CDF of SED and CSED for Rods With Boron-Coated Pellets

Calculation of Through-wall Failure Probability

The above failure probabilities are total, i.e., they do not distinguish between failure initiation and complete through-wall failure. To obtain failure probabilities for the latter, Equation 4-3 Monte Carlo sampling was restricted to rods where the inequality SED ≥ CSED was applied only to failure initiation during open gap, i.e., for SED falling below the curve in Figure 4-16. The results of these calculations gave the following through-wall failure probabilities: 1.0×10^{-5} and 2.0×10^{-5} for the mixed rod population and rods with only boron-coated pellets, respectively. It is interesting to note that these probabilities are of the same order of magnitude predicted for low-to-intermediate burnup fuel in the 1992 Sandia source-term study, SAND90-2406 [16].

Failure Analysis in the Transverse-Tearing and Rod-Breakage Modes

The cask drop calculations consider the cladding to be an elastic-plastic material, but without the ability to sustain damage or failure. This maximizes the forces acting on the fuel rods, which means that the bending moments and axial forces distributions given in Figures 4-7 and 4-8 should be considered bounding, reached only if no cladding damage is possible. The analysis reported in 1013447, 2006 [13] evaluates cladding failure progression through a non-linear incremental-damage analysis in which the damage-based metal/hydride mixture model utilized in the failure criteria development described in Chapter 3 of the present report is used as the cladding constitutive model.

A finite element model of a typical fuel rod is shown in Figure 4-19. The figure also shows contours of the circumferential hydrides distribution in the cladding, derived from Figure 2-4.

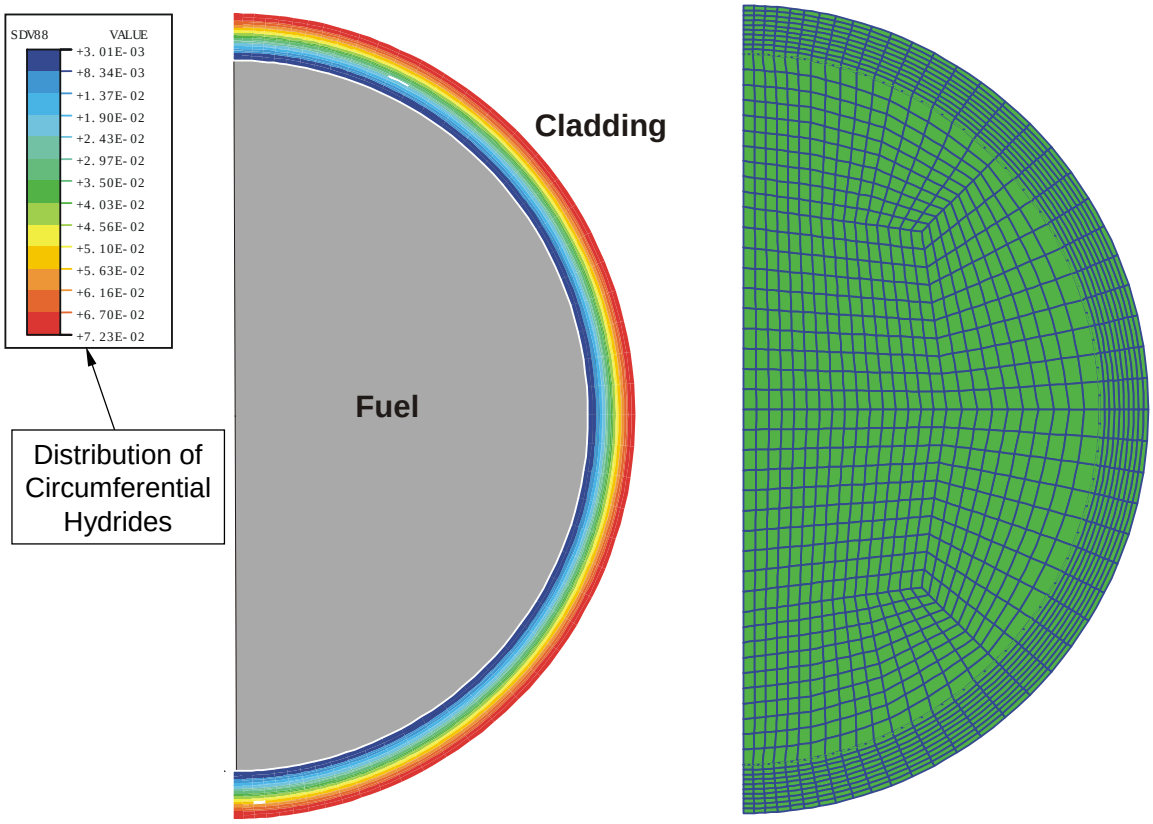

Figure 4-19
Finite Element Representation (Left) of Fuel Rod Cross Section – Fuel Is Modeled With Reduced Stiffness in Compression, (Figure 4-10), and Zero Stiffness in Tension

The structural analysis is carried out using the ABAQUS Finite Element Code [38] in a displacement-controlled procedure, in which displacements and rotations are applied as surrogates for axial forces and bending moments, and ABAQUS automatically calculates the bending moments and axial forces as reaction moments and forces.

The analysis results for Mode-I and partial-Mode-II failure are presented in the next set of figures. The axial force and bending moment that the fuel rod was able to attract are shown in Figures 4-20 and Figure 4-21, respectively. As can be seen in the figures, the axial force and bending moment peaked at 1200 lb and 150 in-lb, respectively, at about the same time, and then began to decline as deformations continued to be applied; the time at which these forces peaked is the onset of damage, which is depicted in Figure 4-22. The net axial force dropped to zero but the bending moment dropped to about half of its peak value. It is interesting to note that the axial force and bending moment in the present analysis did not rise to the levels shown in the distributions depicted in Figures 4-7 and 4-8, respectively. This is the consequence of stress shedding due to damage progression, which weakens the fuel rod and diminishes its ability to attract higher forces under increasing deformations.

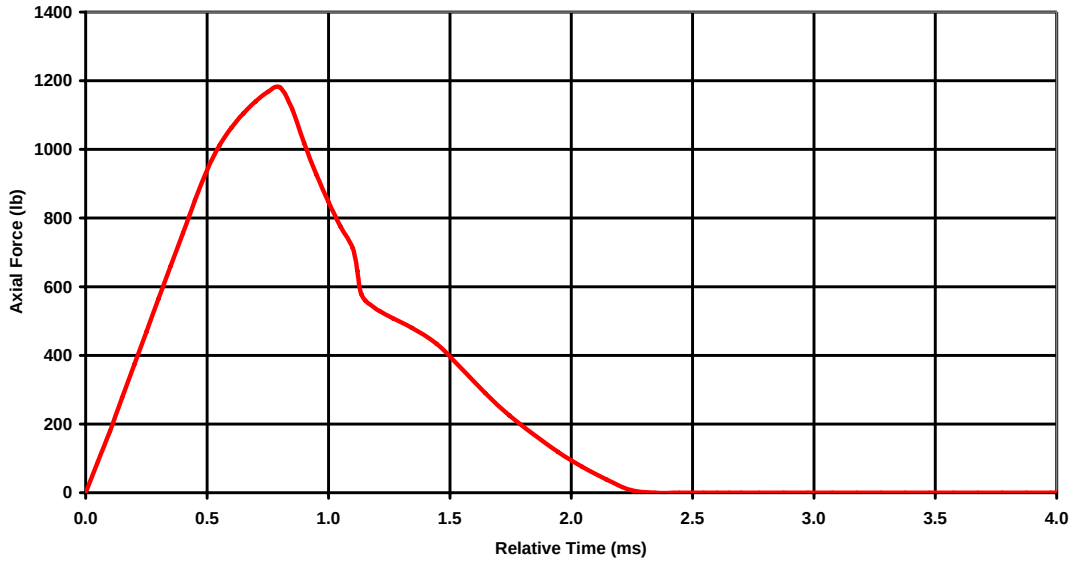

Figure 4-20
Time History of the Axial Force That the Fuel Rod Was Able to Attract, When Combined With the Bending Moment Shown in Figure 4-21

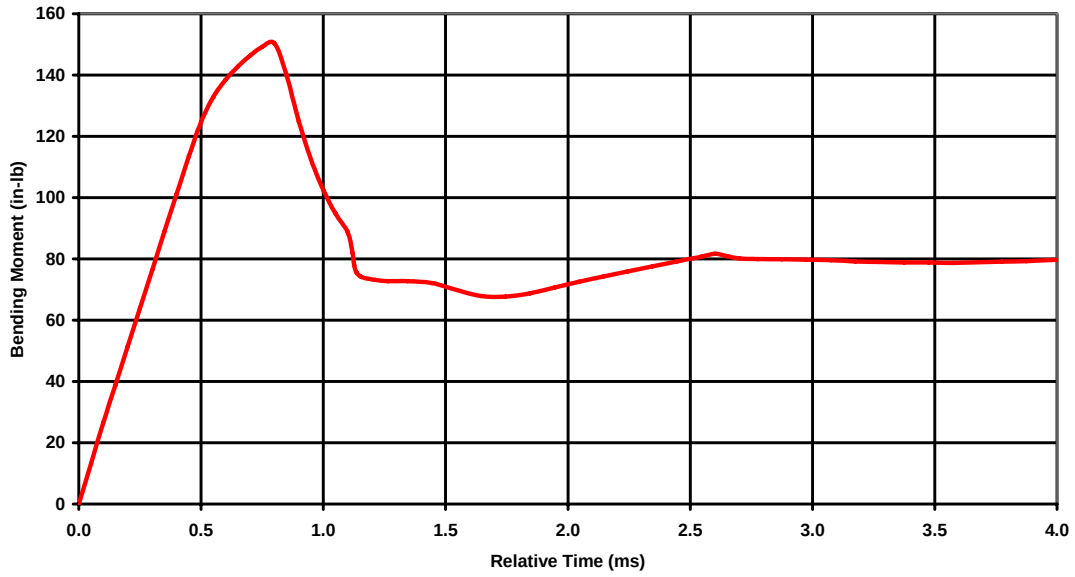

Figure 4-21
Time History of the Bending Moment That the Fuel Rod Was Able to Attract, When Combined With the Axial Force Shown in Figure 4-20

Figure 4-22 shows the axial stress distribution in the cladding at the onset of damage for Mode-I. As can be seen, the stress dropped from a value of over 700 MPa to about 500 MPa, indicating partial stress shedding. At a later time, the damage front penetrated to about 2/3rd of the cladding wall as depicted in Figure 4-23. Completion of Mode-I occurred at a relative time of 1.54 ms, as depicted in Figure 4-24, which shows the zero-contour reaching the inner surface, which is a condition for the formation of a pinhole failure. Damage progression to the final equilibrium state showing partial Mode-II is depicted in Figure 4-25.

The geometry of this failure configuration can be estimated from Figures 4-25 and 4-26, the latter depicting the axial strains (normal to the cross-section) at the equilibrium condition. Figure 4-25 shows the remaining axial stress acting on the lower 40% of the cross-section, where the resultant tension and compression forces are equal and sum-up to zero, as indicated by Figure 4-20. The root of the fracture surface is at the 100-degree angle and the position of the neutral axis, estimated from Figure 4-25, is at the 135-degree angle as measured clockwise from the vertical. Figure 4-26 shows strain variation from about 6.7% at the vertical (zero-degree) position, decreasing to zero at the 135-degree position, with an estimated opening of less than 2 mm at the top outer surface of the cladding decreasing to zero at the 100-degree position.

Comparing the time histories of the axial force and bending moment in Figures 4-20 and 4-21 to their corresponding distributions in Figures 4-7 and 4-8, respectively, indicates that about 7% of the rods may experience an axial force of 1200 lbs or greater, and about 75% of the rods may experience a bending moment of 150 in-lb or greater during the 9-m side drop event. This means that as low as 7% and as high as 75% of the rods can potentially experience Mode-I damage, with potentially pinhole failure geometry. The 7%/75% damage estimate is based on the assumption that the peak axial force and peak bending moment depicted in Figures 4-20 and 4-21, respectively, have equal probability of occurring at the same time in the same rod, which is highly unlikely. Without conducting a time-consuming probabilistic analysis, it is reasonable to use a mean value of 40-50% as the failure probability for partial-Mode-II failure, but no complete rod breakage is predicted. Moreover, the fact that an equilibrium state was reached at the end of the damage process with about 45% of the cladding remaining intact indicates that fuel re-configuration is not an expected outcome of the hypothetical transportation accident.

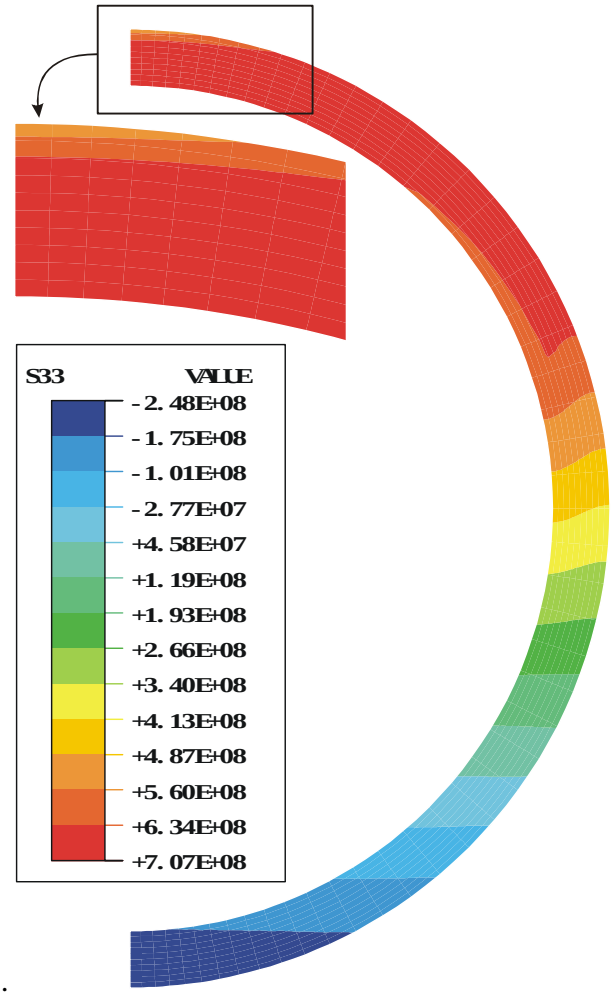

Figure 4-22
Stress Distribution at the Time of Initiation of Damage for Mode-I at 0.8-ms Relative Time in the Analysis Sequence

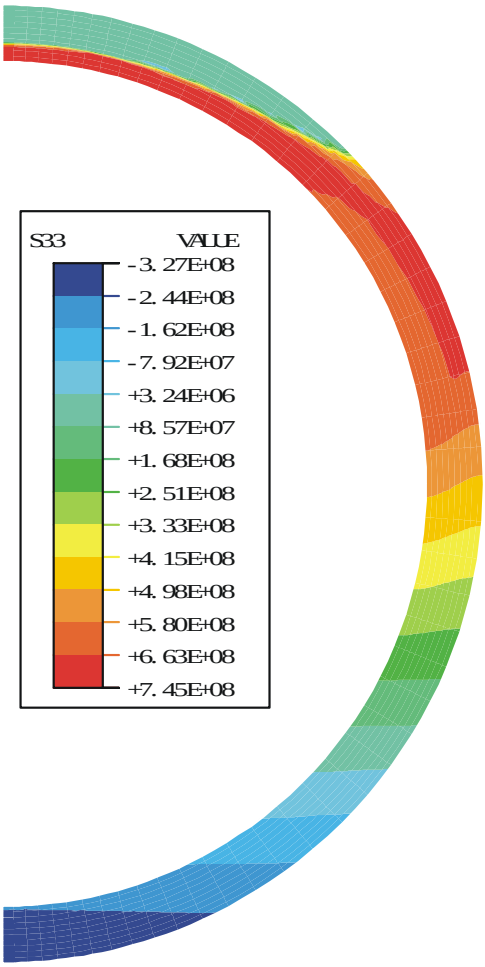

Figure 4-23
Stress Distribution at 1.0-ms Relative Time in the Analysis Sequence Showing Part Through-Wall Damage Progression

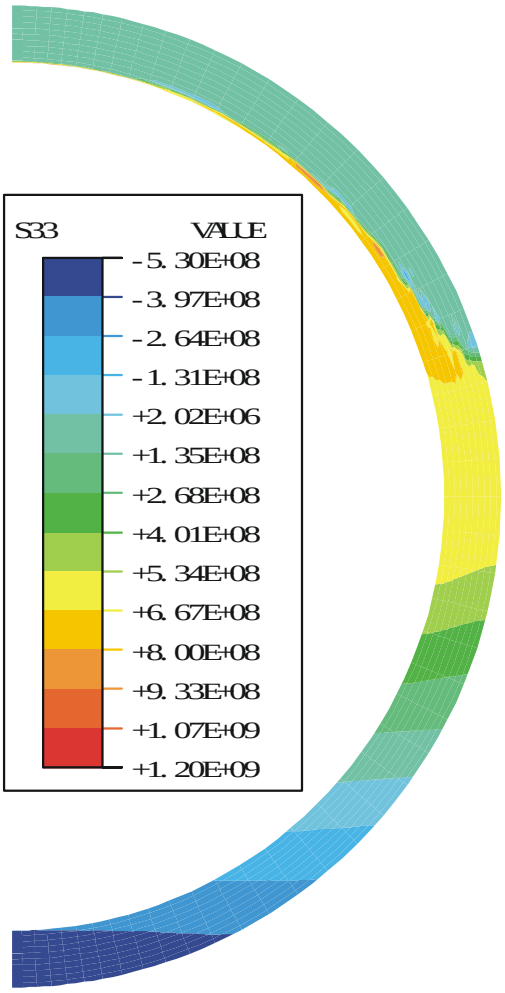

Figure 4-24
Stress Distribution at 1.54-ms Relative Time in the Analysis Sequence Showing Damage State at the Completion of Mode-I

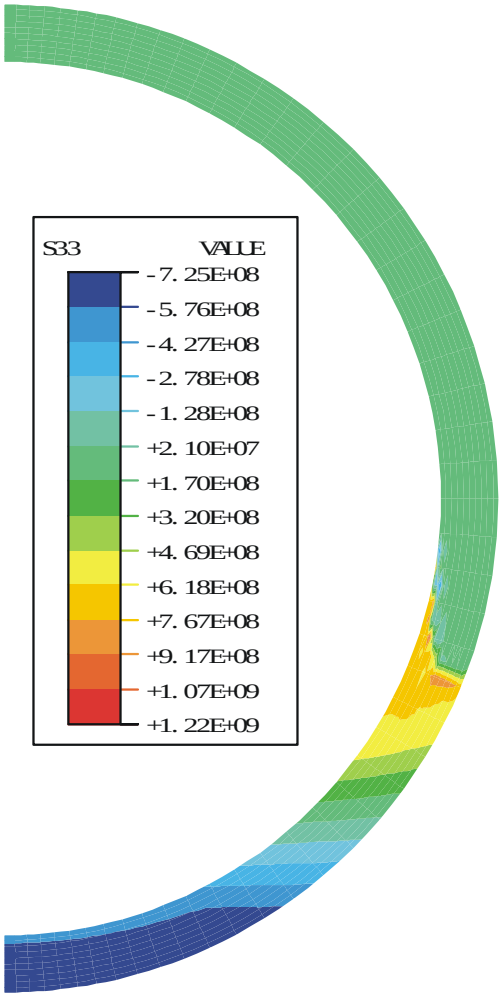

Figure 4-25
Stress Distribution at 4.0-ms Relative Time at the State of Equilibrium at the End of the Analysis Sequence When Damage Progression Stops

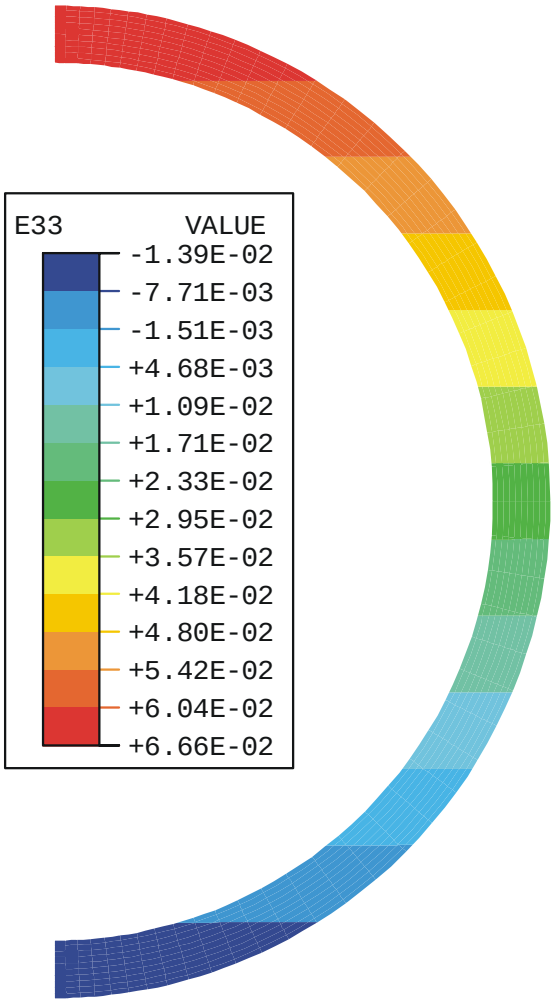

Figure 4-26
Axial Strain Distribution at 4.0-ms Relative Time at the State of Equilibrium at the End of the Analysis Sequence When Damage Progression Stops

5
STRUCTURAL ANALYSIS AND FAILURE EVALUATION OF NORMAL CONDITIONS OF TRANSPORT

The structural analysis and failure evaluation for the normal conditions of transport is described in detail in 1015049, June 2007 [15]. Except for differences in details, the same approach to that used for the hypothetical accident analysis is employed in which a global structural analysis is first performed to calculate the global forces acting on the fuel rods and guide tubes, followed by local analyses to evaluate damage. The differences between the two conditions lie in the definition of the dynamic event and in the definition of the consequences. In the present case, the event is characterized as a 0.3-m drop of a bare cask, i.e., no impact limiters, onto an un-yielding surface. Also, the definition of the consequences, as prescribed in 10 CFR 71.71, is that the geometric form of the package contents should not be substantially altered. This places additional emphasis on the structural integrity of the assemblies, which brings the behavior of the assembly skeleton into the failure evaluation process. In fact, the failure of the guide tubes and/or the plastic collapse of the spacer grids become the object of interest for the normal conditions of transport. This can be deduced from a comparison of the loading demands on the fuel assemblies for the 0.3-m drop and the 9-m drop events, as shown in Table 5-1. The table lists the forces calculated for both events and shows that the forces acting on the fuel rods for the one-foot drop are too low to cause damage, by a factor of two, as demonstrated in 1015049. For this reason, discussion of the results of 1015049 will be limited to the behavior of the guide tubes and spacer grids.

Table 5-1
Comparison of Maximum Forces and Moments for the 30-foot and 1-ft Cask Drops

Force Type (Units)	30-Foot Drop	One-Foot Drop	
	Center Span	Center Span	End Span
Max Pinch Force (lb)	7500 (FR*)	1400 (FR*) / 640 (GT**)	520 (GT**)
Max Axial Force (lb)	1800 (FR*)	600 (FR*)	415 (GT**)
Max Bending Moment (in-lb)	300 (FR*)	175 (FR*)	348 (GT**)

FR* = Fuel Rod; GT** = Guide Tube

Evaluation of Fuel Assembly Damage

Plastic Collapse of the Spacer Grids

The plastic collapse of the spacer grids and the breakage of the guide tubes are the two damage modes that could impair the fuel assembly's geometric continuity. As to the former, Figure 5-1 shows that plastic collapse of the spacer grids does not occur. This is evidenced from the fact that the fuel rod compaction depicted in Figure 5-1 B at the maximum response time of 20-ms recovers upon returning to rest at 40-ms, which is near the end of the analysis as shown in Figure 5-1 C. A longitudinal view of the deformations of the fuel rods and spacer grid for the 0.3-m drop event compared to the 9-m drop event is shown in Figure 5-2. The apparent plastic deformations of the spacer-grid and rod deformations that are evident in the hypothetical accident case are not observed in the 0.3-m drop case, which appears to be only slightly modified from the initial configuration.

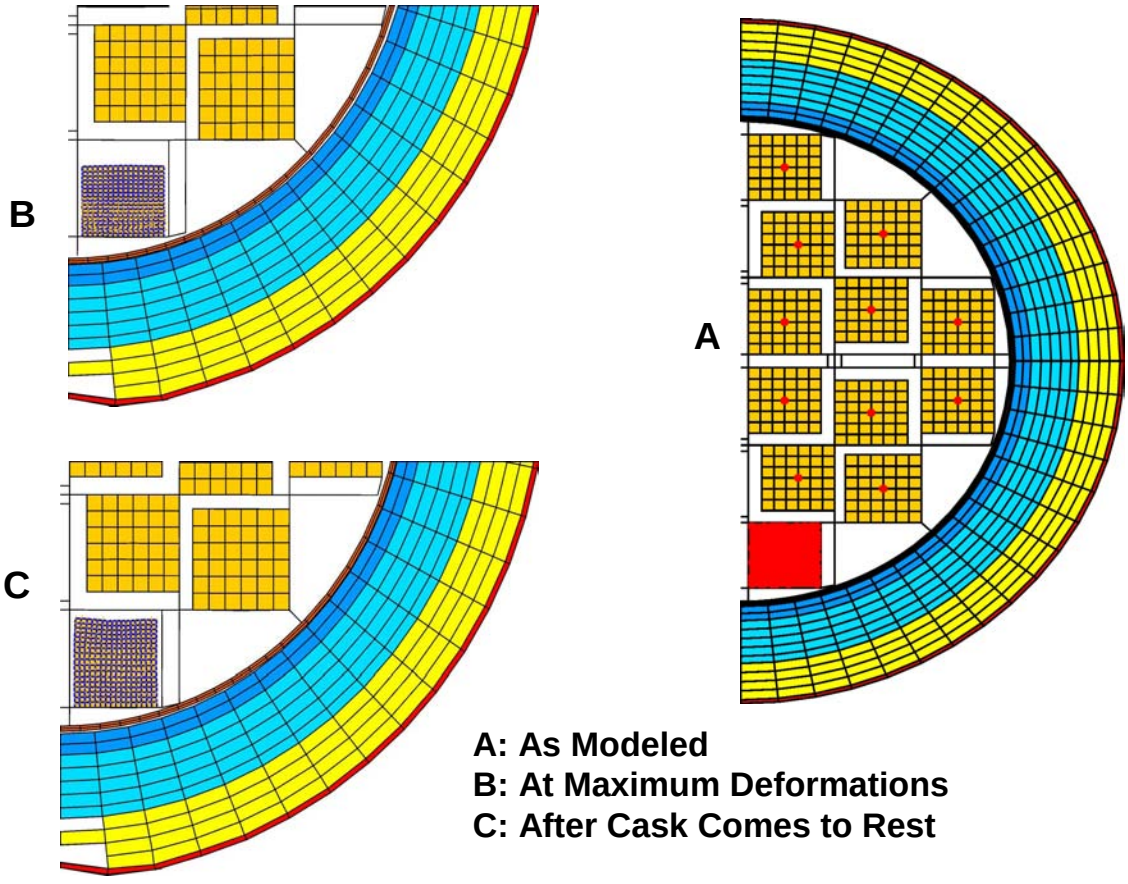

Figure 5-1
End Snapshot View of Cell 24 Assembly Deformations at Maximum Response and After Cask Comes to Rest

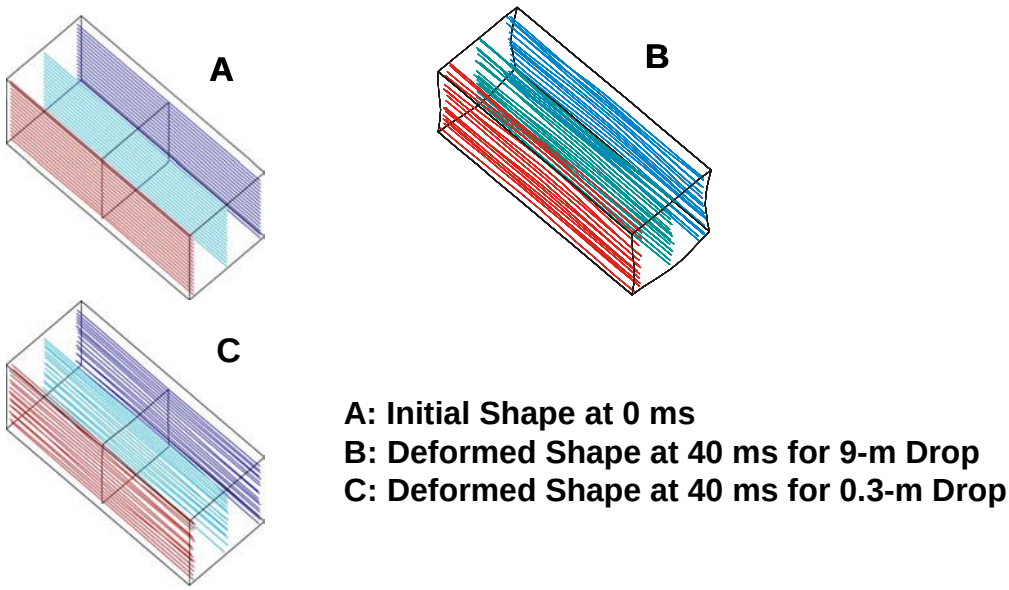

Figure 5-2
Comparison of the 0.3-m Drop and the 9-m Drop Deformations of the Fuel Assembly After Cask Comes to Rest - No Displacement Magnification

Evaluation of Transverse Tearing of Guide Tubes (Mode-I Failure)

The forces that affect the guide tubes transverse tearing are the bending and axial tension forces at the top nozzle. The pinch forces, on the other hand, could cause plastic ovalization and collapse of the guide tubes. These potential damage states are evaluated next in a local failure analysis using Figure 4-19 finite element model, adapted to the geometry of an empty guide tube. The Metal/Hydride Mixture Model [7], with the aid of the position-dependent failure criteria developed in Chapter 3, is used for predicting damage initiation and progression through the wall. The results for potential Mode-I failure are presented in Figures 5-3 through 5-5. The axial force and bending moment that the guide tube was able to attract are shown in Figures 5-3 and Figure 5-4, respectively. As can be seen from these figures and Table 5-1, the guide tube was able to resist 200 lb and 235 in-lb, respectively, before the onset of Mode-I damage, compared to the 415 lb and 348 in-lb shown in Table 5-1. Transverse tearing stopped when the axial force was exhausted and bending came to an equilibrium state of pure bending after tearing has extended to about 20% of the circumference. This can be seen in Figure 5-5, which shows the axial stress and axial strain distributions in the tube.

The consequences of the partial Mode-I failure shown in Figure 5-5 can be evaluated with the help of Figures 5-6 and 5-7. Figure 5-6 shows that about 80% of the guide tubes will exceed the 200 lb force limit shown in Figure 5-3, and Figure 5-7 shows that about 65% of the guide tubes will exceed the moment limit of Figure 5-4. This means that the partial Mode-I failure depicted in Figure 5-5 would occur in about 65-80% of the guide tubes. Taking the higher figure of 80% and considering a loss of cross-sectional area of 20% from Figure 5-5, the load carrying capacity of the guide tube skeleton will be reduced to 64% of its undamaged capacity. To evaluate the relevance of this result, the Metal/Hydride Mixture Model [7] was used to evaluate the ultimate load capacity of the partially damaged guide tube by subjecting the partially damaged guide tube

to a tension force until total loss of tensile capacity was predicted. The force calculated in this manner is 216 lb, which constitutes the residual carrying capacity of the partially damaged guide tube. This is more than 3.5 times higher than required to lift a 1500-lb assembly, assuming all of the 25 guide tubes have sustained the same level of partial Mode-I failure, which is conservative.

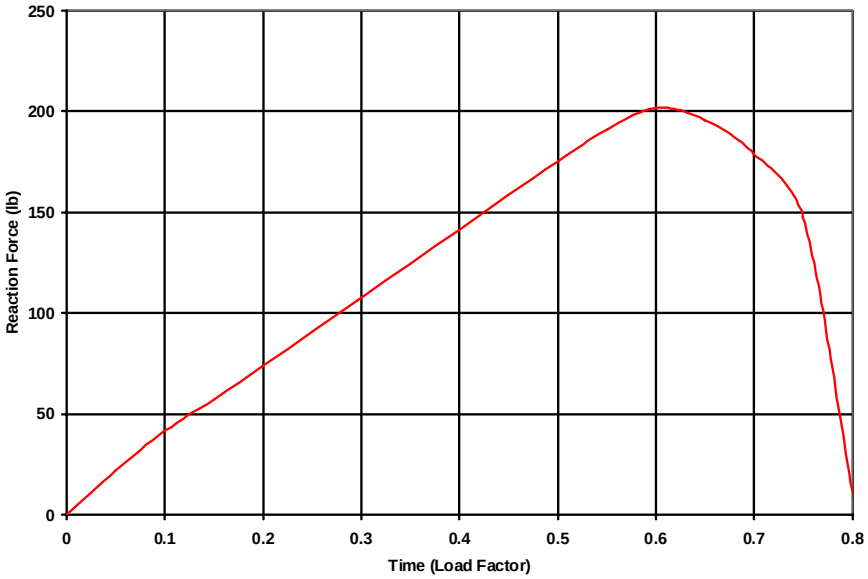

Figure 5-3
Axial Force Resisted by the Guide Tube in Combination With the Bending Moment Shown in Figure 5-4

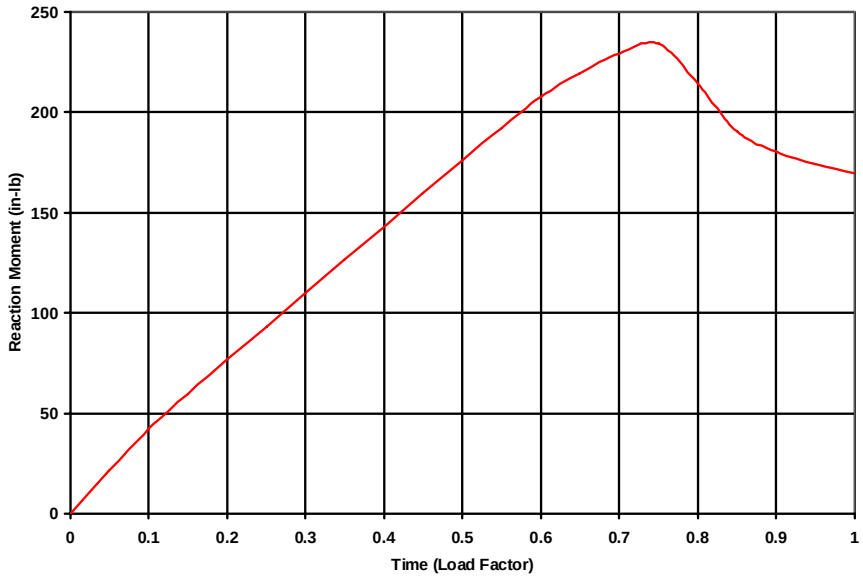

Figure 5-4
Bending Moment Resisted by the Guide Tube in Combination With the Axial Force Shown in Figure 5-3

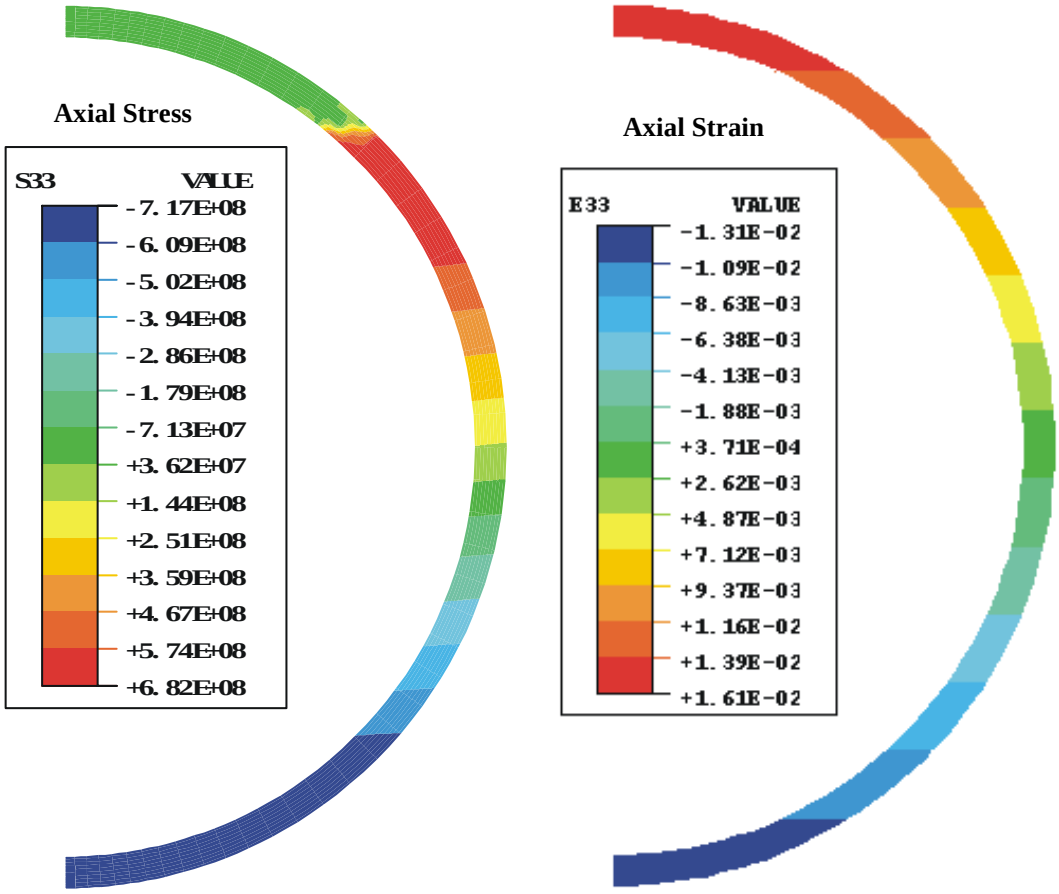

Figure 5-5
Axial Stress and Axial Strain Distributions in the Guide Tube at Maximum Axial Force and Moment

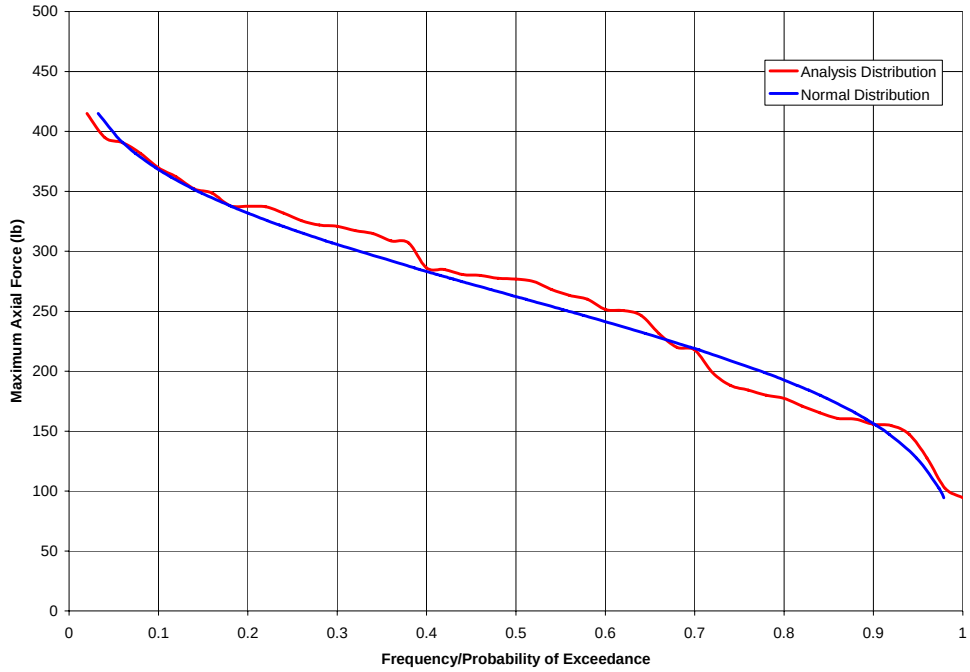

Figure 5-6
Maximum Axial Force Frequency Distribution

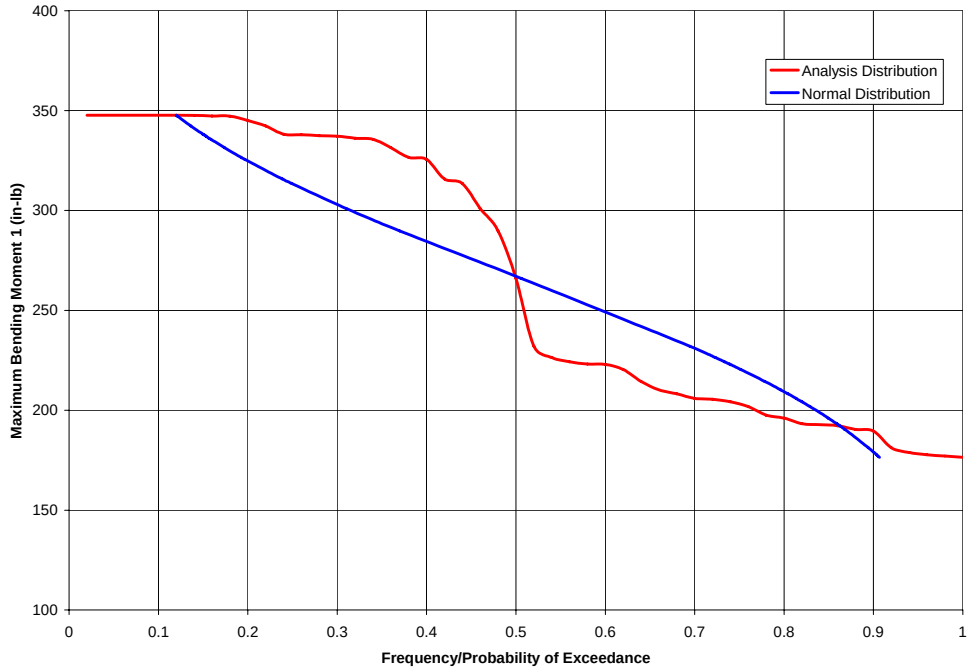

Figure 5-7
Maximum Bending Moment Frequency Distribution

Evaluation of Plastic Collapse of Guide Tubes

A static collapse analysis, employing the Metal/hydride Mixture Model [7], was carried out for a one-inch axial slice of the guide tube, and was found to show that the static collapse load is 130 lb per inch, as shown in Figure 5-8. This is equivalent to a dynamic collapse-load of 260 lb per inch, using a typical load factor of 2. Figure 5-9 shows the un-deformed and deformed shapes and hoop stress contours at the time of maximum load when the analysis ceased to converge. Damage initiation at the ID can be observed in the figure where the stress shedding due to local material fracture begins to occur. Figure 5-8 shows the un-deformed and deformed shapes and hoop stress contours at the time of impending collapse when the analysis ceased to converge. Damage initiation at the ID can be observed in the figure where the stress shedding due to local material fracture begins to occur.

The results of the analysis indicate that the dynamic pinch forces of 640 lb and 520 lb reported in Table 5-1 for the center span and top span, respectively, act over an axial distance of about 2 inches. The 520-lb peak dynamic force is at the static collapse-load capacity of the guide tube for the top span, but the 640-lb force exceeds the capacity of the center span by about 23%. These results indicate that there is sufficient margin against collapse of the guide tubes occurring during the dynamic event. The reason being that, for the guide tube to collapse dynamically, the peak dynamic collapse load must exceed the static capacity by a large factor to account for the inertia effects, which are ignored in the static analysis.

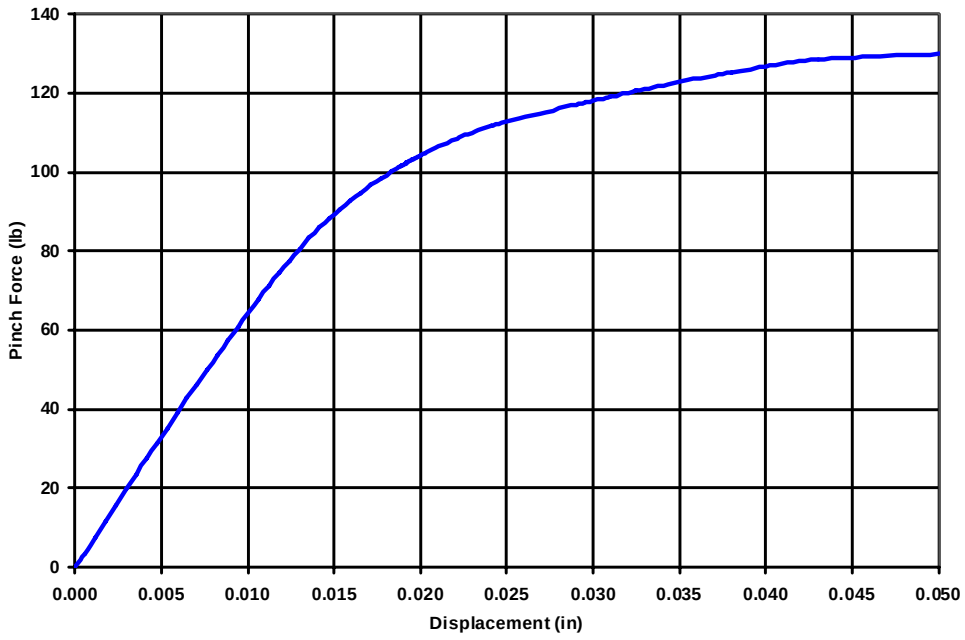

Figure 5-8
Force-Displacement of Guide Tube Cross-Section Subjected to Static Collapse Analysis

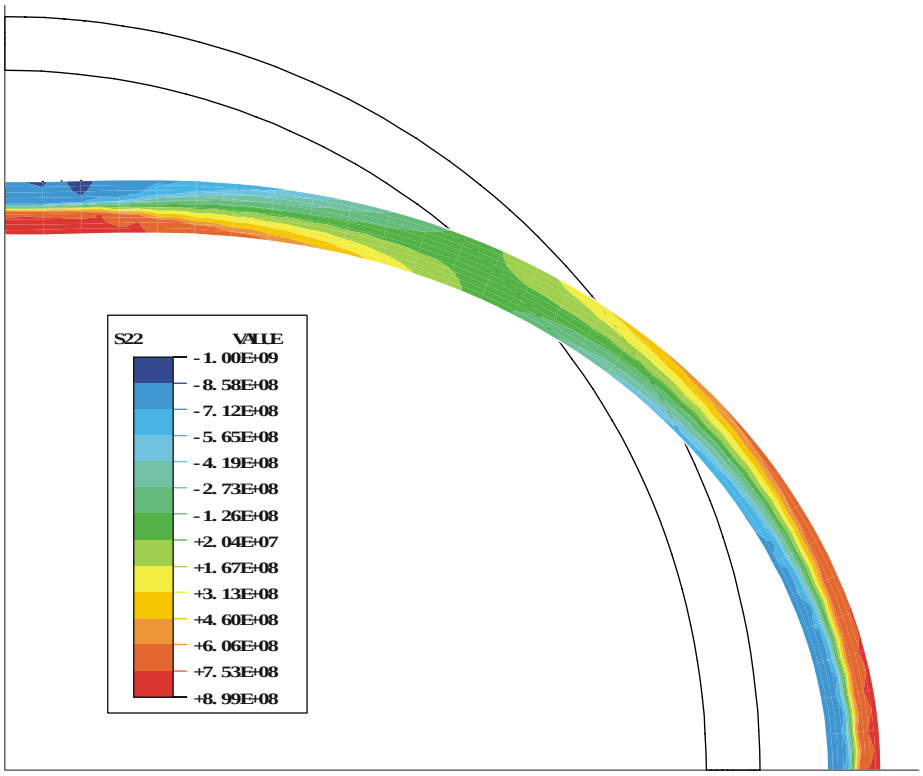

Figure 5-9
Plastic Collapse Analysis of Guide Tubes

6
SUMMARY AND CONCLUSIONS

The results of the analytical studies presented in this report validate the overall conclusion that damage to materials and structures of high-burnup spent fuel systems under prescribed regulatory conditions of dry storage and transportation is tolerably small, with little or no impact on spent fuel operational management. Specific findings, which serve to justify this general conclusion, are summarized below, with reference to the appropriate EPRI product for detailed supporting information.

1. Failure mechanisms postulated to be active during dry storage, namely, Stress Corrosion Cracking (SCC), Delayed Hydride Cracking (DHC) and Creep Rupture (CR), are either inactive or lack sufficient driving forces to cause cladding failure – 1001207, 2000, and 1001281, 2001.
2. Under dry storage conditions, creep is shown to be the governing deformation mechanism for spent fuel. Creep contributes to a rapid decrease of the fuel rod internal pressure, but also results in increasing the fuel-cladding gap size. Under actual dry storage conditions, hydride re-orientation at the end of a 40-year dry storage is predicted to be very limited; increases in radial hydride concentration of less than 20 ppm are calculated. The effects of the fuel-cladding gap on cladding failure led to the development of a "Fail/No-Fail Boundary", which made it possible to distinguish between accident impact loads that result only in crack initiation at the cladding ID and those that are likely to cause the crack to extend to the OD– 1003135, 2001, 1009276, 2003, and Paper # 1038, ICEM05 Conference, 2005.
3. Anticipating the need for evaluating spent fuel rod failure potential under normal and accident conditions, for both the 0.3-m drop and the 9-m drop, the development of the following predictive tools was critical: Metal/Hydride Mixture Model and its derivative product Cladding Failure Criteria as function of local conditions (hydride structure and morphology) in the cladding wall. Both of these tools were indispensable in developing failure information for fuel rods, including: failure size (part-wall fracture versus through-wall rupture), failure mode (longitudinal tearing, circumferential tearing and rod breakage), and failure frequency (number of rods failing in each mode and of what size) – 1009694, 2004, 1009693, 2004, and 1009929, 2005.

4. The consequences of hydride re-orientation, when evaluated for the actual spent fuel behavior regimes during dry storage, do not rise to the level where fuel reconfiguration becomes a likely outcome during transportation accidents. The analysis results of the hypothetical accident for the longitudinal tearing mode, which is the failure mode that is sensitive to radial hydrides, indicate that cladding failure is bi-modal: a state of failure initiation at the cladding ID remaining as part-wall damage, with less than 2% probability of occurrence; and a through-wall failure with a probability of 1E-5, which is of the same order of magnitude as the failure probability calculated in SAND90-2406 [16] for lower burnup fuel. Contributory factors for arriving at this general conclusion are: first, spent fuel rods conditions that would promote the formation of radial hydrides are not sufficient to produce radial hydride concentrations of significant levels, which was the intended result of selecting a peak cladding temperature equal to, or below, 400°C; second, the fuel column, as an integral part of high-burnup spent fuel rods, plays a major role in the cladding resistance to failure under dynamic pinch forces resulting from transportation accidents. The fuel-cladding gap and the radial hydrides concentration are the major protagonists, among all the random variables considered, for failure initiation that has the potential to propagate to through-wall fracture. Only by resorting to highly conservative assumptions did the calculations show a through-wall cladding rupture with a failure probability of 1E-5.
5. Cladding failure mode that could lead to fuel assembly reconfiguration is the rod breakage mode, Mode-II, with the transverse tearing mode, Mode-I, as the precursor. The Metal/Hydride Mixture model, which is capable of predicting and tracking failure progression from initiation to complete failure, was used to calculate the failure geometry, which is necessary for assessing the extent of fuel reconfiguration. The analysis predicts cladding fracture of type Mode-I, which extends radially and circumferentially through the wall to form partial Mode-II failure, but no guillotine break is predicted. The consequence of such a failure configuration can be judged by examining the geometry of the failure mode, specifically the size of the opening. This is estimated to be a maximum of 2 mm at the widest point, decreasing to zero at the root of the tear. The failure frequency in the Mode-I/Partial-Mode-II failure geometry discussed above was estimated to be 50%, but no fuel reconfiguration is predicted.
6. The response analysis for the one-foot drop event shows no fuel rod failures are possible, within a safety factor of two against the longitudinal tearing mode, and no failure is predicted for the transverse tearing (pinhole type) mode; however, stresses at or just below the yield strength of the material are calculated. This implies that damage initiation can be expected, but progression of the damage to form a pinhole failure can be ruled out because the loading is totally exhausted upon damage initiation, in contrast to the hypothetical accident case where damage initiation occurred at 66% of the maximum axial force and 50% of the maximum bending moment. The guide tubes, which form the structural elements of the fuel assembly, are predicted to ovalize but not fracture or totally collapse, which preserves the structural integrity of the assemblies in a non-reconfigured state.

7
REFERENCES

1. Part 71 of Title 10 of the Code of Federal Regulations (10 CFR 71).

2. "Creep as the Limiting Mechanism for Spent Fuel Dry Storage," EPRI, Palo Alto, CA: 2000. 1001207.

3. "Fracture Toughness Data for Zirconium Alloy: Application to Spent Fuel Cladding in Dry Storage," EPRI, Palo Alto, CA, 2001. 1001281.

4. "Creep Modeling and Analysis Methodology for Spent Fuel in Dry Storage," EPRI, Palo Alto, CA: 2001. 1003135.

5. "Dry Storage of High-Burnup Spent Fuel: Responses to Nuclear Regulatory Commission -- Requests for Additional Information and Clarification," EPRI, Palo Alto, CA: 2003. 1009276.

6. Interim Staff Guidance 11, Revision 2 "Cladding Considerations for the Transportation and Storage of Spent Fuel" (NRC 2002).

7. Interim Staff Guidance 11, Revision 3 "Cladding Considerations for the Transportation and Storage of Spent Fuel" (NRC 2003).

8. "Development of Metal/Hydride Mixture Model for Zircaloy Cladding with Mixed Hydride Structure," EPRI, Palo Alto, CA: 2004. 1009694.

9. "Failure Criteria for Zircaloy Cladding using a Damage-Based Metal/Hydride Mixture Model," EPRI, Palo Alto, CA: 2004. 1009693.

10. "Spent Fuel Transportation Applications: Fuel Rod Failure Evaluation Under Simulated Cask Side Drop Conditions," EPRI, Palo Alto, CA. 2005. 1009929.

11. "Application of Critical Strain Energy Density to Predicting High-Burnup Fuel Rod Failure -- *Response to Comments from the Nuclear Regulatory Commission Staff*," EPRI, Palo Alto, CA: 2005. 1011816.

12. "Spent-Fuel Transportation Applications: Global Forces Acting on Spent Fuel Rods and Deformation Patterns Resulting from Transportation Accidents," EPRI, Palo Alto, CA: 2005. 1011817.

13. "Spent-Fuel Transportation Applications: Modeling of Spent-Fuel Rod Transverse Tearing and Rod Breakage Resulting from Transportation Accidents," EPRI, Palo Alto, CA: 2006. 1013447.

14. "Spent-Fuel Transportation Applications: Longitudinal Tearing Resulting from Transportation Accidents," EPRI, Palo Alto, CA: 2006. 1013448.

15. "Spent-Fuel Transportation Applications: Normal Conditions of Transport," EPRI, Palo Alto", CA: 2007: 1015049.

16. Sanders, T. L, Seager, K. D., Rashid, Y. R., et al., "A Method for Determining the Spent-Fuel Contribution to Transport Cask Containment Requirements," SANDIA Report, SAND90-2406, TTC-1019, UC-820, November 1992.

17. Marshall, R. P., and Louthan M. R., "Tensile Properties of Zircaloy with Oriented Hydrides", Transactions of ASM, Vol. 56, 1968.

18. Einziger, R. E., Kohli, R., "Low-Temperature Rupture Behavior of Zircaloy-Clad Pressurized Water Reactor Spent Fuel Rods under Dry Storage Conditions," *Nucl. Tech.*, 67, p. 107-122, 1984.

19. U. S. Nuclear Regulatory Commission (NRC), "Safety Evaluation Report Related to the Topical Safety Analysis Report for CASTOR V/21 Dry Spent Fuel Storage Cask - Appendix A: Analysis of Diffusion Controlled Cavity Growth (DCCG) Damage to Fuel Cladding in Dry Storage," September 1985.

20. Raj, R., Ashby, M F., "Intergranular Fracture at Elevated Temperature," Acta Met., V23, pp. 653-666, 1975.

21. U. S. Nuclear Regulatory Commission, "Standard Review Plan for Dry Cask Storage System: Final Report," NUREG-1536, January 1997.

22. U. S. Nuclear Regulatory Commission, Spent Fuel Project Office Interim Staff Guidance - 11 May 13, 1999.

23. Gilbert, E. R., Beyer, C. E., Simonen, E. P., "Technical Evaluation Report of WCAP-15168, Dry Storage of High Burnup Spent Nuclear Fuel," February 2000.

24. Einziger, R. E., Tsai, H. C., Billone, M. C., Hilton, B. A., "Examination of Spent Fuel Rods after 15 years in Dry Storage", NUREG/CR-6831, ANL-03/17, September 2003.

25. Goll, W., Spilker, H., Toscano, E., "Short-Time Creep and Rupture Tests on High Burnup Fuel Rod Cladding," *J. of N. Mat.*, 289 (2001) 247-253

26. Limon, R., Cappelaere, Ch., Bredel, Th., Bouffioux, P., "A Formulation of the Spent Fuel Cladding Creep Behavior for Long Term Storage", LWR Fuel Performance Meeting, Park City, Utah, April 10-13, 2000.

27. Bouffioux, P., Legras, L. “Effects of Hydriding on the Residual Cold Work Recovery and Creep of Zircaloy-4 Cladding Tubes” LWR Fuel Performance Meeting, Park City, Utah, April 10-13, 2000.

28. Cubicciotti, D., Davies, J. H., Nuclear Science and Engineering, Vol. 60, 1976, p. 314.

29. Roberts, J. T. A., Jones, R. L., Cubicciotti, D., Miller, A. K., Wachob, H. F., Smith, E., Yaggee, F. L., "A Stress Corrosion Cracking Model for Pellet-Cladding Interaction Failures in Light-Water Reactor Fuel Rods," Zirconium in the Nuclear Industry (fourth Conference), ASTM STP 681, American Society for Testing and Materials, 1979, pp. 285-305.

30. Brunisholz, L., Lemaignan, C., "Iodine-Induced Stress Corrosion of Zircaloy Fuel Cladding: Initiation and Growth," Zirconium in the Nuclear Industry: Seventh International Symposium, ASTM STP 939, American Society for Testing and Materials, Philadelphia, 1987, pp. 700-716.

31. Rashid, Y.R. and A.J. Machiels, “Examination of the creep rupture phenomenon and the development of an acceptance criterion for spent fuel dry storage,” Proceedings of the International Conference on Storage of Spent Fuel from Power Reactors, IAEA,Vienna, 2-6 June 2003, pp. 431-441.

32. Bouffioux, Pol, “Interim Dry Storage of PWR’s Spent Fuel – Development of a Creep Law to Assess the Fuel Cladding Integrity”, ICEM01 Conf., Bruges, Belgium, Sept. 30-Oct. 4, 2001.

33. Machiels, A. J., Rashid, Y. R., “Hydride Precipitation in Spent Fuel Cladding During Dry Storage”, Paper # 1038, Proceedings of the 10th. International Conference on Environmental Remediation and Radioactive Waste Management, ICEM05 Paper 1038, Glasgow, Scotland, September 4-8, 2005.

34. Nakatsuka, M., Ogata, K., “Cladding Transient Response NFIR-IV X104-15,” Prepared by Nippon Nuclear Fuel Development Co. Ltd., NFIR Report NFIR-IV/EPRI X104-15-09,” October 2003.

35. Kuo, R.C., et al., “Fuel Cladding Integrity at High Burnup (Part II), Uniaxial Tensile Tests and Slotted Arc Tests on Small Samples,” EPRI, Palo Alto, CA: 2000. 1000606.

36. Yagnik, S.K., Kuo, R-C, Rashid, Y.R., Machiels, A.J., Yang, R.L., “Effect of Hydrides on the Mechanical Properties of Zircaloy-4,” *Proceedings of the 2004 International Meeting on LWR Fuel Performance*, Orlando, Florida, September 19-22, 2004, Paper 1089.

37. Montgomery, R.O., Rashid, Y. R., Zangari, A., "FALCON Fuel Analysis and Licensing Code, Vol. 2, User's Manual," ANATECH Corp., San Diego, California, ANATECH Report No. ANA-97-0230, December 1997.

38. ABAQUS/Standard, ABAQUS/Explicit, Version 5.8, ABAQUS Inc., Providence R.I., 1998.

WARNING: This Document contains information classified under U.S. Export Control regulations as restricted from export outside the United States. You are under an obligation to ensure that you have a legal right to obtain access to this information and to ensure that you obtain an export license prior to any re-export of this information. Special restrictions apply to access by anyone that is not a United States citizen or a permanent United States resident. For further information regarding your obligations, please see the information contained below in the section titled "Export Control Restrictions."

Export Control Restrictions

Access to and use of EPRI Intellectual Property is granted with the specific understanding and requirement that responsibility for ensuring full compliance with all applicable U.S. and foreign export laws and regulations is being undertaken by you and your company. This includes an obligation to ensure that any individual receiving access hereunder who is not a U.S. citizen or permanent U.S. resident is permitted access under applicable U.S. and foreign export laws and regulations. In the event you are uncertain whether you or your company may lawfully obtain access to this EPRI Intellectual Property, you acknowledge that it is your obligation to consult with your company's legal counsel to determine whether this access is lawful. Although EPRI may make available on a case-by-case basis an informal assessment of the applicable U.S. export classification for specific EPRI Intellectual Property, you and your company acknowledge that this assessment is solely for informational purposes and not for reliance purposes. You and your company acknowledge that it is still the obligation of you and your company to make your own assessment of the applicable U.S. export classification and ensure compliance accordingly. You and your company understand and acknowledge your obligations to make a prompt report to EPRI and the appropriate authorities regarding any access to or use of EPRI Intellectual Property hereunder that may be in violation of applicable U.S. or foreign export laws or regulations.

The Electric Power Research Institute (EPRI), with major locations in Palo Alto, California; Charlotte, North Carolina; and Knoxville, Tennessee, was established in 1973 as an independent, nonprofit center for public interest energy and environmental research. EPRI brings together members, participants, the Institute's scientists and engineers, and other leading experts to work collaboratively on solutions to the challenges of electric power. These solutions span nearly every area of electricity generation, delivery, and use, including health, safety, and environment. EPRI's members represent over 90% of the electricity generated in the United States. International participation represents nearly 15% of EPRI's total research, development, and demonstration program.

Together...Shaping the Future of Electricity

Program:

Nuclear Power

Printed on recycled paper in the United States of America

1015048

Electric Power Research Institute
3420 Hillview Avenue, Palo Alto, California 94304-1338 • PO Box 10412, Palo Alto, California 94303-0813 USA
800.313.3774 • 650.855.2121 • askepri@epri.com • www.epri.com